NSF/CEE-81058

WASHINGTON UNIVERSITY IN ST. LOUIS

PB82-148008

Structural Engineering Research Report No. 60

ANALYTICAL METHOD FOR DETERMINING SEISMIC RESPONSE OF COOLING TOWERS ON FOOTING FOUNDATIONS

Phillip L. Gould
Osama El-Shafee
Bor-Jen Lee

October, 1981

DEPARTMENT OF CIVIL ENGINEERING
Washington University
Campus Box 1130
St. Louis, MO 63130

50272-101

REPORT DOCUMENTATION PAGE	1. REPORT NO. NSF/CEE-81058	2.	3. Recipient's Accession No. PB82 148008
4. Title and Subtitle: Analytical Method for Determining Seismic REsponse of Cooling Towers on Footing Foundations			5. Report Date: 1981 6. 008224
7. Author(s): P.L. Gould, O.M. El-Shafee, B.J. Lee			8. Performing Organization Rept. No. 60
9. Performing Organization Name and Address: Washington University, Department of Civil Engineering, St. Louis, MO 63130			10. Project/Task/Work Unit No. 11. Contract(C) or Grant(G) No. (C) (G) PFR7900012
12. Sponsoring Organization Name and Address: Directorate for Engineering (ENG), National Science Foundation, 1800 G Street, N.W., Washington, DC 20550			13. Type of Report & Period Covered 14.

15. Supplementary Notes
Submitted by: Communications Program (OPRM)
National Science Foundation
Washington, DC 20550

16. Abstract (Limit: 200 words)

The development of a finite element model for the dynamic analysis of an axisymmetric thin rotational shell founded on a shallow ring footing is described. The model was developed using high-precision rotational elements for the shell, isoparametric solid elements for the soil, and an energy transmitting boundary at the ring footing. In a sensitivity study of the equivalent boundary system to the driving frequency, the stiffness components were found to be more sensitive than damping components and the rotational components were found to be more sensitive than the translational components. Free vibration, response spectrum, and time history analyses of a hyperbolic cooling tower shell showed that the overall flexibility of the shell increased with a decrease in soil stiffness, reducing many forces in the shell proper and especially in the column support from the values calculated when the interaction is neglected. It is suggested that the structural design and resulting behavior of rotational shells can be improved by considering soil-structure interaction.

17. Document Analysis a. Descriptors

Earthquakes
Hazards
Soils
Construction
Foundation supports
Damping
Foundations
Structural analysis
Mathematical models
Cooling towers
Matrix methods
Computer programs

b. Identifiers/Open-Ended Terms

Man environment interactions
Environmental effects
Ground motion
P.L. Gould, /PI

c. COSATI Field/Group

18. Availability Statement	19. Security Class (This Report)	21. No. of Pages
NTIS	20. Security Class (This Page)	22. Price

ANALYTICAL METHOD FOR DETERMINING SEISMIC RESPONSE OF COOLING TOWERS ON FOOTING FOUNDATIONS

by

Phillip L. Gould

Osama El-Shafee

and

Bor-Jen Lee

Technical Description and Results of

a Research Project Sponsored by the

NATIONAL SCIENCE FOUNDATION

Research Grant No. PFR-7900012

Structural Engineering

Research Report No. 60

Department of Civil Engineering

Washington University

St. Louis, Missouri

October, 1981

SUMMARY

A finite element model for the dynamic analysis of an axisymmetric thin rotational shell founded on a shallow ring footing was developed using high-precision rotational elements for the shell, isoparametric solid elements for the soil, and an energy transmitting boundary at the ring footing. The soil medium and the structure are connected by a frequency dependent dynamic boundary system. A sensitivity study of the equivalent boundary system to the driving frequency revealed that stiffness components were more sensitive than damping components and that the rotational components were more sensitive than the translational components. Free vibration, response spectrum and time history analyses of a hyperbolic cooling tower shell showed that the overall flexibility of the shell increased with a decrease in soil stiffness, reducing many forces in the shell proper and especially in the column supports from the values calculated when interaction is neglected. Relatively large forces and twisting moments are introduced into the ring footing which is, however, massive and capable of resisting these forces. Foundation uplift is investigated and found to be a minor problem. It is suggested that the structural design and resulting behavior of such shells can be improved by consideration of soil-structure interaction. Such an analysis is facilitated by the use of the SHORE-IV computer program developed in conjunction with this research.

TABLE OF CONTENTS

LIST OF FIGURES

LIST OF FIGURES
(continued)

LIST OF FIGURES
(continued)

LIST OF TABLES

1-Introduction

1-1 General

One of the main criteria in selecting a mathematical model is to represent the significant physical behavior of the system as closely as possible. For the dynamic analysis of structures founded on shallow foundations, soil interaction in the structure response is expected, in general, to be notable. The importance of foundation interaction in the structure response depends on the properties of the structure relative to those of the foundation and soil medium.

Although many large shells such as cooling towers are placed on rigid pile or caisson foundations, others may be founded on individual footings or perhaps on a concentric ring footing. With the capability of a soil-structure interaction model for rotational shells, a basis for rationally evaluating the footing option in the list of alternative foundations may be established. Considerable economic benefits may be anticipated from this added option in the form of savings on foundation costs and reduced internal design forces due to the possible amelorating effect of the interaction.

In this report, a dynamic axisymmetric finite element model suitable for shells of revolution founded on ring footings is developed. The analysis is carried out in the time domain while the soil model is based on a driving

frequency identical to the fundamental frequency of the structure on a fixed foundation. The inertial coupling method is used in the analysis and, as a result, no deconvolution is required. The approach used in this research is tempered by the availability and potential of the high precision rotational shell finite element model (1-3). With this factor in mind, the authors of this report developed a compatible representation of the soil medium with the existing shell element foundation, suitable for any type of dynamic analysis.

1-2 Review of Past Work

1-2a General

Although a great deal of attention has been devoted to nuclear containment structures, dams and multistory buildings (4-7), the influence of the surrounding medium on the dynamic response of large towers and other shells of revolution has apparently not been studied extensively. However, it is useful to review the existing knowledge of soil-structure interaction by citing some of the studies carried out by different authors. One may divide the work into three general categories: the approaches to soil-structure interaction, method and techniques, and parameters and applications. Among the last category, there does not appear to have been definitive studies on the interaction between the axisymmetric shells and the foundation system.

Before dealing with each of the preceding categories, it is convenient to introduce the work which is cited for the purpose of assessing the state of the art. A survey of the soil effect on the design of nuclear power plants has been performed by the Ad Hoc Group on Soil-Structure Interaction (1). This paper provides some general insight which may be useful for the specific problem at hand. Veletsos (4) outlined a simple, practically oriented procedure for studying the effects of ground shock and earthquake motions on structure-foundation systems. The procedure is fairly straight forward and it is believed that considerable insight for understanding the general nature of the problem may be gained from such work. A limitation of that analysis is that it is only applicable for structures which may be modeled by a rigid foundation mat supported at the surface of a homogeneous half-space. An additional limitation of the procedure is the assumption of a linear response for the superstructure.

1-2b Approaches to Soil-Structure Interaction

The basic alternative approaches to deal with the soil-structure interaction problem can be divided into *complete* interaction and *inertial* interaction analysis (1). The second approach neglects kinematic interaction and

basically does not explicitly account for the variation of the input ground motion with the depth below the surface. The essential difference between the idealized complete interaction analysis and the inertial interaction analysis lies in the treatment of embedded structures. For embedded structures, the complete interaction analysis is clearly superior from a theoretical viewpoint, but the principal limitation is the cost of analysis.

Vaish and Chopra (2) classified the complete interaction analysis into a combined model and a substructure model. In the combined model, the entire structure-soil medium is treated as a combined system subjected to an excitation at some assumed or actual boundary location such as the soil-rock interface. In the substructure model, the system is separated into substructures. Then the foundation medium is represented as an elastic half-space and is interfaced with the structure through a set of common coordinates at the boundary of the structure and the soil.

1-2c Methods and Techniques

Numerical methods and, in particular, the finite element technique, have usually been used to carry out complete interaction analysis, while inertial interaction analysis has generally been based on analytical solutions. These solutions treat the soil as a viscoelastic half-space or an elastic half space.

A complete interaction analysis for circular footings on layered media is presented by Kausel, Roësset and Waas (8) using a transmitting boundary to represent the far field. Dynamic analysis of rigid circular footings resting on a homogeneous, elastic half space has been carried out by Luco and Westmann (9). In this work numerical results for the analytical solution have been presented for the torsional, vertical, rocking and horizontal oscillations of the rigid disc.

Various approximate methods of superposition for the interaction problem have been recently proposed (10,11,12, 13,14). The methods have differed in the way in which modal damping is calculated, Novak (10), Rainer (12), and Roësset, Whitman and Dobry (13) assigned weighted values of damping based on the energy ratio criterion for evaluation of equivalent modal damping in composite elastic and inelastic structures,whereas Tsai (14) calculated the modal damping by matching the exact and normal modal solutions of the amplitude transfer function for a certain structure location. Bielak (11) assumed that the modal damping can be approximated based on some simplified soil-structure models and the appropriate soil properties.

Clough and Mojtahedi (15) concluded that the most efficient procedure, in case of non-proportional damping system, is to express the response in terms of undamped modal coordinates and to integrate directly the resulting coupled equations.

1-2d Parameters and Applications

The actual properties of the soil medium play the primary role in assessing the actual influence of soil-structure interaction on the structure response. Recently, Pandya and Setlur (16) have defined four cases which provide a range of soil properties useful for comparative analysis and subsequent generalization. It is the opinion of these authors that soil flexibility or compliance is the most important parameter in the soil-structure interaction phenomenon, and that a given flexibility can be realized by a non-unique combination of the basic parameters such as soil depth, shear modulus, etc.

Penzien (17) suggests a system of a non-linear spring and viscous dashpots to represent the soil for determing the properties. In this model, Penzien chooses a non-linear elastic spring with hysteresis characteristics to represent the immediate deformation characteristics of the soil structure under cyclic loading and a viscous dashpot in parallel with the spring, to represent the internal damping within the soil, while the creep behavior of the soil is represented by a viscous element in series with the spring-dashpot combination.

An evaluation of the effects of the foundation damping on the seismic response of simple building-foundation systems is presented by Veletsos and Nair (18). The supporting medium is modeled as a linear viscoelastic half

space. This study shows that a consideration of the effect of energy dissipation by hysteretic action in the soil is to increase the overall damping of the structure-foundation system and to reduce the deformation of the structure.

In the approach taken by Scanlan (19), the seismic wave effect is studied by generalizing the input function in the time domain so as to account for the travel time of the passing wave over the plan dimension of the structural foundation. His study is based on a rigid foundation-soil spring model and suggests that a passing earthquake may excite both lateral and rotational displacements even for a structure which is symmetrical in plan and properties. The study suggests an inherent self-diminishing feature to earthquake excitation relative to the particulars of a given design.

Akiyoshi (20) has proposed a new viscous boundary for shear waves in a one-dimensional discrete model that absorbs the whole energy of the wave traveling toward the boundary. Akiyoshi concluded that a mesh spacing less than one-sixth the wavelength of a sinusoidal wave should be used to obtain the allowable numerical solutions. The limitation of the proposed method is that it is restricted to the case of lumped mass-spring models.

The approaches and methods reviewed above have been applied to different types of structures. Reference was

made previously to three papers dealing with the nuclear containment structures, dams and multistory buildings (1, 2,3). The analysis of a tall chimney, including foundation interaction, for the effects of gusting wind, vortex shedding and earthquake is studied by Novak (10). This study shows that the general trend of the soil-structure interaction effects is to reduce the response to dynamic loads. The effect of embedment and the influence of internal damping is investigated by Kousel (21) for circular foundation on layered media. The case of two-dimensional rigid foundation of semi-elliptical cross-section is studied by Luco, Wong and Trifunac (22) to examine the effects of the embedment depth and the angle of incidence of the seismic waves on the response of the foundation. This study shows that rocking and torsional motion of the foundation is generated in addition to translation.

1-3 SCOPE AND AIM

The aim of the present investigation is to develop a more realistic mathematical model for the dynamic analysis of shells of revolution by including the soil effect as a new factor which should influence the dynamic behavior of such structures. With this proposed model, it is possible to study the effect of the soil condition on the dynamic response of large towers like reinforced concrete cooling towers. In addition to the seismic analysis capability of

the proposed model, it is also applicable to other dynamic loads like wind forces. This wide capability may provide better understanding to the dynamic behavior of the axisymmetric shells and shell-like structures.

A basic theoretical background is furnished in Chapter 2. In that chapter the wave propagation equations in the soil medium are presented and Hamilton's principle is specialized and adapted for the specific problem discussed in this report. The finite element formulation is presented along with the parametric studies concerning the soil model in Chapter 3. The basic formulations of the axisymmetric shell elements and the method of the analysis are given in Chapter 4. In Chapter 5, the seismic analysis of a cooling tower is presented and the results of free vibration, response spectrum, and time history analysis are discussed. Conclusions and recommendations for further investigations are presented in Chapter 6. In addition to this report, two companion volumes, a theoretical manual and a user's manual for the computer program which was developed in the course of this study, have been prepared. The program will be distributed through the NIS/EE, Berkeley, California.

2-Soil Model

2-1 Introduction

In the present chapter, the basic formulation for the wave propagation problem in a layered medium is presented for a general mode ($j \geq 0$). However, if one considers the foundation to be a rigid concentric ring footing, only the first two modes in the series are needed to describe the general motion of the footing acting on the free surface of a soil stratum. These are $j = 0$ for vertical and torsional excitation (axisymmetric modes), and $j = 1$ for rocking and swaying (antisymmetric modes). The soil model along with the connection problem are explained and discussed with respect to several parameters.

2-2 DISPLACEMENTS AND LOADS

Let any point in the soil medium be described by the coordinates r, z,θ as shown in Figure 1. In the cylindrical coordinate system, the displacements in the radial, vertical and tangential directions are denoted by u, w, θ, respectively, while the loads in these directions are denoted by P_r, P_z and P_θ. They can always be expressed in Fourier series by

$$u = \sum_{j=0}^{\infty} (\bar{u}_s^j \cos j\theta + \bar{u}_a^j \sin j\theta)$$

$$w = \sum_{j=0}^{\infty} (\bar{w}_s^j \cos j\theta + \bar{w}_a^j \sin j\theta)$$

$$v = \sum_{j=0}^{\infty} (-\bar{v}_s^j \sin j\theta + \bar{v}_a^j \cos j\theta) \qquad (2\text{-}1)$$

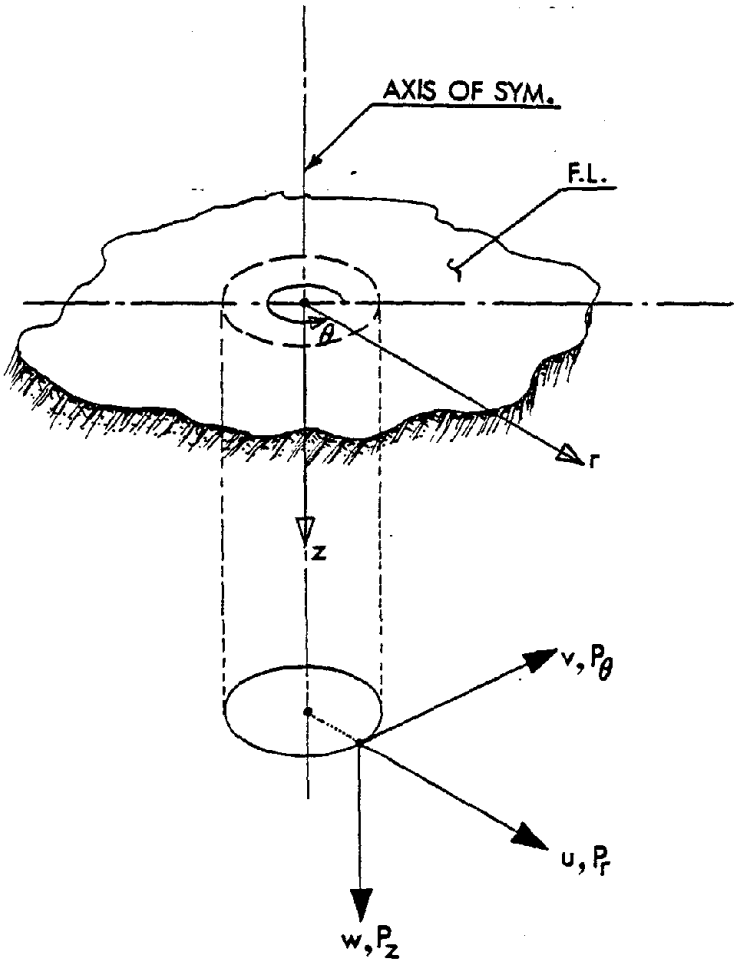

Figure 1. Coordinate System

and,

$$P_r = \sum_{j=0}^{\infty} (\bar{P}^j_{r_s} \cos j\theta + \bar{P}^j_{r_a} \sin j\theta)$$

$$P_z = \sum_{j=0}^{\infty} (\bar{P}^j_{z_s} \cos j\theta + \bar{P}^j_{z_a} \sin j\theta)$$

$$P_\theta = \sum_{j=0}^{\infty} (-\bar{P}^j_{\theta_s} \sin j\theta + \bar{P}^j_{\theta_a} \cos j\theta)$$

where the modal amplitudes with subscript s, a are referred to as the symmetric and antisymmetric displacement (load) components. Equations (2-1) may be rewritten in matrix form as

$$\begin{bmatrix} u \\ \hline w \\ \hline v \end{bmatrix} = \sum_{j=0}^{\infty} \begin{bmatrix} \bar{u}^j_s & \bar{u}^j_a \\ \hline \bar{w}^j_s & \bar{w}^j_a \\ \hline \bar{v}^j_a & -\bar{v}^j_s \end{bmatrix} \begin{bmatrix} \cos j\theta \\ \\ \sin j\theta \end{bmatrix} \qquad (2\text{-}2)$$

with similar expressions for the loads. An alternative notation could be

$$u = \sum_j \bar{u} e^{ij\theta}$$

$$w = \sum_j \bar{w} e^{ij\theta}$$

and

$$v = \sum_j \bar{v} e^{ij\theta} \qquad (2\text{-}3)$$

but since the modal amplitudes are complex for complex moduli, the latter notation is not advantageous.

The negative sign introduced in the sine term for the tangential components has the effect of yielding the same wave equations for both the symmetric and anti-symmetric components (same stiffness matrix in the finite element formulation).

The displacement vector of Equation (2-2) is written in partition form to separate the in-plane components (u,w) from the out-of-plane component (v). The modal displacement vector is then

$$u = \{\bar{u}_1 \vdots \bar{u}_2\} \tag{2-4}$$

where $\bar{u}_1 = \{\bar{u}, \bar{w}\}$

and $$\bar{u}_2 = \bar{v} \tag{2-5}$$

2-3 COMPATIBILITY EQUATIONS

The small strain and rotation-displacement relations expressed in cylindrical coordinates are

$$\begin{aligned} \varepsilon_{rr} &= \frac{\partial u}{\partial r} \\ \varepsilon_{zz} &= \frac{\partial w}{\partial z} \\ \varepsilon_{\theta\theta} &= \frac{u}{r} + \frac{1}{r}\frac{\partial v}{\partial \theta} \\ \gamma_{zr} &= \frac{\partial u}{\partial z} + \frac{\partial w}{\partial r} \end{aligned} \tag{2-6}$$

$$\gamma_{r\theta} = \frac{1}{r}\frac{\partial u}{\partial \theta} + \frac{\partial v}{\partial r} - \frac{v}{r}$$

$$\gamma_{\theta z} = \frac{\partial v}{\partial z} + \frac{1}{r}\frac{\partial w}{\partial \theta}$$

and the Fourier Expansions are

$$\begin{aligned}
\varepsilon_{rr} &= \sum_{j=0}^{\infty} (\bar{\varepsilon}^j_{rr_s} \cos j\theta + \bar{\varepsilon}^j_{rr_a} \sin j\theta) \\
\varepsilon_{zz} &= \sum_{j=0}^{\infty} (\bar{\varepsilon}^j_{zz_s} \cos j\theta + \bar{\varepsilon}^j_{zz_a} \sin j\theta) \\
\varepsilon_{\theta\theta} &= \sum_{j=0}^{\infty} (\bar{\varepsilon}^j_{\theta\theta_s} \cos j\xi + \bar{\varepsilon}^j_{\theta\theta_a} \sin j\theta) \\
\gamma_{zr} &= \sum_{j=0}^{\infty} (\bar{\gamma}^j_{zr_s} \cos j\theta + \bar{\gamma}^j_{zr_a} \sin j\theta) \\
\gamma_{r\theta} &= \sum_{j=0}^{\infty} (-\bar{\gamma}^j_{r\theta_s} \sin j\theta + \bar{\gamma}^j_{r\theta_a} \cos j\theta) \\
\gamma_{\theta z} &= \sum_{j=0}^{\infty} (-\bar{\gamma}^j_{\theta z_s} \sin j\theta + \bar{\gamma}^j_{\theta z_a} \cos j\theta)
\end{aligned} \tag{2-7}$$

where the modal amplitudes are related by

$$\begin{aligned}
\bar{\varepsilon}_{rr} &= \bar{u},r \\
\bar{\varepsilon}_{zz} &= \bar{w},z \\
\bar{\varepsilon}_{\theta\theta} &= \frac{1}{r}(\bar{u}-j\bar{v}) \\
\bar{\gamma}_{zr} &= \bar{u},_z + \bar{w},_r \\
\bar{\gamma}_{r\theta} &= \frac{1}{r}(j\bar{u}-\bar{v}+r\bar{v},_r) \\
\bar{\gamma}_{\theta z} &= j\bar{w}/r + v,z
\end{aligned} \tag{2-8}$$

The above equation may be expressed in matrix form as

$$\bar{\varepsilon} = A\bar{u} \tag{2-9}$$

where $\bar{\varepsilon} = \{\bar{\varepsilon}_{rr}, \bar{\varepsilon}_{zz}, \bar{\varepsilon}_{\theta\theta}, \bar{\gamma}_{zr} | \bar{\gamma}_{r\theta}, \bar{\gamma}_{\theta z}\}$ (2-10)

and A is the partitioned matrix operator

$$A = \left[\begin{array}{cc:c} \frac{\partial}{\partial r} & 0 & 0 \\ 0 & \frac{\partial}{\partial z} & 0 \\ \frac{1}{r} & 0 & -\frac{j}{r} \\ \frac{\partial}{\partial z} & \frac{\partial}{\partial r} & 0 \\ \hdashline \frac{j}{r} & 0 & r\frac{\partial}{\partial r}(\frac{1}{r}) \\ 0 & \frac{j}{r} & \frac{\partial}{\partial z} \end{array}\right] \tag{2-11}$$

It is convenient to write Equation (2-9) in the partitioned form

$$\left[\begin{array}{c} \bar{\varepsilon}_1 \\ \hline \bar{\varepsilon}_2 \end{array}\right] = \left[\begin{array}{c:c} A_{11} & jA_{12} \\ \hline jA_{21} & A_{22} \end{array}\right] \left[\begin{array}{c} \bar{u}_1 \\ \hline \bar{u}_2 \end{array}\right] \tag{2-12}$$

2-4 CONSTITUTIVE EQUATIONS

The stresses can be expanded in the same way as the strains and the modal components of stresses and strains are related by

$$\bar{\sigma} = D\bar{\varepsilon} \tag{2-13}$$

For cross-anisotropy, D(the constitutivity matrix) is restricted to be a function of r and z only. In the present study, only materials with properties not varying with θ will be considered. Matrix D for an isotropic material is given by

$$D = \left[\begin{array}{cccc|cc} \lambda+2\mu & \lambda & \lambda & 0 & & \\ \lambda & \lambda+2\mu & \lambda & 0 & \multicolumn{2}{c}{0} \\ \lambda & \lambda & \lambda+2\mu & 0 & & \\ 0 & 0 & 0 & \mu & & \\ \hline & & & & \mu & 0 \\ \multicolumn{4}{c|}{0} & 0 & \mu \end{array}\right]$$

$$= \left[\begin{array}{c|c} D_1 & 0 \\ \hline 0 & D_2 \end{array}\right] \tag{2-14}$$

where λ and μ are the Lamé constants (complex in general). They are related to Young's modulus, Poisson's ratio and shear modulus through

$$\lambda = \frac{\nu E}{(1+\nu)(1-2\nu)} = \frac{2\nu G}{1-2\nu}$$

$$\mu = \frac{E}{2(1+\nu)} = G \qquad (2\text{-}15)$$

The modal stresses is defined by

$$\bar{\sigma} = \{\bar{\sigma}_1 : \bar{\sigma}_2\}$$

where $$\bar{\sigma}_1 = \{\bar{\sigma}_{rr}, \bar{\sigma}_{zz}, \bar{\sigma}_{\theta\theta}\ \bar{\sigma}_{zr}\} \qquad (2\text{-}16)$$

and $$\bar{\sigma}_2 = \{\bar{\sigma}_{r\theta}, \bar{\sigma}_{\theta z}\}$$

while the true stresses are given by

$$\sigma_1 = \sum_{j=0}^{\infty} (\bar{\sigma}_{1s}^{j}\ \bar{\sigma}_{1a}^{j}) \begin{bmatrix} \cos j\theta \\ \sin j\theta \end{bmatrix}$$

$$\sigma_2 = \sum_{j=0}^{\infty} (\bar{\sigma}_{2s}^{j}\ \bar{\sigma}_{2a}^{j}) \begin{bmatrix} -\sin j\theta \\ \cos j\theta \end{bmatrix} \qquad (2\text{-}17)$$

The partitioning of this matrix into the submatrices D_1 and D_2 is consistent with that of the stresses and strains, and it follows that

$$\bar{\sigma}_1 = D_1\ \bar{\varepsilon}_1$$

$$\bar{\sigma}_2 = D_2\ \bar{\varepsilon}_2 \qquad (2\text{-}18)$$

2-5 WAVE EQUATIONS

The general equations of wave propagation expressed in cylindrical coordinates are (27)

$$\ddot{u} = \frac{1}{\rho}[(\lambda+2\mu)\frac{\partial\Delta}{\partial r} - \frac{\mu}{r}\frac{\partial}{\partial\theta}(\frac{\partial}{\partial r}(rv) - \frac{\partial u}{\partial\theta}) + \mu\frac{\partial}{\partial z}(\frac{\partial u}{\partial z} - \frac{\partial w}{\partial r})]$$

$$\ddot{w} = \frac{1}{\rho}[(\lambda+2\mu)\frac{\partial\Delta}{\partial z} - \frac{\mu}{r}\frac{\partial}{\partial r}r(\frac{\partial u}{\partial z} - \frac{\partial w}{\partial r}) + \frac{\mu}{r}\frac{\partial}{\partial\theta}(\frac{\partial w}{r\partial\theta} - \frac{\partial v}{\partial z})]$$

$$\ddot{v} = \frac{1}{\rho}[(\lambda+2\mu)\frac{1}{r}\frac{\partial\Delta}{\partial\theta} - \mu\frac{\partial}{\partial z}(\frac{1}{r}\frac{\partial w}{\partial\theta} - \frac{\partial v}{\partial z}) + \mu\frac{\partial}{\partial r}(\frac{\partial}{\partial r}(rv) - \frac{\partial u}{\partial\theta})] \qquad (2\text{-}19)$$

where

$$\Delta = \text{volumetric change}$$

$$= \varepsilon_{rr} + \varepsilon_{zz} + \varepsilon_{\theta\theta}$$

$$= -\frac{1}{r}\frac{\partial(ru)}{\partial r} + \frac{\partial w}{\partial z} + \frac{1}{r}\frac{\partial v}{\partial\theta} \qquad (2\text{-}20)$$

For harmonic excitations with frequency Ω, the modal Fourier expansion of Equation (2-19) can be expressed by

$$\sum_{j=0}^{\infty}\bar{u}\begin{bmatrix}\cos j\theta\\ \sin j\theta\end{bmatrix} = \frac{-1}{\rho\Omega^2}\sum_{j=0}^{\infty}[(\lambda+2\mu)\frac{\partial}{\partial r}(\frac{\bar{u}}{r} + \frac{\partial\bar{u}}{\partial r} - \frac{j}{r}\bar{v} + \frac{\partial\bar{w}}{\partial z}) + \frac{\mu j}{r}(\frac{j\bar{w}}{r} - \frac{\partial\bar{v}}{\partial z}) + \mu\frac{\partial}{\partial z}(\frac{1}{r}\frac{\partial(r\bar{v})}{\partial r} - \frac{j\bar{u}}{r})]\begin{bmatrix}\cos j\theta\\ \sin j\theta\end{bmatrix}$$

$$\sum_{j=0}^{\infty}\bar{w}\begin{bmatrix}\cos j\theta\\ \sin j\theta\end{bmatrix} = \frac{-1}{\rho\Omega^2}\sum_{j=0}^{\infty}[(\lambda+2\mu)\frac{\partial}{\partial z}(\frac{\bar{u}}{r} + \frac{\partial\bar{u}}{\partial r} - \frac{j}{r}\bar{v} + \frac{\partial\bar{w}}{\partial z}) - \frac{\mu}{r}\frac{\partial}{\partial r}(\frac{\partial(r\bar{v})}{\partial r} - j\bar{u}) - \frac{\mu j}{r}(\frac{j}{r}\bar{w} - \frac{\partial\bar{v}}{\partial z})]\begin{bmatrix}\cos j\theta\\ \sin j\theta\end{bmatrix}$$

$$\sum_{j=0}^{\infty} \bar{v} \begin{bmatrix} -\sin j\theta \\ \cos j\theta \end{bmatrix} = \frac{-1}{\rho\Omega^2} \sum_{j=0}^{\infty} [(\lambda+2\mu)\ \frac{j}{r}(\frac{\bar{u}}{r} + \frac{\partial \bar{u}}{\partial r} - \frac{j\bar{v}}{r} + \frac{\partial \bar{w}}{\partial z}) - \mu\frac{\partial}{\partial z}(\frac{j\bar{w}}{r} - \frac{\partial \bar{v}}{\partial z}) + \mu\ \frac{\partial}{\partial r}(\frac{\partial \bar{u}}{\partial z} - \frac{\partial \bar{w}}{\partial r})] \begin{bmatrix} -\sin j\theta \\ \cos j\theta \end{bmatrix}$$

(2-21)

For an arbitrary j, it follows that

$$\bar{u} = \frac{-1}{\rho\Omega^2} [(\lambda+2\mu)\frac{\partial}{\partial r}(\frac{\bar{u}}{r} + \frac{\partial \bar{u}}{\partial r} - \frac{j}{r}\bar{v} + \frac{\partial \bar{w}}{\partial z}) + \mu\ \frac{j}{r}(\frac{\partial \bar{u}}{\partial z} - \frac{\partial \bar{w}}{\partial r}) + \frac{\mu}{r}\frac{\partial}{\partial z}\ (\frac{\partial (r\bar{v})}{\partial r} - j\bar{u})]$$

$$\bar{w} = \frac{-1}{\rho\Omega^2} [(\lambda+2\mu)\frac{\partial}{\partial z}(\frac{\bar{u}}{r} + \frac{\partial \bar{u}}{\partial r} - \frac{j}{r}\bar{v} + \frac{\partial \bar{w}}{\partial z}) - \frac{\mu}{r}\frac{\partial}{\partial r}\ (\frac{\partial (r\bar{v})}{\partial r} - j\bar{u}) - \frac{\mu j}{r}\ (\frac{j}{r}\bar{w} - \frac{\partial \bar{v}}{\partial z})]$$

$$\bar{v} = \frac{-1}{\rho\Omega^2} [(\lambda+2\mu)\frac{j}{r}(\frac{\bar{u}}{r} + \frac{\partial \bar{u}}{\partial r} - \frac{j\bar{v}}{r} + \frac{\partial \bar{w}}{\partial z}) - \mu\ \frac{\partial}{\partial z}(\frac{j}{r}\bar{w} - \frac{\partial \bar{v}}{\partial z}) + \mu\ \frac{\partial}{\partial r}(\frac{\partial \bar{u}}{\partial z} - \frac{\partial \bar{w}}{\partial r})]$$

(2-22)

which shall be called the Modal Wave Equations (MWE). They are only functions of r and z, with the parameter j = 0, 1, 2,...dependent on the Fourier decomposition of the loadings or prescribed displacements. The general solution of MWE is (28)

$$\bar{u} = e^{i\Omega t}\left[(kAe^{-\ell z} - mCe^{-mz})\frac{\partial H_j^{(2)}(kr)}{\partial r} + \frac{j}{r} B H_j^{(2)}(kr) e^{-mz}\right]$$

$$\bar{w} = e^{i\Omega t}\left[(Cke^{-mz} - \ell Ae^{-\ell z}) k H_j^{(2)}(kr)\right]$$

$$\bar{v} = e^{i\Omega t}\left[(kAe^{-\ell z} - mCe^{-mz})\frac{j}{r} H_j^{(2)}(kr) + B \frac{\partial H_j^{(2)}(kr)}{\partial r} e^{-mz}\right]$$

(2-23)

in which $H_j^{(2)}(kr)$ are second Hankel functions of order j (order of Fourier component), A, B, C are integration constants, k is an arbitrary parameter (wave number), and

$$\ell = \pm \sqrt{k^2 - \frac{\Omega^2}{v_p^2}}$$

$$m = \pm \sqrt{k^2 - \frac{\Omega^2}{v_s^2}} \qquad (2\text{-}24)$$

and

$$\frac{1}{v_p} = \sqrt{\frac{\rho}{\lambda+2\mu}}$$

$$\frac{1}{v_s} = \sqrt{\frac{\rho}{\mu}}$$

where v_p and v_s are the compression and shear wave velocities, respectively.

In the particular solutions given by (2-23), analagous expressions containing first Hankel functions $H_j^{(1)}(kr)$ have been omitted, since they correspond, in combination with the factor $e^{i\Omega t}$, to waves travelling from infinity towards the origin and thus must be disregarded in accordance with Sommerfeld's radiation principle (29). (Sources confined to the vicinty of the origin). For this reason, the index (2) and the argument (kr) in the Hankel functions will be dropped.

The solution of the modal wave equations may be written as

$$\bar{u} = e^{i\Omega t}(f_1(z)H_j' + f_3(z)\frac{j}{r}H_j)$$

$$\bar{w} = kf_2(z)H_j\, e^{i\Omega t} \qquad (2\text{-}25)$$

$$\bar{v} = e^{i\Omega t}(f_1(z)\frac{j}{r}H_j + f_3(z)H_j')$$

where $H_j' = \frac{\partial}{\partial r} H_j^{(2)}(kr)$

and

$$\begin{aligned} f_1(z) &= kAe^{-\ell z} - mCe^{-mz} \\ f_2(z) &= kCe^{-mz} - \ell Ae^{-\ell z} \\ f_3(z) &= Be^{-mz} \end{aligned} \qquad (2\text{-}26)$$

Dropping the time dependent term $e^{i\Omega t}$ from (2-25) together with (2-26) one gets

$$\bar{Y} = HF \tag{2-27}$$

where $\bar{Y}$ is the modal displacement without the time dependent term, and

$$F = \{f_1, f_2, f_3\}$$

and

$$H = \begin{bmatrix} H_j' & 0 & \frac{j}{r} H_j \\ 0 & kH_j & 0 \\ \frac{j}{r} H_j & 0 & H_j' \end{bmatrix} \tag{2-28}$$

In the above equation F is only a function of z while H is a function of r and the harmonic number j.

Also, expressions for the strains and stresses in terms of the functions f_i will be needed later. Substituting (2-27) into (2-8) results in

$$\bar{\varepsilon}_{rr} = f_1 H_j'' + f_3 \frac{j}{r} \left(H_j' - \frac{H_j}{r}\right)$$

$$\bar{\varepsilon}_{zz} = f_2' \cdot k \cdot H_j$$

$$\bar{\varepsilon}_{\theta\theta} = f_1\left(\frac{H_j'}{r} - \frac{j^2}{r^2} H_j\right) + f_3 \frac{j}{r}\left(\frac{H_j}{r} - H_j'\right)$$

$$\bar{\gamma}_{zr} = f_1' H_j' + f_2 k H_j' + f_3' \frac{j}{r} H_j \qquad (2\text{-}29)$$

$$\bar{\gamma}_{r\theta} = f_1 \frac{j}{r}\left(2H_j' - \frac{H_j}{r}\right) + f_3\left(\frac{j^2}{r^2} H_j - \frac{1}{r} H_j' + H_j''\right)$$

$$\bar{\gamma}_{\theta z} = f_1' \frac{j}{r} H_j + f_2 k \frac{j}{r} H_j + f_3' H_j'$$

and with

$$\bar{\Phi} = (f_2' - k f_1) k H_j \qquad (2\text{-}30)$$

the stresses follow as

$$\begin{aligned}
\bar{\sigma}_{rr} &= 2\mu\varepsilon_{rr} + \lambda\bar{\Phi} \\
\bar{\sigma}_{zz} &= 2\mu\varepsilon_{zz} + \lambda\bar{\Phi} \\
\bar{\sigma}_{\theta\theta} &= 2\mu\varepsilon_{\theta\theta} + \lambda\bar{\Phi} \\
\bar{\sigma}_{zr} &= \mu\gamma_{zr} \\
\bar{\sigma}_{r\theta} &= \mu\gamma_{r\theta} \\
\bar{\sigma}_{\theta z} &= \mu\gamma_{\theta z}
\end{aligned} \qquad (2\text{-}31)$$

The modal wave equations (2-22) may be expressed in matrix form using Equations (2-25) through (2-28) as

$$H \cdot Z = 0 \qquad (2\text{-}32)$$

where H is given by (2-28) and Z is a vector depends only on z

$$Z = \begin{bmatrix} z_1 \\ z_2 \\ z_3 \end{bmatrix} = \begin{bmatrix} (\lambda+2\mu)(kf_2'-k^2f_1)+\mu(f_1''-kf_2')+\rho\Omega^2 f_1 \\ (\lambda+2\mu)(f_2''-kf_1')+\mu k(f_1'-kf_2)+\rho\Omega^2 f_2 \\ \mu(f_3''-k^2f_3)+\rho\Omega^2 f_3 \end{bmatrix} \quad (2\text{-}33)$$

The above form of MWE is suitable for the finite element formulations as we will discuss later.

2-6 PRINCIPLE OF VIRTUAL DISPLACEMENTS

In dynamics, the generalization of the principle of virtual displacements into a law of kinetics by use of D'Aambert's principle is referred to as Hamilton's principle. For conservative systems, the principle states that the work performed by the applied external loads and inertial forces during an arbitrary virtual displacement field that is consistent with the constraints is equal to the change in strain energy plus the energy dissipated by internal friction during that virtual displacement.

Hamilton's principle shall be specialized and adapted for the specific problem discussed in this report in which the coordinate system is cylindrical, and the viscoelastic constants are complex. By applying two Fourier transformations, one in the time domain, and one in the θ

coordinate, the principle of virtual displacements for axisymmetric systems subjected to a general harmonic excitation shall be developed.

A general form of Hamilton's principle in elasticity is

$$\int_{t_0}^{t_1}\left[\int_V \delta\varepsilon_{ij}\sigma_{ij}dV - \int_V \delta u_i(b_i-\rho\ddot{u}_i)dV - \int_S \delta u_i p_i dA\right]dt = 0 \tag{2-34}$$

where $\delta\varepsilon_{ij}$ is the virtual strain field corresponding to the displacement field δu_i which is consistent with the constraints and vanishes at the time t_0 and t_1. The term $\delta\varepsilon_{ij}\ \sigma_{ij}$ represents the change in strain energy as well as the energy lost due to internal friction. S corresponds to that portion of the boundary where the forces are prescribed.

Since the prescribed virtual displacements are arbitrary, a set of displacements can be chosen of the form

$$\left.\begin{aligned}\delta u_i(x,t) &= \delta\tilde{u}_i(x)\cdot\delta(t)\\ \delta\varepsilon_{ij}(x,t) &= \delta\tilde{\varepsilon}_{ij}(x)\cdot\delta(t)\end{aligned}\right\} \quad t_0 \leq t \leq t_1 \tag{2-35}$$

where x stands for the coordinate system,

$$x = (x_1,\ x_2,\ x_3) \tag{2-36}$$

and $\delta(t)$ is the Dirac delta function. Substitution in (2-34) and integration over the time domain yields

$$\int_V \delta\tilde{\varepsilon}_{ij}\sigma_{ij}\, dV - \int_V \delta\tilde{u}_i(b_i-\rho\ddot{u}_i)dV - \int_S \delta\tilde{u}_i\, p_i dA = 0 \qquad (2\text{-}37)$$

where σ_{ij}, b_i, u_i and p_i are evaluated at the time t.

Alternatively, it is possible to arrive at this result starting from the equilibrium equations (wave equation) and the boundary force equations, and constraining the time variable to remain constant while the virtual displacements are applied, that is, the real motion is stopped while the virtual displacements are performed; however, the inertial forces must be assumed to persist. In other words, it is assumed that the performance of the virtual displacements consumes no time (30).

Applying a Fourier transformation (FT) to (2-37) and defining

$$\tilde{\sigma}_{ij}(\Omega) = FT(\sigma_{ij}(t)),\ \tilde{b}_i(\Omega) = FT(b_i(t)),\ \tilde{p}_i(\Omega) = FT(p_i(t)),$$

$$\tilde{u}_i(\Omega) = FT(u_i(t)),\ -\Omega^2\tilde{u}_i(\Omega) = FT(\ddot{u}_i(t)) \qquad (2\text{-}38)$$

yields

$$\int_V \delta\tilde{\varepsilon}_{ij}\tilde{\sigma}_{ij}\, dV - \int_V \delta\tilde{u}_i(\tilde{b}_i+\rho\Omega^2\tilde{u}_i)dV - \int_S \tilde{p}_i\, \delta\tilde{u}_i dA = 0 \tag{2-39}$$

where the transformed quantities are in general complex.

For real elastic moduli, the stresses will be real and in phase with the strains and displacements whereas, for complex moduli, they will be complex and there will be a phase lag between these two quantities. The relation between the transformed stresses $\tilde{\sigma}_{ij}$ and strains $\tilde{\varepsilon}_{ij}$ is given by equation (2-13).

An alternate form of equation (2-39) is obtained using integration by parts, resulting in

$$\int_V \delta\tilde{u}_i(\tilde{\sigma}_{ij,j} + \tilde{b}_i + \rho\Omega^2\tilde{u}_i)dV + \int_S \delta\tilde{u}_i(\tilde{p}_i - n_j\tilde{\sigma}_{ij})dA = 0 \tag{2-40}$$

which, for arbitrary variations of the virtual displacements δu_i yields the body and boundary equilibrium equations. Using the stress-strain relation, the term in parenthesis in the first integral becomes the wave equation, which shall be useful later on. Switching now from tensor to matrix notation and dropping the superscript $\sim$ with the implicit understanding that the applied forces (displacements) are harmonic, equation (2-39) becomes

$$\int_V \delta\varepsilon^T \sigma dV - \int_V \delta u^T (b+\rho\Omega^2 u) dV - \int_S \delta u^T p dA = 0 \qquad (2\text{-}41)$$

For a cylindrically orthotropic (cross anisotropic) material, integration w/r to θ, with $dV = rdrd\theta dz$, and using

$$\int_0^{2\Pi} \sin m\theta \sin n\theta \, d\theta = (\delta_{mn} - \delta_{m\theta}\,\delta_{n\theta})\Pi = \begin{cases} \Pi & \text{for } m=n\neq 0 \\ 0 & \text{otherwise} \end{cases}$$

$$\int_0^{2\Pi} \cos m\theta \cos n\theta \, d\theta = (\delta_{mn} + \delta_{m\theta}\delta_{n\theta})\Pi = \begin{cases} \Pi & \text{for } m=n\neq 0 \\ 2\Pi & \text{for } m=n=0 \\ 0 & \text{otherwise} \end{cases}$$

$$\int_0^{2\Pi} \sin m\theta \cos n\theta \, d\theta = 0 \qquad \text{for any values of m and n}$$

yields for the principle of virtual displacements

$$\iint \delta\bar{\varepsilon}^T D \bar{\varepsilon} \, rdrdz - \iint \rho\Omega^2 \, \delta\bar{u}^T \bar{u} rdrdz$$

$$= \int_S \delta\bar{u}^T \bar{p} rds \qquad (2\text{-}42)$$

where the superscript bar refers to the Fourier modal amplitude. Similarly, by substituting Equation (2-32) into Equation (2-40), we find

$$\iint \delta\bar{u}^T \cdot H \cdot Z \cdot rdrdz + \int \delta\bar{u}^T (\bar{p} - \bar{\sigma}^*) rds = 0 \qquad (2\text{-}43)$$

where $\bar{\sigma}^* = \{n_j \bar{\sigma}_{ij}\}$ are the projection of the modal stresses on the unit outward boundary normal nj

$H \cdot Z =$ the modal wave equation (2-32).

Equation (2-43) is preferable to equation (2-42) or (2-41) when using the principle of virtual displacements to define the eigenvalue problem for the viscoelastic energy absorbing boundary since it does not require a cumbersome integration of products of the Hankel functions over the coordinate r.

3. FINITE ELEMENT FORMULATION

3-1 INTRODUCTION

Numerical techniques have been used successfully in the stress analysis of many complex structures. In particular, the finite element technique has been the major tool for analyzing different types of structures such as solids of revolution and shells of revolution. These two classes of structures are of special importance in modelling the axisymmetric shell-soil system. The use of highly efficient rotational shell finite elements to model the superstructure suggested that the soil medium be represented in a similar manner. A main problem in this case is to account for the proper boundary conditions at the edges of a finite domain which will not introduce undesirable reflections of waves into the region of interest. A possible solution is to place the boundaries at a substantial distance from the footing if there is internal dissipation of energy in the soil. This approach requires a very large number of elements and is therefore expensive.

This chapter presents the finite element model used to represent the soil medium where axisymmetrical isoparametric quadratic solid elements with transmitting vertical boundaries placed directly at the outer edge of the structure

are employed (Figure 2). With the energy transmitting boundary, the finite element region is reduced to minimum, resulting in a high order sophisticated model with comparatively few elements as has been the continuing objective in previous investigations at Washington University. The formulation of the rotational shell elements is presented elsewhere (2, 3).

3-2 SOLID ELEMENT FORMULATION

The core region of Figure 2 is modelled by means of axisymmetric isoparametric quadratic solid elements. For each nodal circle there are three degrees-of-freedom; two of them are in-plane, u and w, while the third, v, is out-of-plane. These in-plane and out-of-plane degrees-of-freedom are separated in the formulations of the element stiffness and mass matrices. The name "isoparametric" derives from use of the same interpolation functions to define the element shape as are used to define the displacements within the element.

If ϕ denotes the expansion vector for the isoparametric formulation,

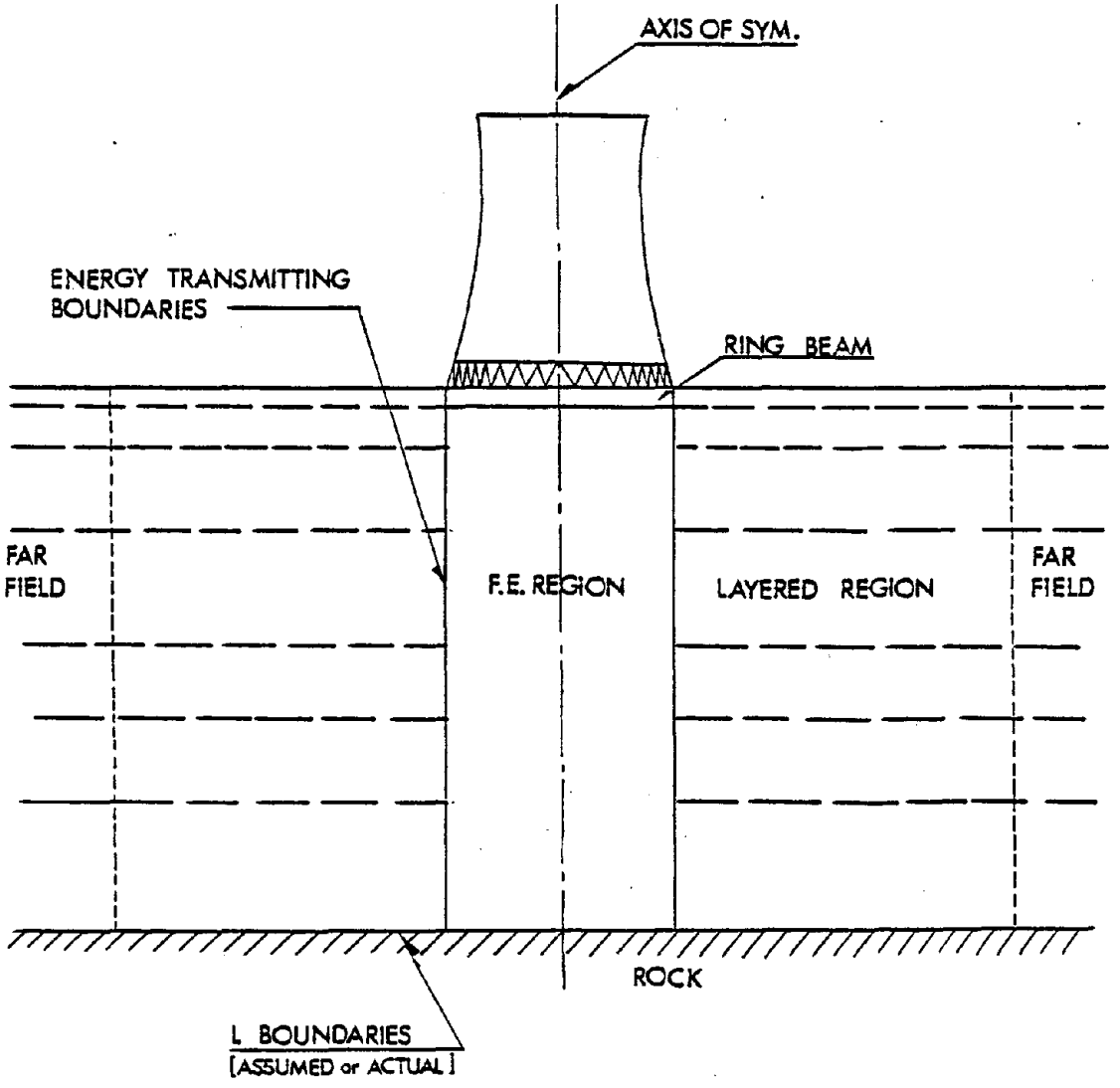

Figure 2. Finite Element Model for the Soil Medium

$$r = \sum_{i=1}^{n} \phi_i r_i$$

$$z = \sum_{i=1}^{n} \phi_i z_i \qquad (3\text{-}1)$$

where n = number of nodes per element.

In vector notation

$$r = \phi^T r_o$$

$$z = \phi^T z_o \qquad (3\text{-}2)$$

where $r_o^T = \{r_1, r_2, \ldots r_n\}$

$$z_o^T = \{z_1, z_2, \ldots z_n\} \qquad (3\text{-}3)$$

Using the same expansions for the displacements,

$$u = \Phi^T u_o \qquad (3\text{-}4)$$

where

$$u = \begin{bmatrix} \bar{u} \\ \bar{w} \\ \bar{v} \end{bmatrix}, \quad u_o^T = \{\bar{u}_1, \bar{u}_2, \ldots, \bar{u}_n, \bar{w}_1, \bar{w}_2, \ldots, \bar{w}_n, \bar{v}_1, \bar{v}_2, \ldots, \bar{v}_n\}$$

and $$\Phi^T = \begin{bmatrix} \phi^T & 0 & \\ & \phi^T & \\ 0 & & \phi^T \end{bmatrix} \qquad (3\text{-}5)$$

In equation (3-4), Φ^T is called the expansion matrix. From (2-10) and (3-4), one can write

$$\begin{bmatrix} \bar{\varepsilon}_1 \\ 4\times 1 \\ \hline \bar{\varepsilon}_2 \\ 2\times 1 \end{bmatrix}_{6\times 1} = \left[\begin{array}{c|c} A_{11} & A_{12} \\ 4\times 2 & 4\times 1 \\ \hline A_{21} & A_{22} \\ 2\times 2 & 2\times 1 \end{array}\right]_{6\times 3} \begin{bmatrix} \phi^T & & \\ & \phi^T & \\ & & \phi^T \end{bmatrix}_{3\times 3n} \begin{bmatrix} \bar{u}_1 \\ \bar{u}_2 \\ \vdots \\ \bar{u}_n \\ \bar{w}_1 \\ \bar{w}_2 \\ \vdots \\ \bar{w}_n \\ \hline \bar{v}_1 \\ \bar{v}_2 \\ \vdots \\ \bar{v}_n \end{bmatrix}_{3n\times 1} \tag{3-6}$$

or $\bar{\varepsilon} = B\, u_o$

$$\text{where } B = \left[\begin{array}{c|c} b_{11} & b_{12} \\ 4\times 2n & 4\times n \\ \hline b_{21} & b_{22} \\ 2\times 2n & 2\times n \end{array}\right]_{6\times 3n} \tag{3-7}$$

Substitution into equation (2-42) gives

$$\sum_{\text{elements}} \delta u_o^T \{\int\int (B^T D B - \rho\Omega^2 \Phi\Phi^T) u_o r\,dr\,dz - \int \Phi \bar{p} r\,ds\} = 0 \tag{3-8}$$

For the k<u>th</u> element, the consistent mass matrix M_k, the stiffness matrix K_k and the load vector P_k are defined as:

$$M_k = \int\int \rho \Phi \Phi^T \, r dr dz$$
$$K_k = \int\int B^T D B \, r dr dz \qquad (3\text{-}9)$$
$$P_k = \int \Phi \bar{P} \, r ds$$

3-2a Isoparametric Formulations

For quadratic elements, the total number of nodes per element n is equal to eight and the shape functions $\phi_i = g_i$ (i=1,...,8) may be chosen as functions of the dimensionless coordinates ξ and η. In Table 1 the expressions for g_i, $g_{i,\xi}$ and $g_{i,\eta}$ are given.

The Jacobian is defined by

$$Jac = \begin{bmatrix} g_{1,\xi} & g_{2,\xi} & g_{3,\xi} & g_{4,\xi} & g_{5,\xi} & g_{6,\xi} & g_{7,\xi} & g_{8,\xi} \\ g_{1,\eta} & g_{2,\eta} & g_{3,\eta} & g_{4,\eta} & g_{5,\eta} & g_{6,\eta} & g_{7,\eta} & g_{8,\eta} \end{bmatrix} \begin{bmatrix} r_1 & z_1 \\ r_2 & z_2 \\ r_3 & z_3 \\ r_4 & z_4 \\ r_5 & z_5 \\ r_6 & z_6 \\ r_7 & z_7 \\ r_8 & z_8 \end{bmatrix}$$

$$\text{or } Jac = \begin{bmatrix} \sum_{i=1}^{8} g_{i,\xi} r_i & \sum_{i=1}^{8} g_{i,\xi} z_i \\ \sum_{i=1}^{8} g_{i,\eta} r_i & \sum_{i=1}^{8} g_{i,\eta} z_i \end{bmatrix} \qquad (3\text{-}10)$$

The inverse of the Jacobian IJ is, then, given by

$$IJ = \begin{bmatrix} IJ_{11} & IJ_{12} \\ IJ_{21} & IJ_{22} \end{bmatrix}$$

Table 1. Shape Functions and First Derivatives for Expansion Vector

i	g_i	$g_{i,\xi}$	$g_{i,\eta}$
1	$-\frac{1}{4}(1-\xi)(1-\eta)(1+\xi+\eta)$	$\frac{1}{4}(1-\eta)(2\xi+\eta)$	$\frac{1}{4}(1-\xi)(2\eta+\xi)$
2	$\frac{1}{2}(1-\xi^2)(1-\eta)$	$-\xi(1-\eta)$	$-\frac{1}{2}(1-\xi^2)$
3	$\frac{1}{4}(1+\xi)(1-\eta)(\xi-\eta-1)$	$\frac{1}{4}(1-\eta)(2\xi-\eta)$	$\frac{1}{4}(1+\xi)(2\eta-\xi)$
4	$\frac{1}{2}(1+\xi)(1-\eta^2)$	$\frac{1}{2}(1-\eta^2)$	$-\eta(1+\xi)$
5	$\frac{1}{4}(1+\xi)(1+\eta)(\xi+\eta-1)$	$\frac{1}{4}(1+\eta)(2\xi+\eta)$	$\frac{1}{4}(1+\xi)(2\eta+\xi)$
6	$\frac{1}{2}(1-\xi^2)(1+\eta)$	$-\xi(1+\eta)$	$\frac{1}{2}(1-\xi^2)$
7	$\frac{1}{4}(1-\xi)(1+\eta)(\eta-\xi-1)$	$\frac{1}{4}(1+\eta)(2\xi-\eta)$	$\frac{1}{4}(1-\xi)(2\eta-\xi)$
8	$\frac{1}{2}(1-\xi)(1-\eta^2)$	$-\frac{1}{2}(1-\eta^2)$	$-\eta(1-\xi)$

where
$$IJ_{11} = \left(\sum_{i=1}^{8} g_{i,\eta} z_i\right) / |Jac|$$
$$IJ_{12} = -\left(\sum_{i=1}^{8} g_{i,\xi} z_i\right) / |Jac|$$
$$IJ_{21} = -\left(\sum_{i=1}^{8} g_{i,\eta} r_i\right) / |Jac| \qquad (3\text{-}11)$$
and
$$IJ_{22} = \left(\sum_{i=1}^{8} g_{i,\xi} r_i\right) / |Jac|$$

where $|Jac|$ is the determinant of the Jacobian matrix of equation (3-10). The inverse of the Jacobian is necessary for the transformation from r-z coordinates to ξ-η natural coordinates,

$$( )_{,r} = IJ_{11} \cdot ( )_{,\xi} + IJ_{12} \cdot ( )_{,\eta}$$
$$( )_{,z} = IJ_{21} \cdot ( )_{,\xi} + IJ_{22} \cdot ( )_{,\eta} \qquad (3\text{-}12)$$

3-2b Element Mass and Stiffness Matrices

Using partitioned form of the B, D and Φ matrices we get:

$$M_k = \begin{bmatrix} m & 0 & 0 \\ 0 & m & 0 \\ 0 & 0 & m \end{bmatrix}_{24\times 24}$$

where $m_{8\times 8} = \int\int \rho\phi\phi^T \, r dr dz$ (3-13)

and $K_k = \left[\begin{array}{c|c} K_1 & K_2 \\ \hline K_2^T & K_3 \end{array}\right]_{24\times 24}$

where $K_1 = \int\int (b_{11}^T D_1 b_{11} + b_{21}^T D_2 b_{21}) r dr dz$

$K_2 = \int\int (b_{11}^T D_1 b_{12} + b_{21}^T D_2 b_{22}) r dr dz$

$K_3 = \int\int (b_{22}^T D_2 b_{22} + b_{12}^T D_1 b_{12}) r dr dz$ (3-14)

From (3-7), the submatrices b_{11}, b_{12}, b_{21} and b_{22} are given by (See Appendix I).

$$b_{11} = \begin{bmatrix} g_{1,r} & g_{2,r} \cdots\cdots g_{8,r} & 0 & 0 \cdots\cdots 0 \\ 0 & 0 \cdots\cdots 0 & g_{1,z} & g_{2,z} \cdots g_{8,z} \\ g_{1/r} & g_{2/r} \cdots\cdots g_{8/r} & 0 & 0 \cdots\cdots 0 \\ g_{1,z} & g_{2,z} \cdots\cdots g_{8,z} & g_{1,r} & g_{2,r} \cdots g_{8,4} \end{bmatrix}_{4\times 16} \quad (3\text{-}15\text{-}a)$$

$$b_{12} = \frac{-j}{r} \begin{bmatrix} 0 & 0.....0 \\ 0 & 0.....0 \\ g_1 & g_2.....g_8 \\ 0 & 0.....0 \end{bmatrix}_{4\times 8} \qquad (3\text{-}15\text{-}b)$$

$$b_{21} = \frac{j}{r} \begin{bmatrix} g_1 & g_2.....g_8 & 0 & 0.....0 \\ 0 & 0.....0 & g_1 & g_2.....g_8 \end{bmatrix}_{2\times 16} \qquad (3\text{-}15\text{-}c)$$

$$b_{22} = \begin{bmatrix} r\frac{\partial}{\partial r}(g_1/r) & r\frac{\partial}{\partial r}(g_2/r)....r\frac{\partial}{\partial r}(g_8/r) \\ g_{1,z} & g_{2,z}.....g_{8,z} \end{bmatrix}_{2\times 8} \qquad (3\text{-}15\text{-}d)$$

and $\phi\phi^T$ is given by:

$$\phi\phi^T = \begin{bmatrix} g_1^2 & g_1g_2 & g_1g_3....g_1g_8 \\ g_2g_1 & g_2^2 & g_2g_3 & g_2g_8 \\ g_3g_1 & g_3g_2 & g_3^2.....g_3g_8 \\ \vdots & \vdots & \vdots & \vdots \\ g_8g_1 & g_8g_2 & g_8g_3.... g_8^2 \end{bmatrix}_{8\times 8} \qquad (3\text{-}16)$$

With RG defined as

$$RG = \sum_{i=1}^{8} g_i r_i \tag{3-17}$$

$$\text{and } \int\int (\ )\,r\,dr\,dz = \int_{-1}^{1}\int_{-1}^{1} (\ )\,RG \det Jac\, d\xi\, d\eta \tag{3-18}$$

the mass matrix M_k and the stiffness matrix K_k are obtained for a general Fourier harmonic j; however, M_k is independent of j as one can see from equations (3-13) and (3-16).

The integration in each element is carried out by means of four points Gaussian integration with the dimensionless coordinates ξ, η. Since in the Gaussian quadrature scheme, there are no points on the boundary of the elements, no problems are encountered with the singularity of the integrand of the symmetry axis (r=0) for those elements adjacent to it.

The details of the isoparametric formulation for the element stiffness matrix is presented in Appendix I.

3-3 THE BOUNDARIES

It is assumed that the finite element region has a fixed lower boundary, which may be true if we are dealing with a stratum over rock of infinite horizontal extent. The lower boundary location factor will be studied in case of a deep stratum or half space.

Now, for the total mass matrix M, total stiffness matrix K, and the total load vector P we have the following equation

$$(K - \Omega^2 M)u = P \qquad (3\text{-}19)$$

where u stands for the total nodal displacements.

The above equation needs to be modified to include the effect of the far field on the stiffness of the core region. This can be achieved by considering the equilibrium of the vertical boundaries of the core region. If the core region of Figure 2 is removed and replaced by equivalent distributed forces corresponding to the internal stresses, the dynamic equilibrium of the far-field will be preserved. Since no other prescribed forces act on the far-field, the displacements at the boundary and at any other point in the far-field will be uniquely defined in terms of these boundary forces. The relation between these boundary forces and the corresponding boundary displacements is the dynamic boundary matrix to be added to the total dynamic stiffness matrix of equation (3-19).

For a consistent boundary (8), it is always possible to express the displacements in the far-field in terms of eigenfunctions corresponding to the natural modes of wave propagation in the stratum. The general solution to the problem is given by Equation (2-23) where k is an undetermined parameter of the wave number. In an unbounded medium,

any value of k, and thus any wave length, is admissible; for a layered stratum, however, only a discrete set of values of k (each one with a corresponding propagation mode) will satisfy the boundary condition. At a given frequency, Ω, there are thus, an infinite but discrete set of propagation modes and wave numbers k, which can be found by solving a transcendental eigenvalue problem. For each eigenfunction one can determine the distribution of stresses up to a multiplicative constant, the participation factor of the mode. Combining these modal stresses so as to match any given distribution of stresses at the boundary, one can compute the participation factors and, correspondingly, the dynamic stiffness function relating boundary stresses to boundary displacements.

The solution of the actual transcendental eigenvalue problem for the continuum problem is difficult and time consuming requiring, in general, search procedures. A discrete eigenvalue problem can be obtained by substituting the actual dependence of the displacements on the z variable, as given by Equations (2-25) and (2-26), by an assumed expansion consistent with that used for the finite elements. The result is an algebraic eigenvalue problem with a finite number of eigenvectors and eigenvalues, for which efficient numerical solutions are available.

3-3a Wave Numbers and Modes of Propagation

Consider the toroidal section of the far-field limited by two cylindrical surfaces of radii r_o and r_1, as shown in Figure 3. The stratum is discretized in horizontal layers, the interfaces of which match the nodal circles of the finite element mesh in the core region. For the nth layer there are three nodes i, i+1, i+2, for the ith node the three degrees of freedom are:

$$x_i = \{x_1, x_2, x_3\}_i \tag{3-20}$$

The exact values for these three nodal displacements are given by Equation (2-25),

$$x_i = H \cdot F_i$$

and for the layer number n,

$$x_n = \{x_{1_i}, x_{2_i}, x_{3_i}: x_{1_{i+1}}, x_{2_{i+1}}, x_{3_{i+1}}: x_{1_{i+2}}, x_{2_{i+2}}, x_{3_{i+2}}\} \tag{3-21}$$

Approximate solution for the nodal displacements may be obtained using the same expansions as for the coordinates and displacements in the finite element region

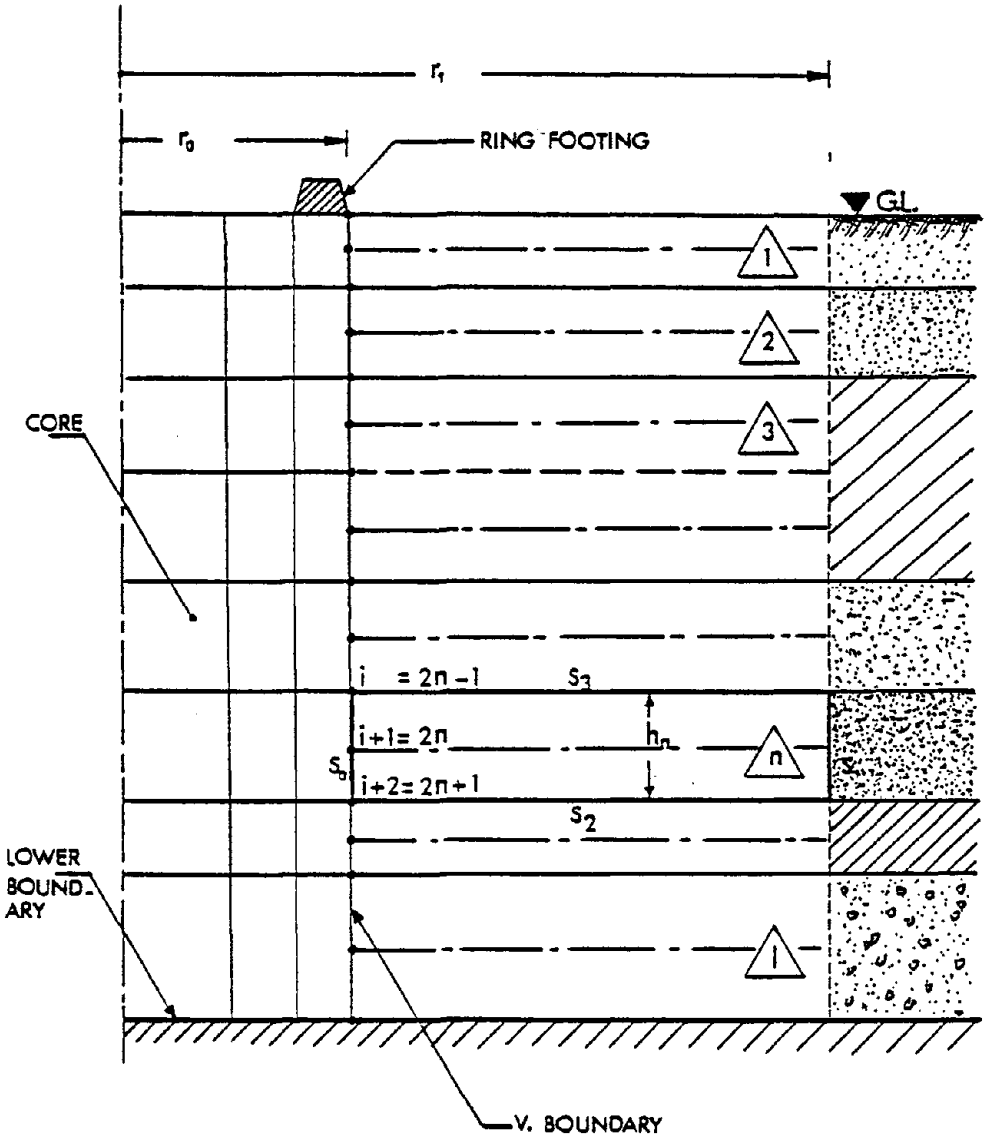

Figure 3. Toroidal Section of the Far Field

$$F_i = N\, X_i \tag{3-22}$$

where

$$N = [g_1 I, g_2 I, g_3 I]_{3\times 9} \tag{3-23}$$

in which I is a 3×3 identity matrix, and g_i represents the expansion coefficients. For a quadratic expansion,

$$g_1 = \frac{1}{2}(\eta^2-\eta),\ g_2 = 1-\eta^2 \text{ and } g_3 = \frac{1}{2}(\eta^2+\eta) \tag{3-24}$$

Combining Equations (3-20) to (3-24) yield

$$U_{app_n} = N\, U_{o_n} \tag{3-25a}$$

= the approximate nodal displacements for the nth layer

and

$$U_{o_n} = \begin{bmatrix} x_{1i} H_j' + \frac{j}{r_o} x_{3i} H_j \\ kx_{2i} H_j \\ \frac{j}{r_o} x_{1i} H_j + x_{3i} H_j' \\ x_{1i+1} H_j' + \frac{j}{r_o} x_{3i+1} H_j \\ kx_{2i+1} H_j \\ \frac{j}{r_o} x_{1i+1} H_j + x_{3i+1} H_j' \\ x_{1i+2} H_j' + \frac{j}{r_o} x_{3i+2} H_j \\ kx_{2i+2} H_j \\ \frac{j}{r_o} x_{1i+2} H_j + x_{3i+2} H_j' \end{bmatrix}_n \tag{3-25b}$$

Using the same basic procedure for the finite element formulation as previously employed, an approximate solution is obtained by substituting the displacement expansion into the expression of the principle of virtual displacements (2-43), integrating over the region, and requiring the result to vanish for an arbitrary δu.

Substituting the above approximate displacements in (2-43) and summing over the ℓ layers yields

$$\sum_{n=1}^{\ell} \left[\iiint \delta\bar{u}^T \cdot H \cdot Z \cdot r dr dz + \int_{s_o} \delta\bar{u}^T (\bar{p}-\bar{\sigma}^*) r ds + \int_{s_1} \delta\bar{u}^T (\bar{p}-\bar{\sigma}^*) r ds \right.$$

$$\left. + \int_{s_2} \delta\bar{u}^T (\bar{p}-\bar{\sigma}^*) r ds + \int_{s_3} \delta\bar{u}^T (\bar{p}-\bar{\sigma}^*) r ds \right] = 0 \qquad (3\text{-}26)$$

In the above equation, consistent nodal forces $\bar{p}_o$ and $\bar{p}_1$ are applied at each of the boundaries r_o and r_1 such that the integrands over s_o and s_1 vanish

$$\sum_{n=1}^{\ell} \left[\delta\bar{u}_o^T \bar{P}_o = \int_{s_o} \delta\bar{u}^T \bar{p} r ds = \int_{s_o} \delta\bar{u}^T \bar{\sigma}^* \, r ds \right] \qquad (3\text{-}27)$$

$$\sum_{n=1}^{\ell} \left[\delta\bar{u}_1^T \bar{P}_1 = \int_{s_1} \delta\bar{u}^T \bar{p} r ds = \int_{s_1} \delta\bar{u}^T \bar{\sigma}^* \, r ds \right]$$

with no external prescribed forces acting at the layer interfaces;

$$\sum_{n=1}^{\ell}\left[\iint \delta\bar{u}^{T} H\, Z\, r dr dz - \int_{s_2} \delta\bar{u}^{T}\bar{\sigma}^{*} r ds - \int_{s_3} \delta\bar{u}^{T}\bar{\sigma}^{*} r ds\right] = 0 \tag{3-28}$$

in which

$$\bar{\sigma}^{*} = \begin{cases} \{\bar{\sigma}_{rz}, \bar{\sigma}_{zz}, \bar{\sigma}_{\theta z}\} & \text{for } s_2 \\ -\{\bar{\sigma}_{rz}, \bar{\sigma}_{zz}, \bar{\sigma}_{\theta z}\} & \text{for } s_3 \end{cases} \tag{3-29}$$

From Equations (2-29), (2-30) and (2-31)

$$\bar{\sigma}^{*} = \begin{bmatrix} \bar{\sigma}_{rz} \\ \bar{\sigma}_{zz} \\ \bar{\sigma}_{\theta z} \end{bmatrix} = \begin{bmatrix} \mu\{(f_1'+kf_2)H_j' + \frac{j}{r} H_j f_3'\} \\ kH_j\{(\lambda+2\mu) f_2' - \lambda k f_1\} \\ \mu\{(f_1'+kf_2)\frac{j}{r} H_j + f_3' H_j'\} \end{bmatrix} \tag{3-30-a}$$

$$\text{or} \quad \bar{\sigma}^{*} = H \cdot \bar{Z}_2 \cdot F \tag{3-30-b}$$

where $\bar{Z}_2$ is an operator matrix

$$\bar{Z}_2 = \begin{bmatrix} \mu\frac{\partial}{\partial z} & \mu k & 0 \\ -\lambda k & (\lambda+2\mu)\frac{\partial}{\partial z} & 0 \\ 0 & 0 & \mu\frac{\partial}{\partial z} \end{bmatrix} \tag{3-31}$$

The wave equation H·Z, Equation (2-32), may be written as

$$W = H \cdot \bar{Z}_1 \cdot F \tag{3-32}$$

in which $\bar{Z}_1$ is an operator matrix

$$\bar{Z}_1 = \begin{bmatrix} \rho\Omega^2+\mu\frac{\partial^2}{\partial z^2} - k^2(\lambda+2\mu) & k(\lambda+\mu)\frac{\partial}{\partial z} & 0 \\ -k^2(\lambda+\mu)\frac{\partial}{\partial z} & \rho\Omega^2-\mu k^2+(\lambda+2\mu)\frac{\partial^2}{\partial z^2} & 0 \\ 0 & 0 & \rho\Omega^2-\mu k^2+\mu\frac{\partial^2}{\partial z^2} \end{bmatrix} \tag{3-33}$$

With $\delta\bar{u} = H\cdot N\cdot\delta X$ and $F = N\cdot X$, Equation (3-28) becomes

$$\sum_{n=1}^{\ell} \int_r \left\{ \int_z \delta X^T N^T H^T H(\bar{Z}_1-\bar{Z}_1')NX dz - \int_z \delta X^T N'^T H\bar{Z}_2 NX dz\, rdr \right\} = 0 \tag{3-34}$$

In the above equation,

$$N^T N = [g_i \cdot g_k] \quad , \quad N' = \frac{\partial N}{\partial z} = [g_i' \; I_i]$$

in which i = 1, 2, 3 and k = 1, 2, 3.

Also, in Equation (3-34);

$N^T H^T H = \bar{H} N^T$ and $N'^T H^T H = \bar{H} N'^T$, where

$$\bar{H} = \left[\begin{array}{ccc|ccc|ccc} H_1 & 0 & H_2 & & & & & & \\ 0 & H_3 & 0 & & 0 & & & 0 & \\ H_2 & 0 & H_1 & & & & & & \\ \hline & & & H_1 & 0 & H_2 & & & \\ & 0 & & 0 & H_3 & 0 & & 0 & \\ & & & H_2 & 0 & H_1 & & & \\ \hline & & & & & & H_1 & 0 & H_2 \\ & 0 & & & 0 & & 0 & H_3 & 0 \\ & & & & & & H_2 & 0 & H_1 \end{array}\right] \qquad (3\text{-}35)$$

in which

$$H_1 = H_j'^2 + \left(\frac{j}{r}\right)^2 H_j^2$$

$$H_2 = \frac{2j}{r} H_j' H_j$$

$$H_3 = k^2 H_j^2$$

Factoring out the $\bar{H}$ matrix, which is independent of z, from Equation (3-34) and rearranging the equation yields

$$\sum_{n=1}^{\ell} \delta X^T \left[\int_{r_o}^{r_1} \bar{H} r dr\right] \left[\int_0^{h_n} N^T (\bar{Z}_1 - \bar{Z}_2') N dz - \int_0^{h_n} N'^T \bar{Z}_2 N dz\right] X = 0 \qquad (3\text{-}36)$$

For an arbitrary δX and with $\int_{r_o}^{r_1} \bar{H} r dr \neq 0$ (non singular matrix) which is the same for all layers in the case of vertical boundaries, the following equation must hold:

$$\sum_{n=1}^{\ell} \left[\int_0^{h_n} N^T(\bar{Z}_1 - \bar{Z}_2')N dz - \int_0^{h_n} N'^T \bar{Z}_2 N dz \right] X = 0 \qquad (3\text{-}37)$$

and with

$$\int_0^h g_i g_k dz = \frac{h}{30} \begin{bmatrix} 4 & 2 & -1 \\ 2 & 16 & 2 \\ -1 & 2 & 4 \end{bmatrix}$$

$$\int_0^h g_i g_k' dz = \frac{1}{6} \begin{bmatrix} -3 & 4 & -1 \\ -4 & 0 & 4 \\ 1 & -4 & 3 \end{bmatrix} \qquad (3\text{-}38)$$

and $$\int_0^h g_i' g_k' dz = \frac{1}{3h} \begin{bmatrix} 7 & -8 & 1 \\ -8 & 16 & -8 \\ 1 & -8 & 7 \end{bmatrix}$$

equation (3-37) becomes

$$\sum_{n=1}^{\ell} ([S]_n - K[B]_n - k[A]_n)\{X\} = 0 \qquad (3\text{-}39)$$

in which

$$[S]_n = \frac{1}{3h_n}$$

$$\begin{bmatrix}
0.4h_n^2\rho\Omega^2 - 7\mu & 0 & 0 & 0.2h_n^2\rho\Omega^2 + 8\mu & 0 & 0 & -0.1h_n^2\rho\Omega^2 - \mu & 0 & 0 \\
 & 0.4h_n^2\rho\Omega^2 - 7(\lambda+2\mu) & 0 & 0 & 0.2h_n^2\rho\Omega^2 + 8(\lambda+2\mu) & & & -0.1h_n^2\rho\Omega^2 - (\lambda+2\mu) & \\
 & & 0.4h_n^2\rho\Omega^2 - 7\mu & 0 & 0 & 0.2h_n^2\rho\Omega^2 + 8\mu & 0 & 0 & -0.1h_n^2\rho\Omega^2 - \mu \\
 & & & 1.6h_n^2\rho\Omega^2 - 16\mu & 0 & 0 & 0.2h_n^2\rho\Omega^2 + 8\mu & & 0 \\
 & & & & 1.6h_n^2\rho\Omega^2 - 16(\lambda+2\mu) & 0 & & 0.2h_n^2\rho\Omega^2 + 8(\lambda+2\mu) & 0 \\
 & & \text{SYM.} & & & 1.6h_n^2\rho\Omega^2 - 16\mu & 0 & 0 & 0.2h_n^2\rho\Omega^2 + 8\mu \\
 & & & & & & 0.4h_n^2\rho\Omega^2 - 7\mu & 0 & 0 \\
 & & & & & & & 0.4h_n^2\rho\Omega^2 - 7(\lambda+2\mu) & 0 \\
 & & & & & & & & 0.4h_n^2\rho\Omega^2 - 7\mu
\end{bmatrix}$$

(3-40-a)

$$[A]_n = \frac{h_n}{30}\begin{bmatrix} 4(\lambda+2\mu) & 0 & 0 & 2(\lambda+2\mu) & 0 & 0 & -(\lambda+2\mu) & 0 & 0 \\ & 4\mu & 0 & 0 & 2\mu & 0 & 0 & -\mu & 0 \\ & & 4\mu & 0 & 0 & 2\mu & 0 & 0 & -\mu \\ & & & 16(\lambda+2\mu) & 0 & 0 & 2(\lambda+2\mu) & 0 & 0 \\ & & & & 16\mu & 0 & & 2\mu & 0 \\ & & \text{SYM} & & & 16\mu & 0 & 0 & 2\mu \\ & & & & & & 4(\lambda+2\mu) & 0 & 0 \\ & & & & & & & 4\mu & 0 \\ & & & & & & & & 4\mu \end{bmatrix}$$

and

(3-40-b)

$$[B]_n = \frac{1}{30}\begin{bmatrix} 0 & 15(\lambda-\mu) & 0 & 0 & -20(\lambda+\mu) & 0 & 0 & 5(\lambda+\mu) & 0 \\ & 0 & 0 & 20(\lambda+\mu) & 0 & 0 & -5(\lambda+\mu) & 0 & 0 \\ & & 0 & 0 & 0 & 0 & 0 & 0 & 0 \\ & & & 0 & 0 & 0 & 0 & -20(\lambda+\mu) & 0 \\ & & & & 0 & 0 & 20(\lambda+\mu) & 0 & 0 \\ & & \text{SYM} & & & 0 & 0 & 0 & 0 \\ & & & & & & 0 & -15(\lambda-\mu) & 0 \\ & & & & & & & 0 & 0 \\ & & & & & & & & 0 \end{bmatrix}$$

For the whole stratum, the assembled matrices of (3-40) leads to

$$(S-KB-k^2A)X = 0 \tag{3-41}$$

which is an eigenvalue problem in k_i^2, the wave number of the propagation mode X_i. The order of this eigenvalue problem is 6ℓ, where ℓ is the total number of layers in the stratum.

3-3b Dynamic Stiffness Matrix of the Energy Absorbing Boundary

Consider Equation (3-27) with ds = dz and r = r_o, i.e.

$$\sum_{n=1}^{\ell} \left[P_o = r_o \int_0^{h_n} N^T \bar{\sigma}^* dz \right]$$ for an arbitrary variation of the nodal displacements. But

$$P_s = \alpha_s r_o \int_0^{h} N^T \bar{\sigma}_s^* \, dz \tag{3-42}$$

where P_s = the nodal forces for the $s^{\underline{th}}$ propagation mode

α_s = the participation factor for the $s^{\underline{th}}$ propagation mode

$\bar{\sigma}_s^*$ = the $s^{\underline{th}}$ modal boundary stresses vector

$= \{-\sigma_{rr}, -\sigma_{zr}, -\sigma_{\theta r}\}_s$

Therefore, from Equations (2-31) and (2-29)

$$\bar{\sigma}_s^* = -\begin{bmatrix} 2\mu H_j'' - \lambda k^2 H_j & (\lambda k H_j)\frac{\partial}{\partial z} & 2\mu\frac{j}{r_o}(H_j' - H_j/r_o) \\ (\mu H_j')\frac{\partial}{\partial z} & \mu k H_j & (\mu\frac{j}{r_o}H_j)\frac{\partial}{\partial z} \\ 2\mu\frac{j}{r_o}(H_j' - H_j/r_o) & 0 & \mu(H_j'' - \frac{H_j'}{r_o} + (\frac{j}{r_o})^2 H_j) \end{bmatrix} \begin{bmatrix} f_1 \\ f_2 \\ f_3 \end{bmatrix}$$

$$= -\begin{bmatrix} s_1 & 0 & s_2 \\ 0 & s_3 & 0 \\ s_2 & 0 & s_4 \end{bmatrix} \begin{bmatrix} f_1 \\ f_2 \\ f_3 \end{bmatrix} - \begin{bmatrix} 0 & T_1 & 0 \\ T_2 & 0 & T_3 \\ 0 & 0 & 0 \end{bmatrix} \begin{bmatrix} f_1' \\ f_2' \\ f_3' \end{bmatrix}$$

$$= -[s]\{f\} - [T]\{f'\} \qquad (3\text{-}43)$$

where;

$$\begin{aligned} s_1 &= 2\mu H_j'' - \lambda k^2 H_j \\ s_2 &= 2\mu \frac{j}{r_o}(H_j' - \frac{1}{r_o} H_j) \\ s_3 &= \mu k H_j' \\ s_4 &= \mu(H_j'' - \frac{1}{r_o} H_j' + \frac{j^2}{r_o^2} H_j) \qquad (3\text{-}44) \\ T_1 &= \lambda k H_j \\ T_2 &= \mu H_j' \end{aligned}$$

and $$T_3 = \mu \frac{j}{r_o} H_j$$

With $\{f\} = [N]\{X\}$ and $\{f'\} = [N']\{X\}$

$$N^T\bar{\sigma}_s^* = (N^TN\bar{S} + N^TN'\bar{T})x \tag{3-45}$$

where

$$\bar{S} = \begin{bmatrix} S & & \\ & S & \\ & & S \end{bmatrix}_{9\times 9} \quad \text{and} \quad \bar{T} = \begin{bmatrix} T & & \\ & T & \\ & & T \end{bmatrix}_{9\times 9} \tag{3-46}$$

which leads to the following equation for the nodal forces in the sth mode:

$$P_s = \alpha_s r_o([\int_0^h N^TNdz]\bar{S} + [\int_0^h N^TN'dz]\bar{T})X \tag{3-47}$$

Matrices S and T may be simplified by taking advantage of the property of Hankel functions

$$\begin{aligned} H_j'' &= -\frac{1}{r}H_j' - [k^2 - \frac{j^2}{r^2}]H_j \\ H_j' &= k\,H_{j-1} - \frac{j}{r}H_j \\ H_{-1} &= -H_1 \end{aligned} \tag{3-48}$$

which yields

$$S = k^2 S1 + kS2 + S3$$

and

$$T = kT1 + T2 \qquad (3\text{-}49)$$

with

$$S1 = \begin{bmatrix} \lambda+2\mu & 0 & 0 \\ 0 & \mu & 0 \\ 0 & 0 & \mu \end{bmatrix} \begin{bmatrix} H_j & 0 & 0 \\ 0 & -H_{j-1} & 0 \\ 0 & 0 & H_j \end{bmatrix} \qquad (3\text{-}50a)$$

$$S2 = \frac{\mu}{r_o} \begin{bmatrix} -2 & 0 & 2j \\ 0 & j & 0 \\ 2j & 0 & -2 \end{bmatrix} \begin{bmatrix} -H_{j-1} & 0 & 0 \\ 0 & H_j & 0 \\ 0 & 0 & -H_{j-1} \end{bmatrix} \qquad (3\text{-}50b)$$

$$S3 = \frac{2\mu j(j+1)}{r_o^2} (-1) \begin{bmatrix} 1 & 0 & -1 \\ 0 & 0 & 0 \\ -1 & 0 & 1 \end{bmatrix} \begin{bmatrix} H_j & 0 & 0 \\ 0 & -H_{j-1} & 0 \\ 0 & 0 & H_j \end{bmatrix} \qquad (3\text{-}50c)$$

$$T1 = \begin{bmatrix} 0 & -\lambda & 0 \\ \mu & 0 & 0 \\ 0 & 0 & 0 \end{bmatrix} \begin{bmatrix} -H_{j-1} & 0 & 0 \\ 0 & H_j & 0 \\ 0 & 0 & -H_{j-1} \end{bmatrix} \qquad (3\text{-}50d)$$

$$\text{and } T2 = -\frac{\mu j}{r_o} \begin{bmatrix} 0 & 0 & 0 \\ -1 & 0 & 1 \\ 0 & 0 & 0 \end{bmatrix} \begin{bmatrix} H_j & 0 & 0 \\ 0 & -H_{j-1} & 0 \\ 0 & 0 & H_j \end{bmatrix} \qquad (3\text{-}50e)$$

Defining the modal vectors XA_s and XB_s

where

$$XA_s = \{XA_1^T \; XA_2^T \ldots . XA_i^T \ldots XA_{2\ell}^T\}$$

$$XB_s = \{XB_1^T \; XB_2^T \ldots . XB_i^T \ldots XB_{2\ell}^T\} \qquad (3\text{-}51)$$

$$\{XA_i\}_s = \begin{bmatrix} H_j & & \\ & -H_{j-1} & \\ & & H_j \end{bmatrix} \begin{bmatrix} x_1 \\ x_2 \\ x_3 \end{bmatrix}_i$$

$$\{XB_i\}_s = \begin{bmatrix} -H_{j-1} & & \\ & H_j & \\ & & -H_{j-1} \end{bmatrix} \begin{bmatrix} x_1 \\ x_2 \\ x_3 \end{bmatrix}_i$$

and the boundary load vector P_{bs} as

$$P_{bs} = \alpha_s r_o \{[A]\{XA\}_s k_s^2 + [G]\{XB\}_s \; k_s + [E]\{XA\}_s\} \qquad (3\text{-}52)$$

the nodal load vector for the whole stratum assembled from P_s for each discrete layer where matrices A, E and G are formed from the layer matrices A_n, E_n and G_n in a similar fashion as in the eigenvalue problem.

A_n is the matrix given by Equation (3-40-b)

$$E_n = \int_0^{h_n} \frac{\mu j}{r_o^2} \left[\begin{bmatrix} 2(j+1)g_i g_m & 0 & -2(j+1)g_i g_m \\ r_o g_i g_m' & 0 & -r_o g_i g_m' \\ -2(j+1)g_i g_m & 0 & 2(j+1)g_i g_m \end{bmatrix}_{3\times3} \right]_{9\times9} \qquad (3\text{-}53)$$

and

$$G_n = \int_0^{h_n} \frac{2}{r_o} \left[\begin{bmatrix} -\mu g_i g_m & -\frac{\lambda r_o}{2} g_i g_m' & j g_i g_m \\ \frac{\mu r_o}{2} g_i g_m' & \frac{j\mu}{2} g_i g_m & 0 \\ j g_i g_m & 0 & -\mu g_i g_m \end{bmatrix}_{3\times3} \right]_{9\times9}$$

with $i = 1, 2, 3$

$m = 1, 2, 3$

Adding up the contributions of each mode gives for the boundary load vector

$$P_b = \sum_{s=1}^{6\ell} \alpha_s r_o \{ [A]\{XA\}_s k_s^2 + [G]\{XB\}_s k_s + [E]\{XA\}_s \}$$

or

$$P_b = r_o \left[[A][XA][K^2] + [G][XB][K] + [E][XA] \right] \{\alpha\} \qquad (3\text{-}54)$$

In (3-54)

$$[XA] = [\{XA\}_1 \{XA\}_2 \ldots \{XA\}_s \ldots \{XA\}_{6\ell}]_{6\ell x 6\ell}$$

$$[XB] = [\{XB\}_1 \{XB\}_2 \ldots \{XB\}_s \ldots \{XB\}_{6\ell}]_{6\ell x 6\ell}$$

$[K^2]$ and $[K]$ are diagonal matrices with k_s^2 and k_s on the main diagonal respectively

(s=1 to 6ℓ)

and $\{\alpha\} = \{\alpha_1, \alpha_2, \alpha_3, \ldots, \alpha_s, \ldots, \alpha_{6\ell}\}$

The modal participation factors $\{\alpha\}$ are the only unknown vector in the RHS of Equation (3-54). The next step, then, is to calculate the boundary displacement vector in terms of the modal participation factors, and to relate the boundary load vector to the boundary displacement vector to form the boundary matrix.

At any particular node i, the displacement vector is given by

$$u_i = \sum_{s=1}^{\ell} \alpha_s \, H(s) X_i(s) \qquad (3\text{-}55)$$

or

$$u_i = \sum_{s=1}^{\ell} \alpha_s \begin{bmatrix} uI_s \\ uJ_s \\ uK_s \end{bmatrix}_i$$

where

$$\begin{bmatrix} uI_s \\ uJ_s \\ uK_s \end{bmatrix}_i = \begin{bmatrix} H_j'(k_s r_o) X_1(s) + \frac{j}{r_o} H_j(k_s r_o) X_3(s) \\ k_s H_j(k_s r_o) X_2(s) \\ \frac{j}{r_o} H_j(k_s r_o) X_1(s) + H_j'(k_s r_o) X_3(s) \end{bmatrix}_i$$

Therefore

$$\begin{bmatrix} \bar{u} \\ \bar{w} \\ \bar{v} \end{bmatrix}_i = \begin{bmatrix} uI(1) & uI(2) \ldots uI(s) \ldots uI(6\ell) \\ uJ(1) & uJ(2) \ldots uJ(s) \ldots uJ(6\ell) \\ uK(1) & uK(2) \ldots uK(s) \ldots uK(6\ell) \end{bmatrix}_i \begin{bmatrix} \alpha_1 \\ \alpha_2 \\ \vdots \\ \alpha_s \\ \vdots \\ \alpha_{6\ell} \end{bmatrix} = [\bar{uu}]_i \{\alpha\} \tag{3-56}$$

Defining $\{u_b\}_{6\ell \times 1}$ as the boundary displacement vector, and with u_i as a general nodal vector, $\{u_b\}$ may be written as

$$u_b = \begin{bmatrix} [\bar{uu}]_1 \\ [\bar{uu}]_2 \\ \vdots \\ [\bar{uu}]_i \\ \vdots \\ [\bar{uu}]_{2\ell} \end{bmatrix}_{6\ell \times 6\ell} \{\alpha\} = [\bar{uu}] \cdot \{\alpha\} \tag{3-57}$$

$$\therefore \quad \{\alpha\} = [\bar{uu}]^{-1} u_b \tag{3-58}$$

The dynamic stiffness matrix of the energy absorbing boundary R_b is defined through the following relation:

$$P_b = R_b u_b \tag{3-59}$$

Substituting (3-58) into (3-54) for $\{\alpha\}$ and equating the resulting RHS to the RHS of (3-59) for an arbitrary u_b, it follows that

$$R_b = r_o \left[[A][XA][K^2] + [G][XB][K] + [E][XA] \right] [\bar{u}\bar{u}]^{-1} \tag{3-60}$$

3.4 TOTAL DYNAMIC STIFFNESS MATRIX OF THE SOIL MEDIUM

Consider the boundary load vector of Equation (3-59) as an external load vector acting with negative sign on the finite element region, Equation (3-19) becomes;

$$(K - \Omega^2 M)u = P - R_b u_b$$

and by increasing the size of R_b by adding zero rows and columns to match the dimension of K and M, one can get

$$(K - \Omega^2 M + R)u = P \tag{3-61}$$

or

$$K_c u = P$$

where K_c is the total dynamic stiffness matrix of the soil medium,

$$K_c = K - \Omega^2 M + R \tag{3-62}$$

Equation (3-61) may be solved by conventional numerical methods to obtain the nodal displacements. Although neither the total dynamic stiffness matrix of Equation (3-62) nor the formula of Equation (3-61) will be used in their present form in the structure-soil system of the next chapter, these are very useful in checking the finite element model of the soil medium and the effectiveness of the vertical energy absorbing boundaries. The checking of the model presented in this chapter is part of the study described in the following section.

3-5 STUDY OF ENERGY ABSORBING BOUNDARY

In order to check the applicability and effectiveness of the energy absorbing boundary based on the preceding theory, a time history analysis is carried out for two cycles of a sinusoidal ground acceleration applied at the lower boundary of the finite element region of Figure 4. The sinusoidal ground acceleration has a maximum amplitude of 20%g and a frequency equals to 10 radians per second. For $j = 1$, the dynamic analysis is performed using two models which are the same, except for the vertical boundaries. The first model has an energy absorbing boundary which is represented by the dynamic boundary matrix $[R]_b$ of Equation (3-60) while the second has a roller boundary which allows the nodal points along the vertical boundary to move freely

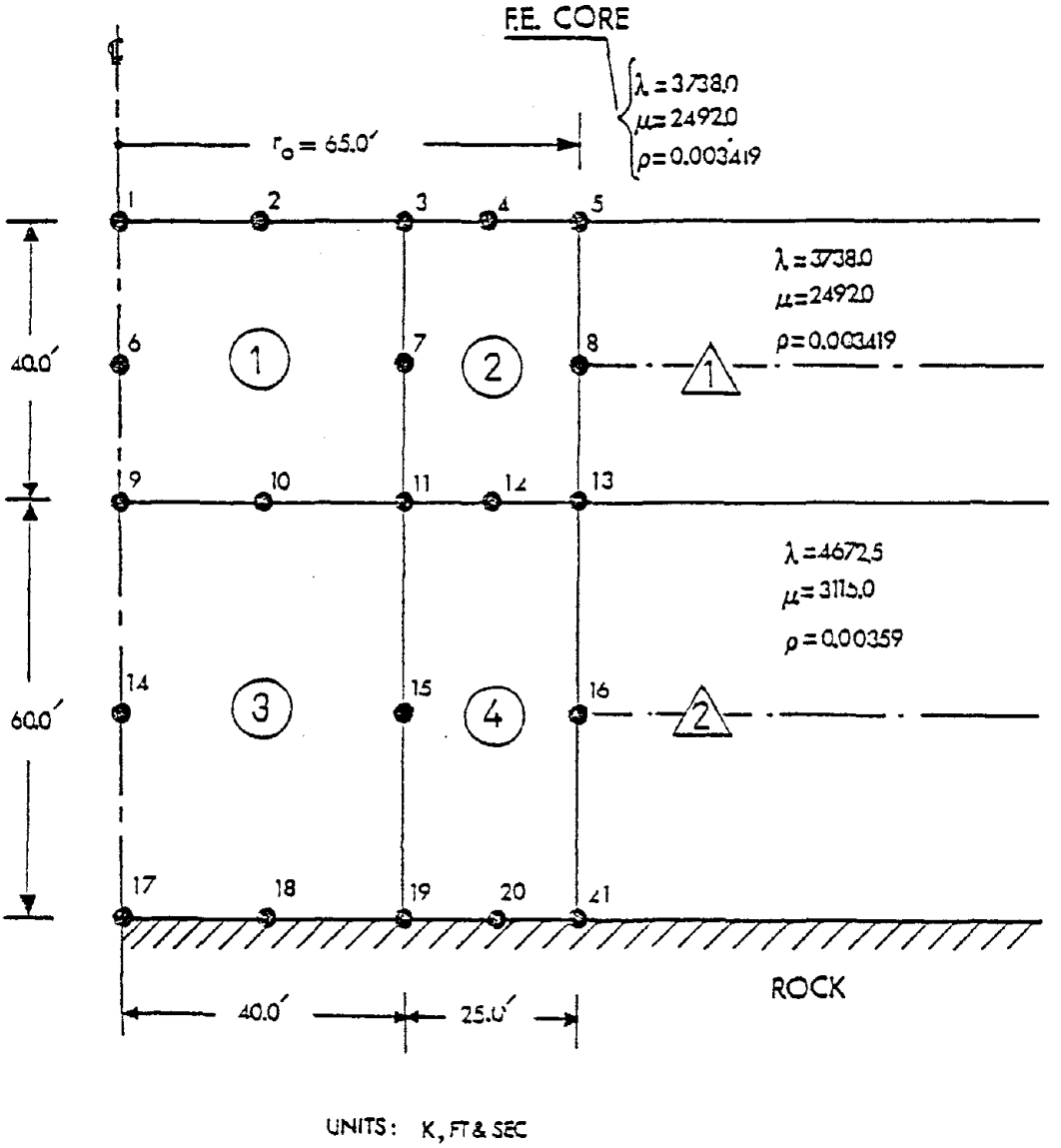

Figure 4. F.E. Mesh for the Time History Analysis of Two Cycles of a Sinusoidal Acceleration

in the vertical and circumferential directions, while restricting radial motion. Numerical computations herein are conducted using the Newmark method with $\beta = 1/4$ and a time step of 0.005 second.

The three components of the response acceleration of node 4 in the radial, vertical, and circumferential directions ($\ddot{u}$, $\ddot{w}$, and $\ddot{v}$, respectively) are given in Figure 5. The response accelerations show that, in contrast to the undamped response in the model with a roller boundary (solid lines), the model with an energy absorbing boundary produced a damped response (dashed lines). These results are comparable to those given in Akiyoshi's study for viscous boundaries (20). However, the compatible viscous boundary in Akiyoshi's model proved to be more effective in absorbing the entire energy of the wave traveling toward the boundary; it is yet to be examined for an axisymmetric solid model.

To check for the correctness of the present model, a classical problem from the literature is considered, namely the dynamic analysis of a rigid circular footing on an elastic half space (32). The vertical displacement δ of the footing is calculated from the relation (see Figure 6)

$$\delta\, e^{i\Omega t} = \frac{P_o}{K} F\, e^{i\Omega t} \tag{3-63}$$

where

$$\delta = \delta_r + i\, \delta_i \tag{3-64}$$

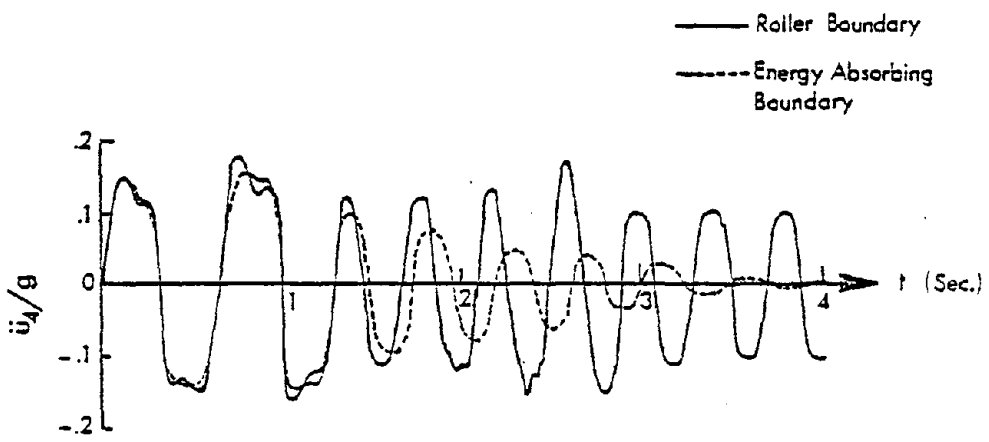

Fig. 4-a

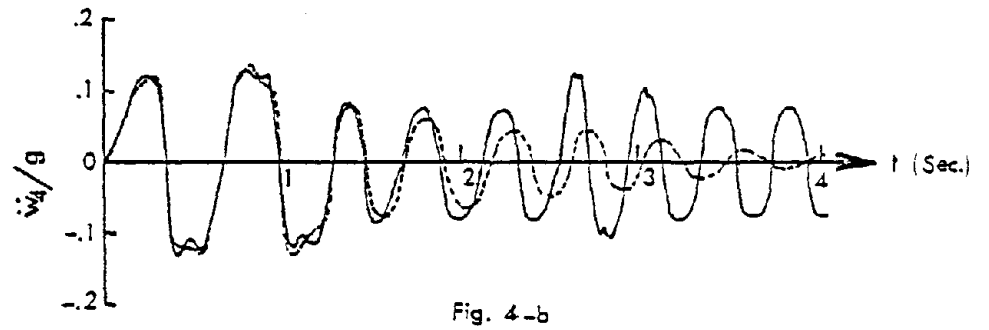

Fig. 4-b

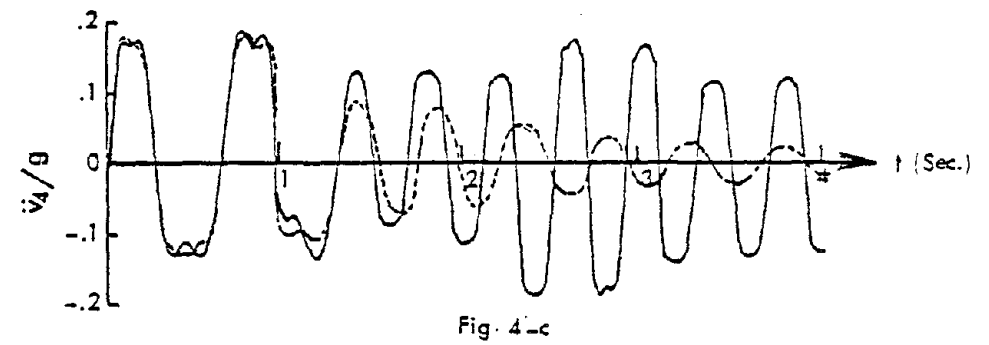

Fig. 4-c

Figure 5. Response Accelerations of 4 Sec. Time History Analysis

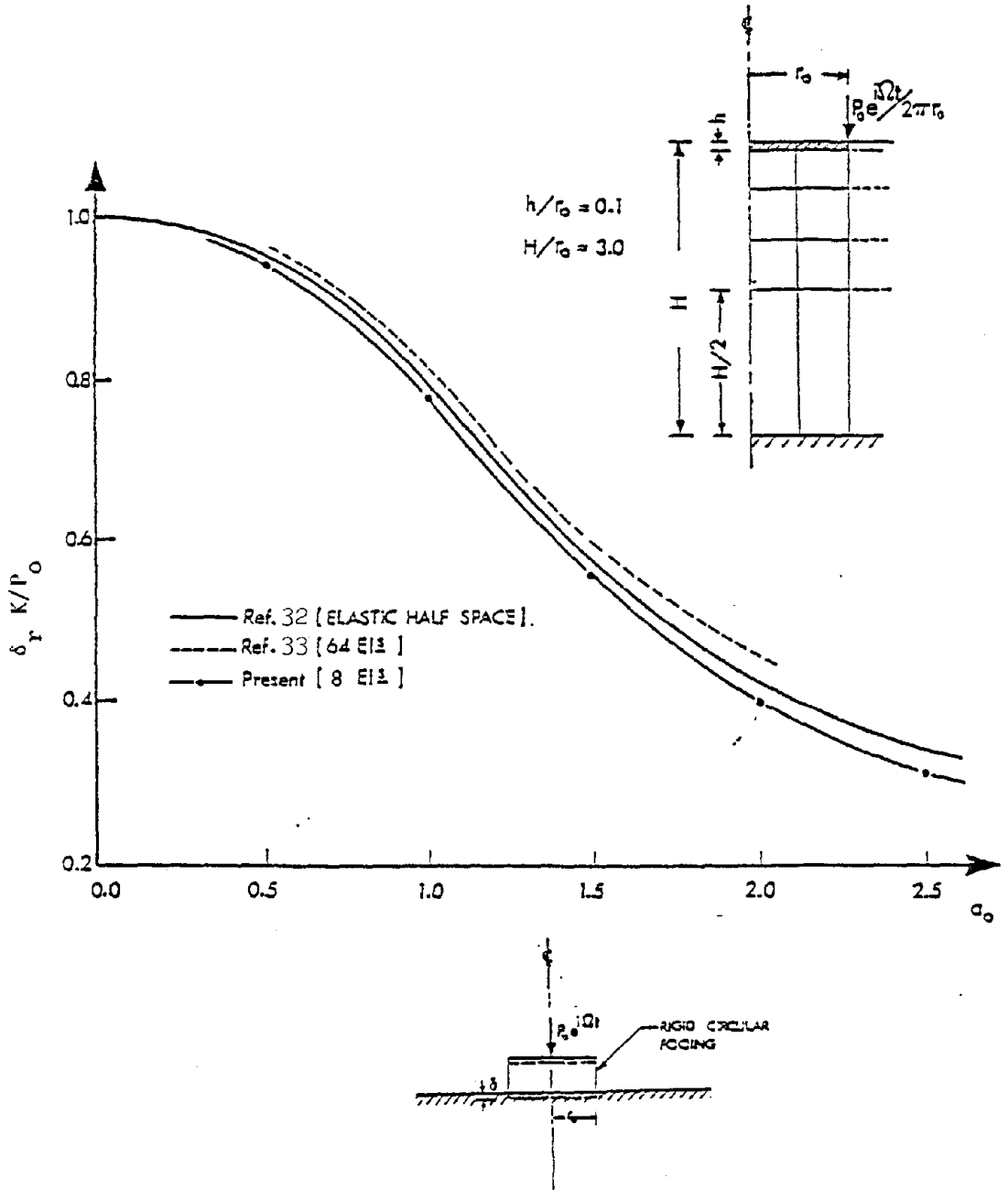

Figure 6. Vertical Displacement for Rigid Circular Footing on Elastic Half Space

in which P_o and Ω = the amplitude and frequency, respectively, of the exciting force; t = time; and K = the static spring constant. It may be shown that

$$K = \frac{4GR_o}{1-\nu} \qquad (3\text{-}65)$$

The dimensionless quantity F, herein designated the displacement function, is a function of Poisson's ratio ν and the dimensionless frequency ratio a_o.

The rigid circular plate is idealized by a row of massless finite elements of very high rigidity (10^6 times greater than that of the stratum) as shown in Figure 6. The equivalent value for the force amplitude in the finite element model is taken as $P_o/2\pi r_o$ and is concentrated along the foundation edge; the material damping, defined explicitly in Equation 3-68, is taken as 5%. In the figure the real part of the displacement in the w direction δ_r is plotted against the dimensionless frequency ratio a_o, for P_o = 1.0 K, r_o = 10', G = 2492 K/Ft^2 and ν = 1/3. The results for the finite element model with an energy absorbing boundary show good agreement, especially in the lower frequency range in which the shear wave length Λ becomes longer and the element size ratio ℓ/Λ becomes smaller. The results for the same problem obtained by Lysmer and Kuhlemeyer (33) are also plotted. It can be seen that the present model with only 10 elements gave results comparable to those of Lysmer

and Kuhlemeyer for which 64 elements were used. This provides a check for the correctness of the present model and suggests its applicability for very deep stratums although it would be desirable to use the actual H/r_o in a physical situation.

3-6 Impedance Matrix

The impedance matrix is the dynamic stiffness to be added to the superstructure matrices to complete the structure-soil model. It is composed of the dynamic stiffness coefficients corresponding to the common degrees of freedom between the superstructure and the soil model. For structure-foundation systems idealized in three dimensions, three boundary value problems for the foundation with a unit harmonic force $e^{i\Omega t}$ applied individually for each of the three degrees of freedoms of each connection nodal point need to be solved.

Considering Equation (3-61), with the RHS all equated to zero except for the value at one of the common d.o.f. which is set to unity, and solving for the displacements at the common d.o.f., the complex compliance matrix for the foundation $[C]$ can be obtained. The complex impedance matrix $[\bar{K}]$ is then found by inverting the compliance matrix $[C]$, i.e.,

$$[\bar{K}] = [C]^{-1} \tag{3-66}$$

Herein, prescribed forces rather than displacements are used to avoid the complex mixed boundary value problem which could result from enforcing the traction free condition outside the structure-foundation interface. However, it may appear preferable to solve the problem with prescribed displacements to ensure compatibility of the deformations at the surface of the foundation with the deformations in a displacement formulation of the finite element system representing the structure (34). The applicability of the latter procedure to the problem at hand has not been investigated.

3-7 Connection Model

The connection between the soil medium and the ring footing is established by eliminating the six degrees of freedoms at the corners D and F shown in Figure 7 while forming the rotational d.o.f. at E from the eliminated degrees of freedom; in other words, the nine d.o.f. are lumped into five d.o.f. at the mid point of the footing base. The base uplift is treated by restricting the contact stresses between the soil and the footing to be compressive or shearing, but not tensile. Mild tension may be admissible,but no quantitative results are available as yet.

In order to formulate the soil stiffnesses and damping at the connecting nodal point, the following method is commonly used:

$$K = \bar{K}_r - 2D\bar{K}_i \tag{3-67}$$

$$C = (\bar{K}_i + 2D\bar{K}_r)/\Omega \tag{3-68}$$

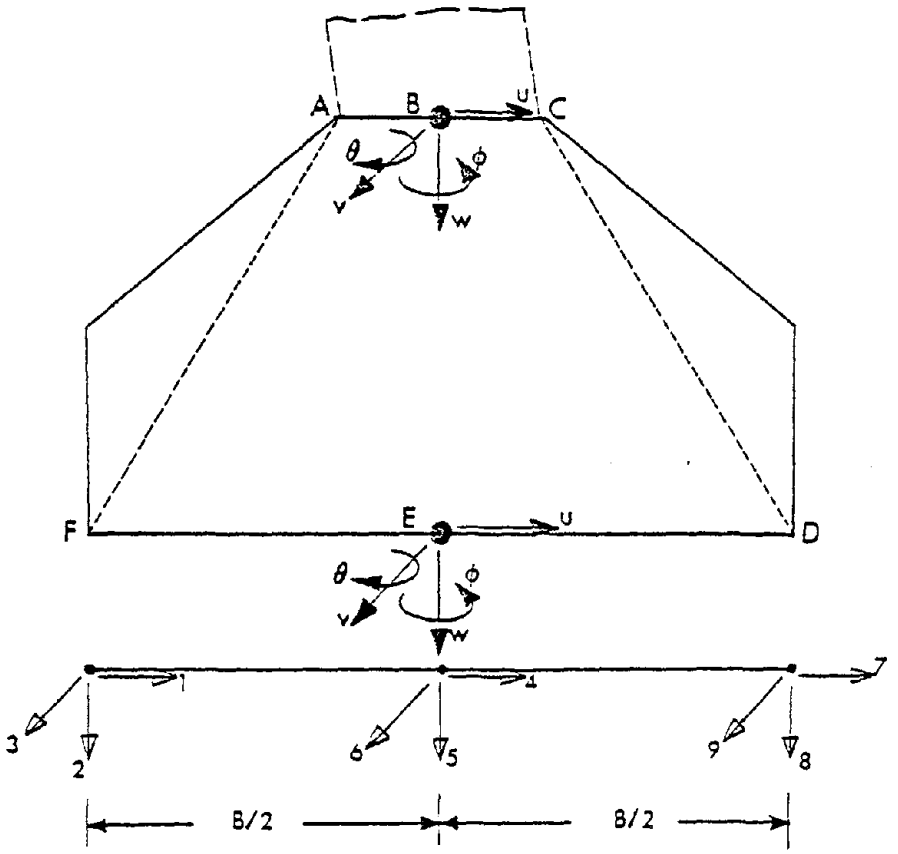

Figure 7. Ring Footing Cross Section

where $\bar{K}_r + i\bar{K}_i$ is the complex soil-stiffness with no material damping and D is the material damping parameter independent of the driving frequency Ω. It is obvious that both K and C of Equation (3-67) and (3-68) are frequency dependent since $\bar{K}_r$ and $\bar{K}_i$ are frequency dependent and the material damping affects both stiffness and damping.

The nine stiffness elements of Figure 8 are obtained from Equation (3-67) by considering each stiffness element on the main diagonal as a linear spring in the corresponding direction. The stiffness elements of the connection model are formulated from these nine stiffnesses:

$$\begin{aligned} K_u &= K_1 + K_4 + K_7 \\ K_w &= K_2 + K_5 + K_8 \\ K_v &= K_3 + K_5 + K_9 \\ K_\theta &= B^2/4\ (K_2 + K_8) \\ K_\phi &= B^2/4\ (K_3 + K_9) \end{aligned} \tag{3-69}$$

The damping system is formulated from matrix C (Equation 3-68) in a way similar to the stiffness elements of the connection model discussed above. The resultants in the five degrees of freedom at the center point E of Figure 7 are evaluated as follows:

$$\begin{aligned} C_u &= C_1 + C_4 + C_7 \\ C_w &= C_2 + C_5 + C_8 \\ C_v &= C_3 + C_6 + C_9 \\ C_\theta &= B^2/4\ (C_2 + C_8) \\ C_\phi &= B^2/4\ (C_3 + C_9) \end{aligned} \tag{3-70}$$

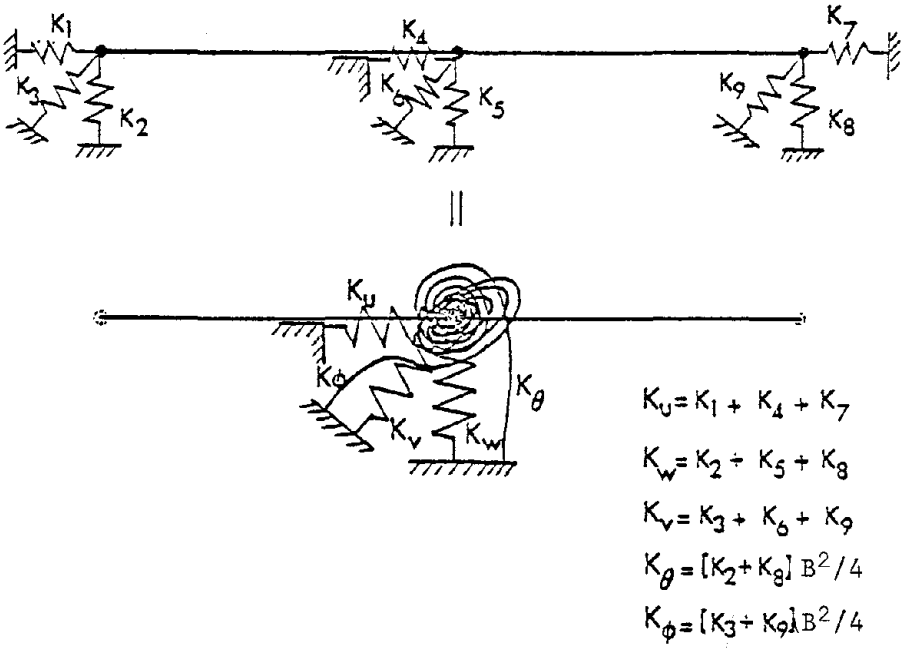

Figure 8. Equivalent Boundary Stiffnesses

For obvious reasons the connecting model is called the Equivalent Boundary System (EBS) for the ring footing. The EBS is frequency dependent and must be updated for each Fourier harmonic. In Equations (3-69) and (3-70) the K's and C's are modal values which are expressed in Fourier series in the θ direction. Figure 9 shows the resultant translational and the rotational stiffness and damping elements at the midpoint of the footing base.

3-8 SENSITIVITY STUDY OF THE EBS

3-8a Effect of the Stratum Depth

The depth of the stratum for a given ring footing dimension affects the results for the stiffnesses and damping of the EBS since the dynamic response of the nodes at the foundation level is significantly influenced by the reflections at the rock-soil surface.

To evaluate the convergence of the EBS quantities for the case of a very deep stratum, six meshes with the same element size throughout were considered. Figure 10 shows the dimensions of the meshes, which progress from a shallow stratum to a very deep one. Table 2 gives the soil material properties which are used for all meshes and the stiffnesses and damping of the EBS are shown in Figures 11 and 12, respectively. These results indicate the importance of the stratum depth factor for the stiffnesses. On the other hand, the damping elements are less sensitive to the depth

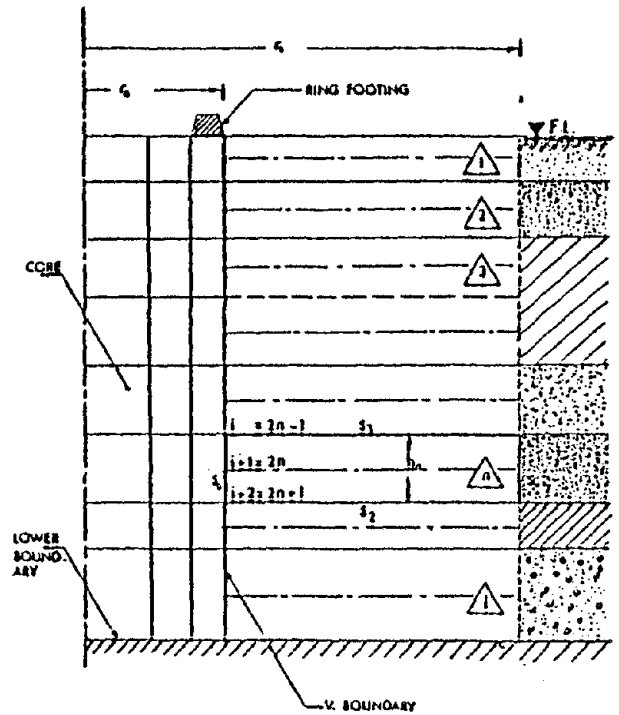

a. F.E. Model

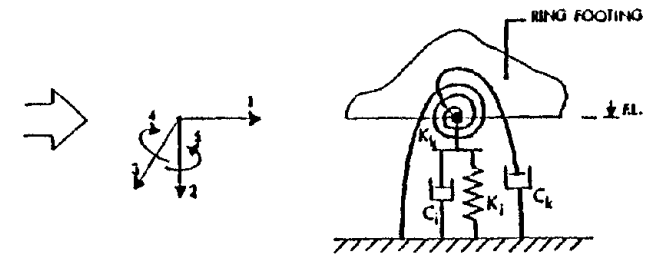

b. E.B.S.

Figure 9. Soil Model

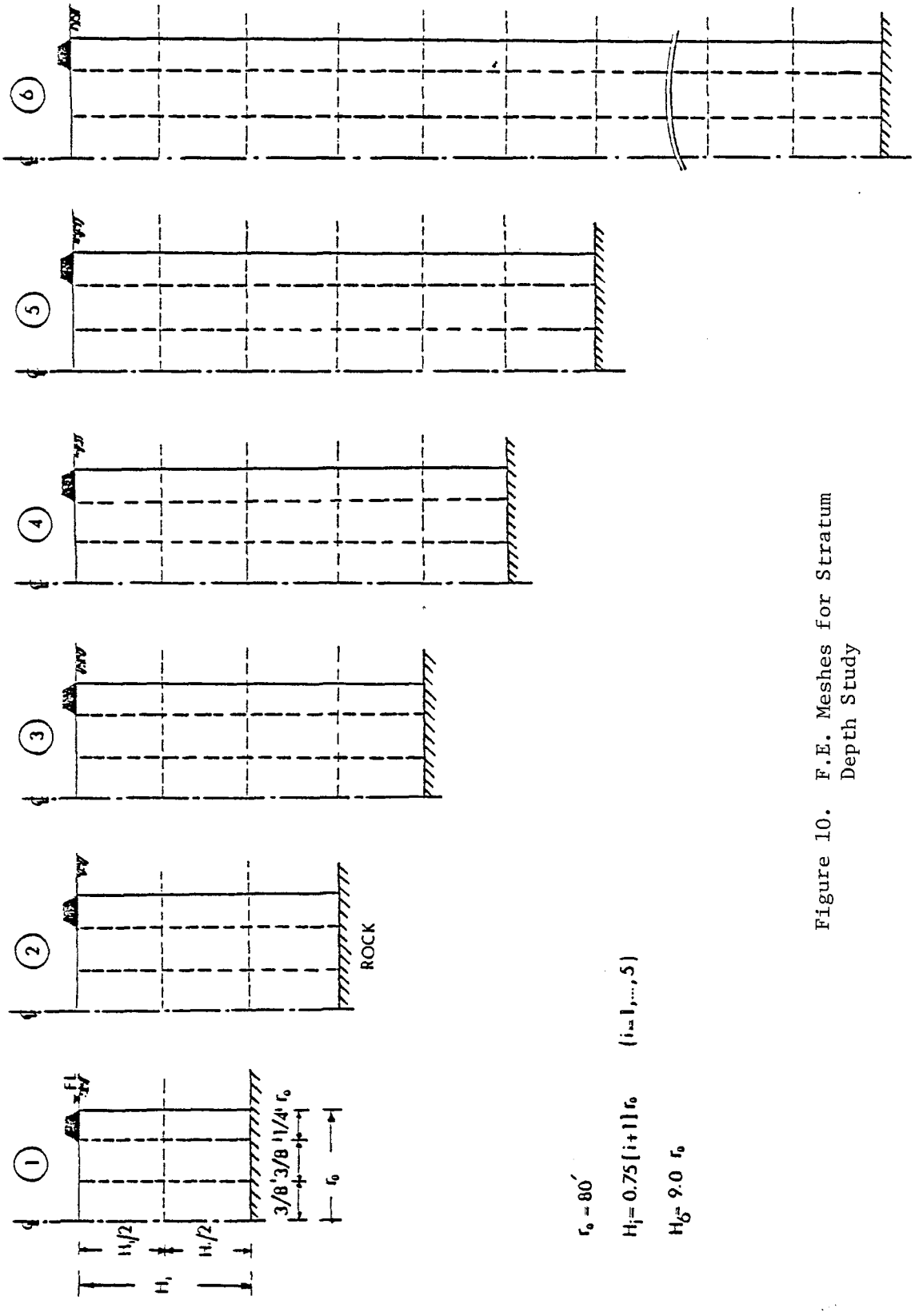

Figure 10. F.E. Meshes for Stratum Depth Study

Table 2. Soil Material Properties

Soil Properties	λ	μ	ρ	a_o	v_s	v_p
All Finite Elements	3738.0	2492.0	0.003419	1.64	853.74	1599.81
All Layers	3738.0	2492.0	0.003419	1.64	953.74	1599.71

Units: K, Ft and Sec.

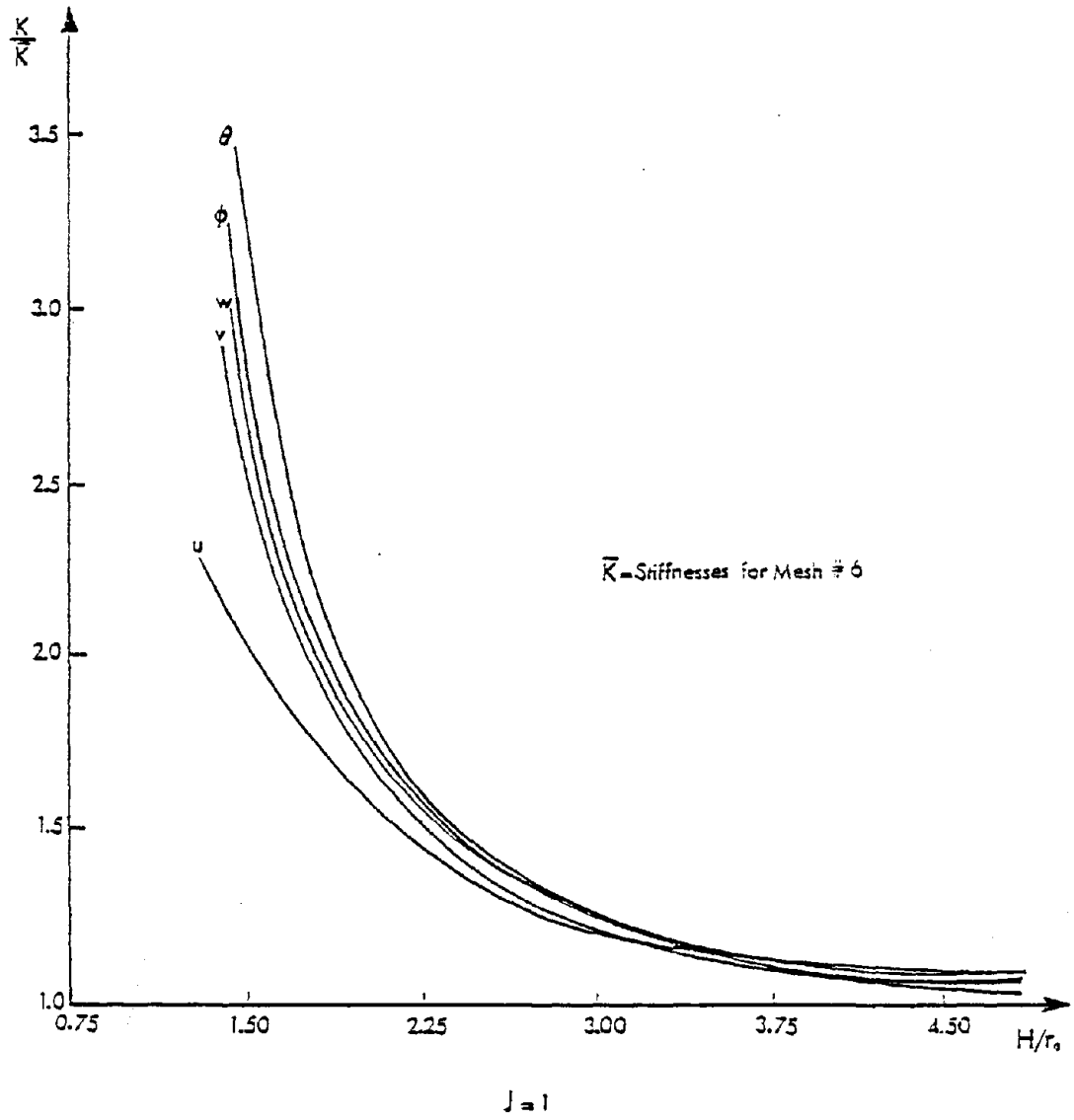

Figure 11. Effect of Stratum Depth on Stiffnesses

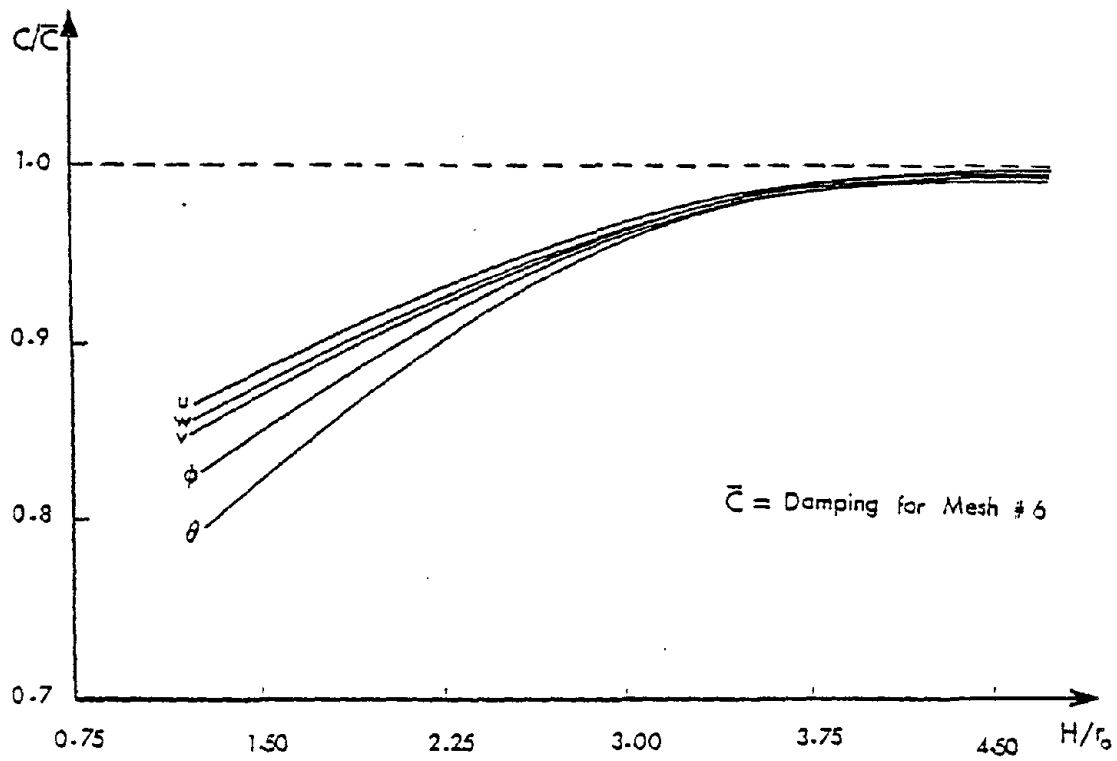

J = 1

a_0 = 1.64

r_0 = 80'

D = 0.05

Figure 12. Effect of Stratum Depth on the Damping

factor as may be observed from Figure 12. The lesser sensitivity of the damping elements with the stratum depth suggests that the damping is mainly due to the radiation of the waves horizontally in the far-field and that the vertical radiation of the waves is not a major factor.

The study of the stratum depth presented herein suggests some useful guidelines which may expedite the parametric study. One very important finding is that the stiffness elements are the most sensitive of the EBS components. Also, the results reveal that the assumption of a fixed lower boundary at a depth $H = 3r_o$ is reasonable.

3-8b Effect of the Driving Frequency

To study the effect of the driving frequency on the EBS components, a frequency ratio a_o is considered for the range $1/\pi$ to 2 (8), where

$$a_o = \frac{\Omega r_o}{v_s} \tag{3-71}$$

and v_s is the shear wave velocity for the stratum. The antisymmetrical Fourier harmonic (j=1) is considered in the study using mesh of Figure 10 with the ratio $H/r_o = 3$.

Figure 13 shows the dependence of the stiffness elements on the driving frequency. It is evident that both translational and rotational stiffnesses are very sensitive to the change of a_o. The sensitivity of the stiffness elements may be understood by examining Equation (1-61), where the

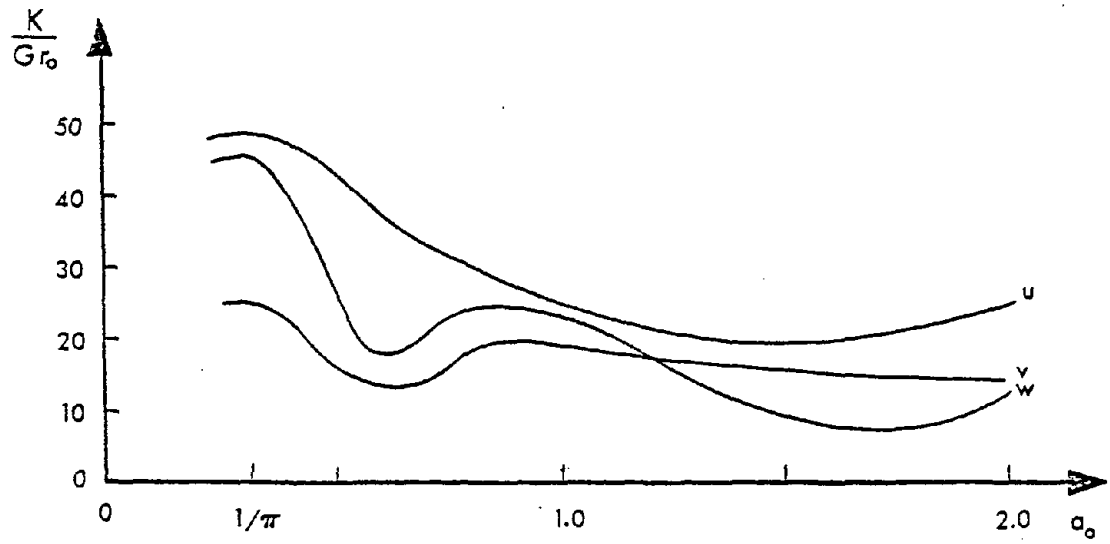

13-a

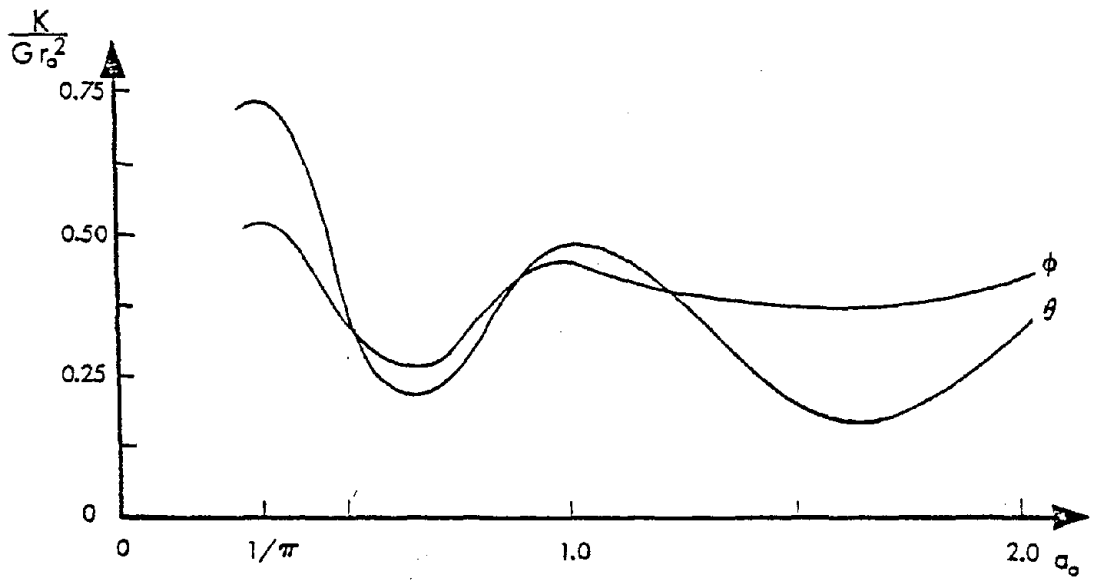

13-b

Figure 13. Driving Frequency Effect on Stiffness in Antisymmetrical Modes

second and third terms of the RHS of the equation are functions of the driving frequency Ω. Similar observations may be applied to the damping elements in Figure 14. However, the damping elements are less dependent on the excitation frequency than the stiffness elements. This conclusion agrees with the results presented in References 8 and 35.

3-8c Higher Harmonics

In Figures 15 and 16 the results of the first six Fourier harmonics (j = 0 to 5) are shown. The same mesh used for the driving frequency study is retained and the excitation frequency ratio a_o is taken equal to 1.64. It is interesting to notice that the EBS parameters for $j > 1$ are approximately constant for the u, v and ϕ components, while the w and θ components (vertical and rocking), show more variation. This observation may be useful in reducing the size of the problem if the stiffnesses and damping elements of the higher harmonics are considered to be independent of the Fourier number j and suggests a helpful procedure to determine the EBS components for $j > 1$ with the aid of one harmonic number j, $(j \geq 2)$.

3-8d Mesh Study

To evaluate the convergence of the finite element solution with decreasing element size, four meshes with a depth ratio $H/r_o = 3$ were considered. Soil material properties used in the analysis are given in Table 1. The four meshes along with the results are shown in Figure 17.

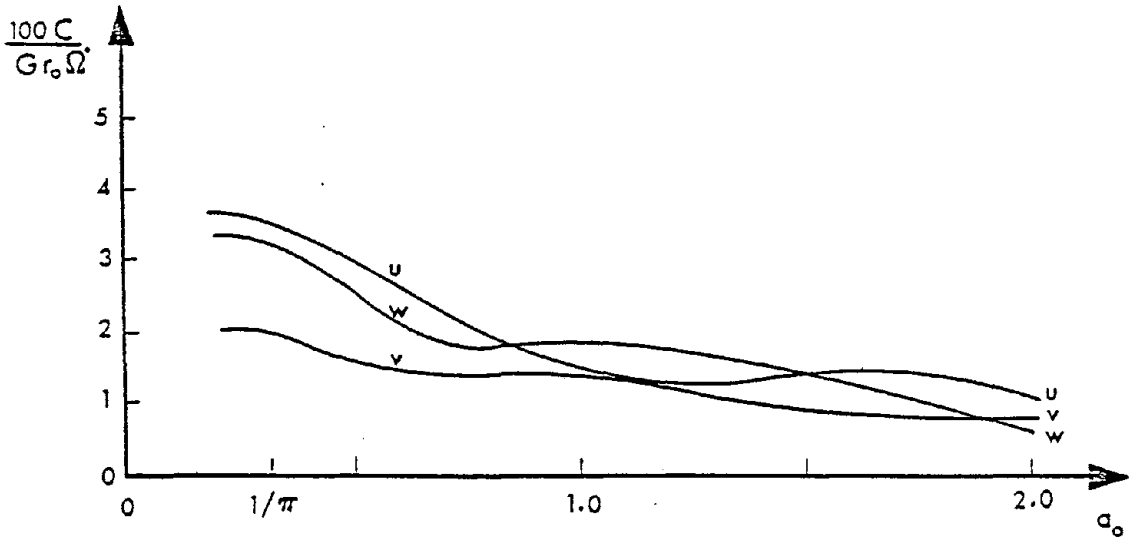

14-a

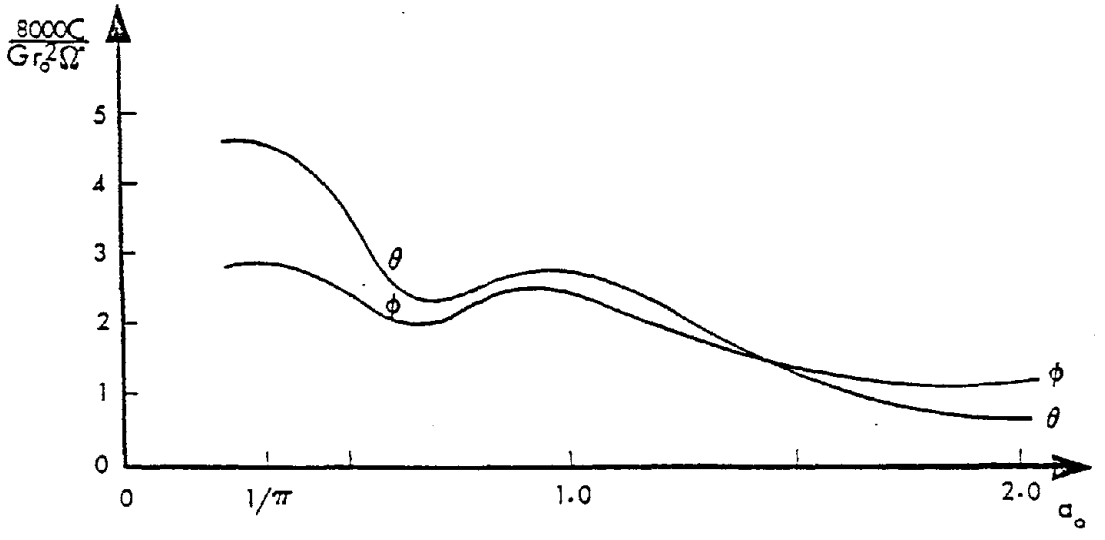

14-b

$\dot{\Omega} = \Omega|_{a_0 = 1.64}$

Figure 14. Driving Frequency Effect on Damping in Antisymmetrical Modes

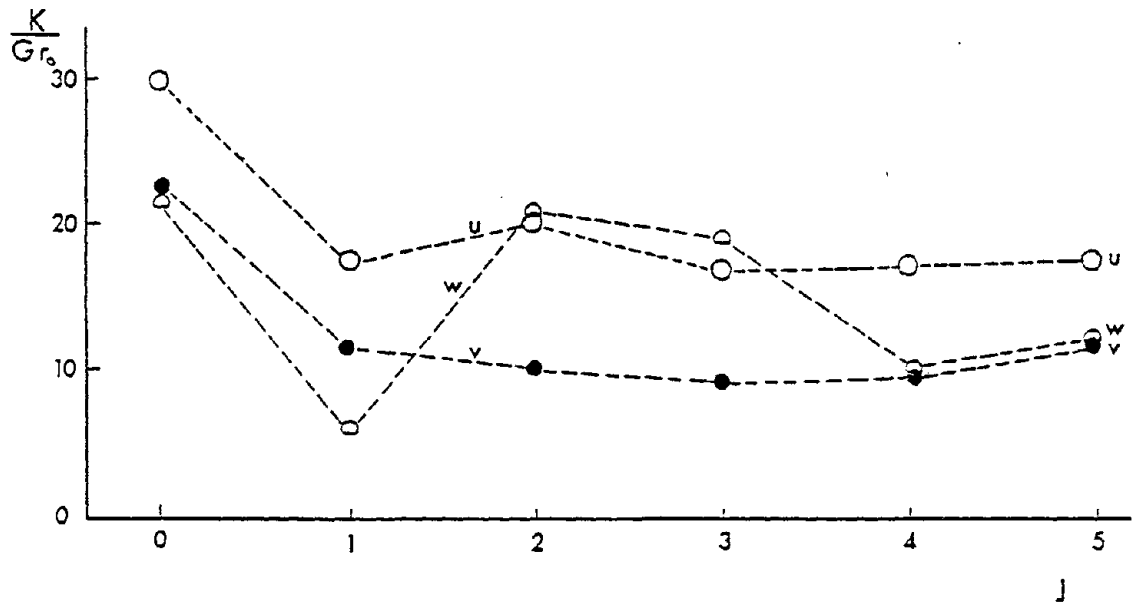

15 – a

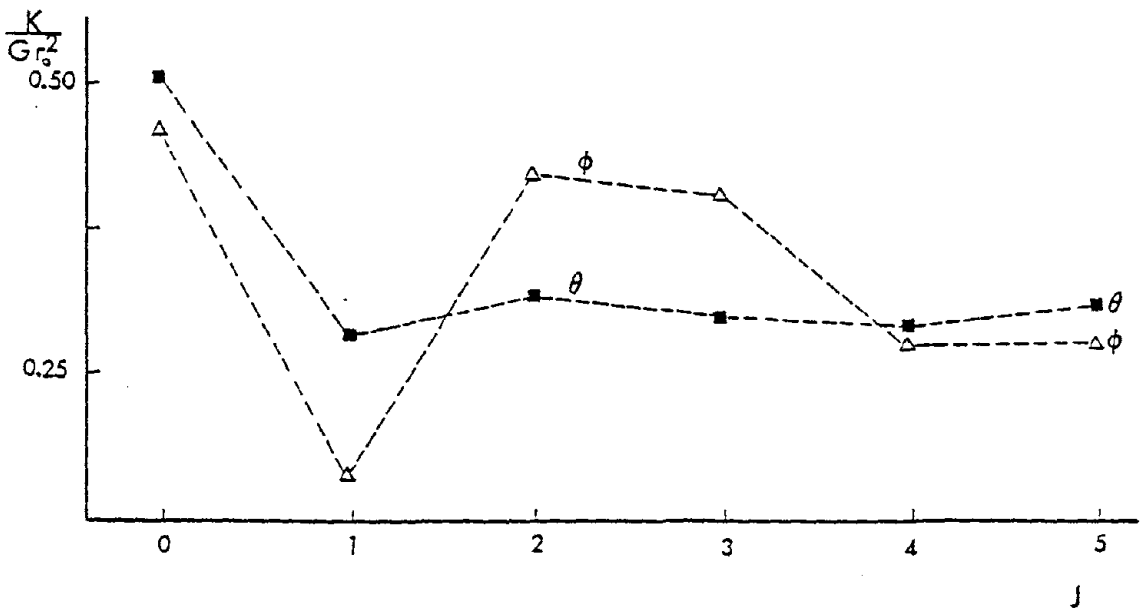

15 – b

$a_0 = 1.64$

Figure 15. Stiffness Elements in Higher Fourier Harmonics

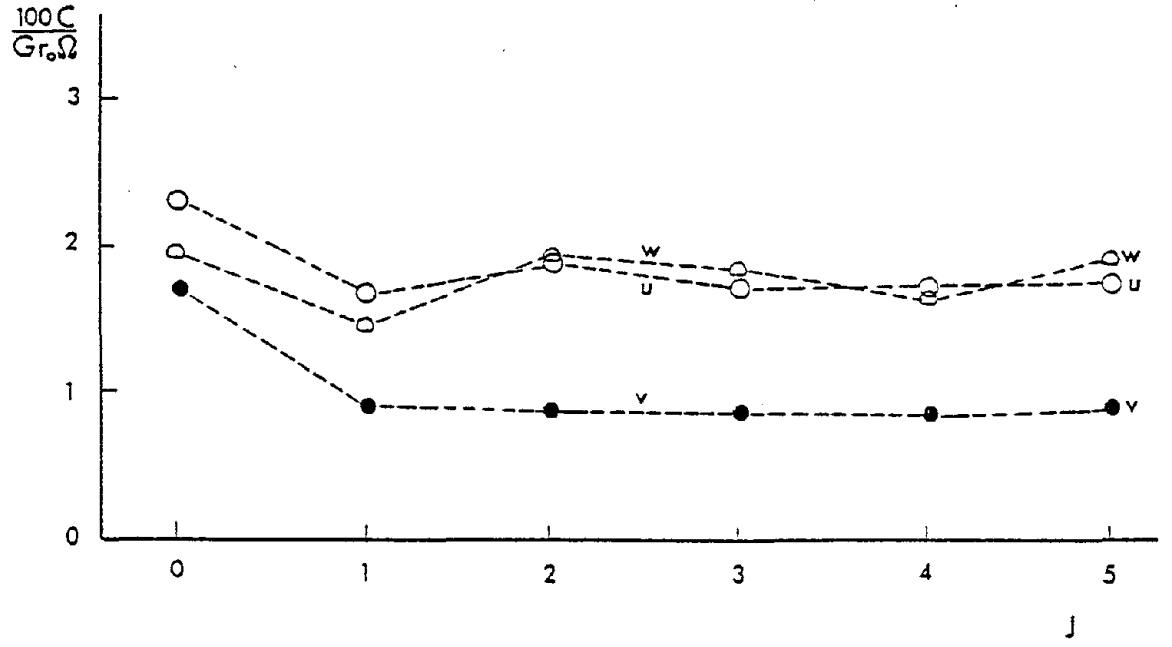

16 – a

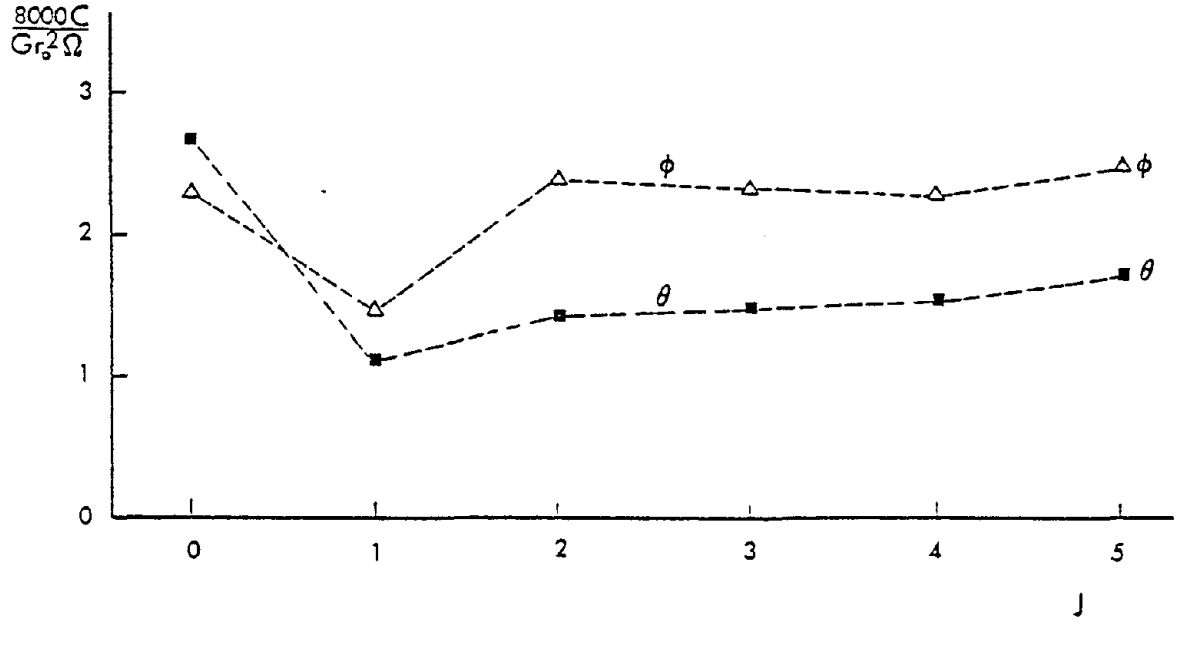

16 – b

$a_0 = 1.64$

Figure 16. Damping Elements in Higher Fourier Harmonics

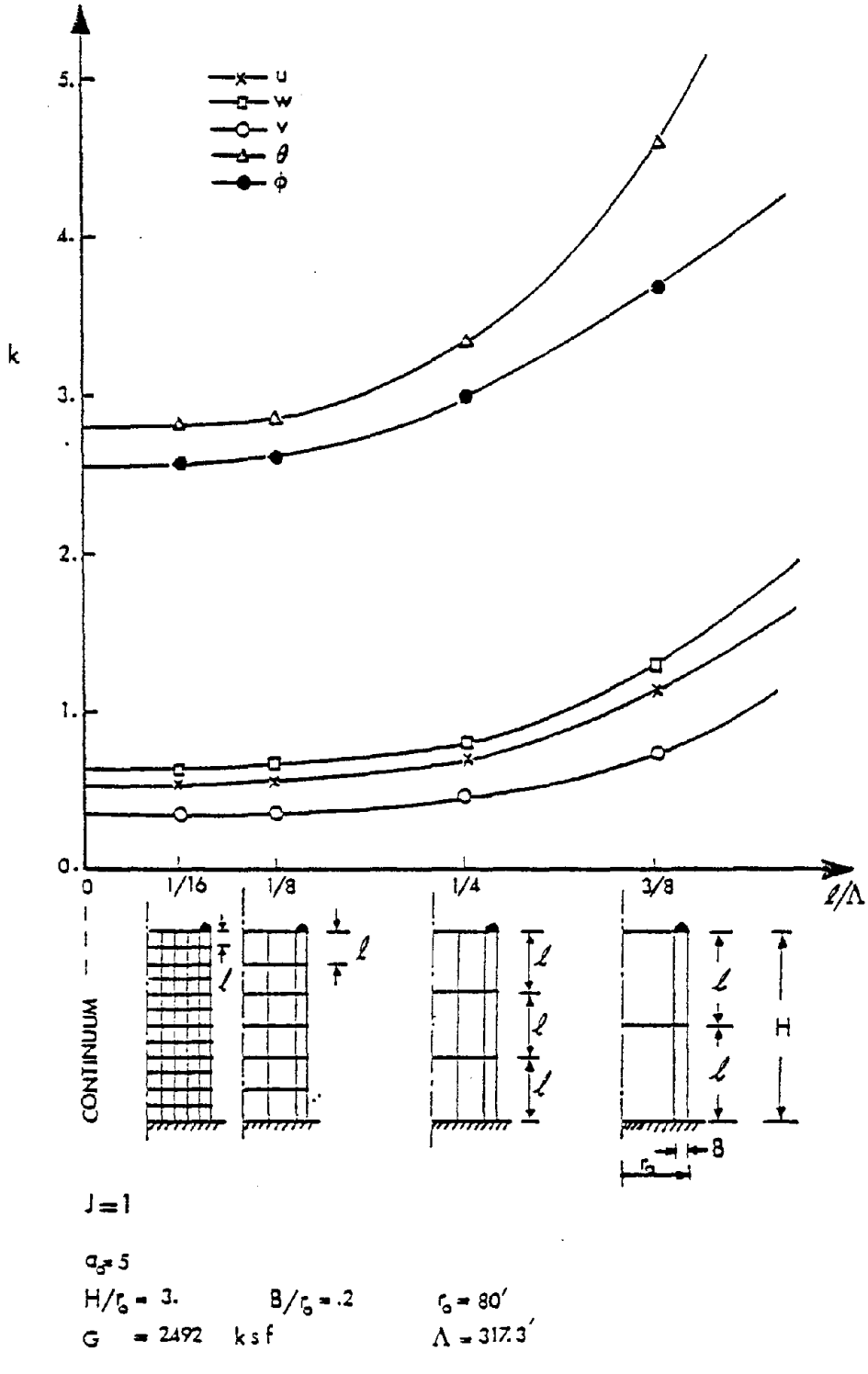

Figure 17. Element Size Effect
(Uniform Layers)

Only the dimensionless stiffness elements k are plotted against the element size ratio ℓ/Λ, where

$$\begin{aligned} k &= K/Gr_o \qquad (u,w,v) \\ &= K/Gr_oB \qquad (\theta,\phi) \end{aligned} \tag{3-72}$$

ℓ is the longest element dimension in the mesh, and Λ is the shear wave length.

In Figure 17 the continuum solution could be extrapolated by the intersection of the curves with the vertical axis ($\ell/\Lambda = 0$). The results indicate that the largest element dimension in the mesh should not exceed $\Lambda/6$ for satisfactory results in case of a uniform mesh. Also, it may be observed that the rate of convergence for the five components is approximately the same and that it is very slow for element size ratio less than 1/8.

In order to investigate the possibility of using larger elements with increasing depth, another four meshes are considered with same soil properties and depth ratio as those used in the convergence study. Knowing the continuum solution for the EBS from the convergence study, the errors in the finite element solution of the four meshes are calculated and plotted against the ratio 100/n, where n is the total number of elements in a mesh, Figure 18. Also, the four meshes used in the study are shown in the same figures.

It is interesting to notice that the mesh with twenty elements produced results with error as small as 0.7% of

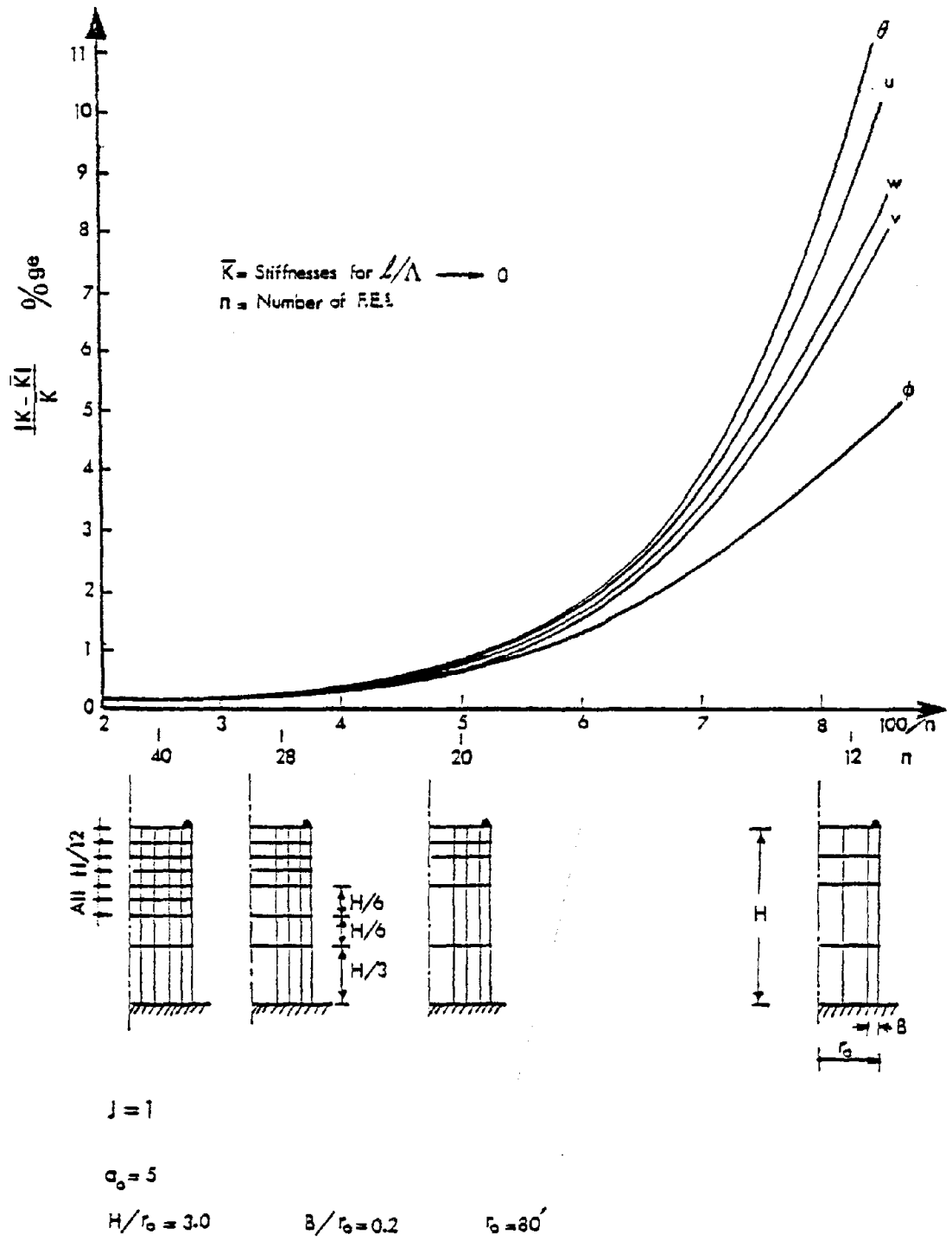

Figure 18. Mesh-Effect
(Non-Uniform Layers)

the continuum solution, although elements with dimensions equal to $\Lambda/4$ are used. Also, the results indicate only negligible differences between the two meshes with twenty eight and forty elements, which suggests that the spurious reflection of the elastic waves may be significant in these types of grids; however, more study is needed to substantiate this observation (36).

It should be noted here that the geometry of the foundation, which is a ring footing, affects the mesh size and the elements refinement near the foundation level. In extreme cases, where B/r_o gets small (less the 0.1), the zone of influence or the so-called dynamic pressure bulb will take a toroidal shape below the ring footing and, consequently, more economical finite element meshes may be used with large elements away from the footing, radially towards the axis of symmetry and downwards away from the dynamic pressure bulb towards the lower boundary.

4-SOIL-STRUCTURE ANALYSIS

4-1 Introduction

As mentioned earlier, many large shells such as cooling towers, are placed on rigid pile or caisson foundations. In such cases the soil-structure interaction is expected to be minimal, and in general, the dynamic analysis without the soil effect may yield more conservative results. However, other shells may be founded on individual footings, or perhaps on a concentric ring footing. The soil-structure interaction in this latter case could prove very important, and as a result, the analysis without the soil interaction may be incomplete. Due to the possible amelorating effect of the interaction, the internal design forces may be reduced.

In this section, the shell model is quickly reviewed and the complete model of shell-soil system is presented. The dynamic analysis is carried out in the time domain, and the soil components are formulated at a driving frequency identical to the fundamental frequency of the structure on a fixed foundation. The study is conducted on a cooling tower on a hypothetical foundation, with a variety of soil conditions chosen to generate a trend of results from which some conclusions may be drawn.

4-2 Soil-Structure Model

Figure 19 shows the finite element model for the shell-soil system. The shell is represented by high-precision

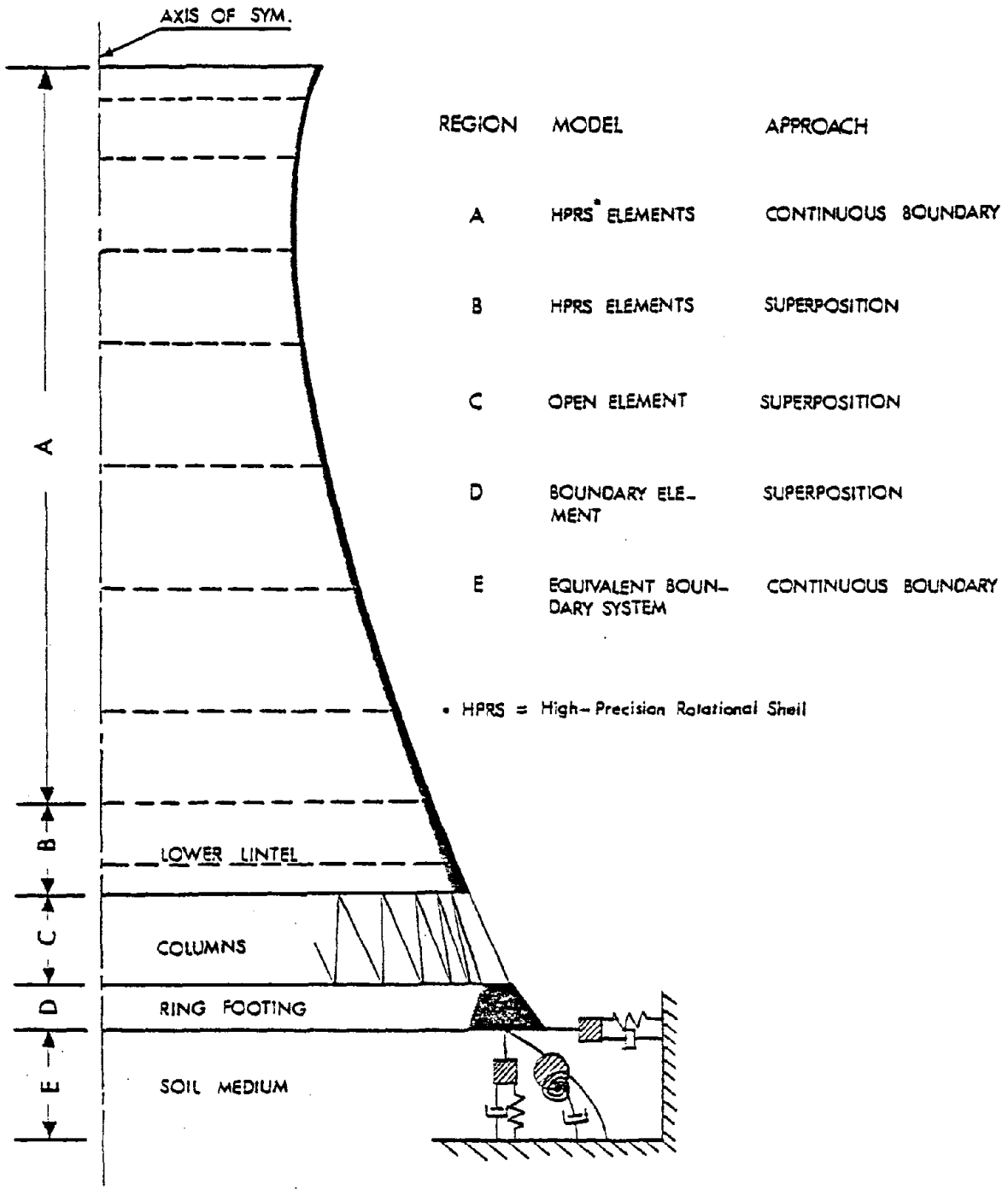

Figure 19. Proposed Model for a Cooling Tower Shell

rotational shell finite elements, while the soil medium is represented by a dynamic boundary system at the common degrees of freedom between the shell foundation and the underlaying soil.

For the shell elements (Figure 20), the strain-displacement relationships used in the formulation include the effect of transverse shear deformations. In forming the element stiffness and mass matrices, displacement fields of arbitrary order, i.e., linear to sixth order, can be used, and because only C^o continuity is required to be satisfied, the extra coefficients in quadratic and higher order displacement-fields are eliminated by kinematic condensation at the element level. Proportional damping is assumed and the damping matrix is arrived at through a linear combination of the condensed stiffness and mass matrices.

4-3 SCHEME OF COMPUTATION

The master flow chart of the computation scheme is presented in Figure 21. In this model the calculation of the displacements and stresses in a shell of revolution subjected to a general loading (static or dynamic loading which may be symmetrical, antisymmetrical or with any distribution pattern around the axis of symmetry of the shell) is treated. The simplest case of loading is static, for which no soil effect need be considered in the analysis; however, the load distribution may be complicated and a Fourier series expansion

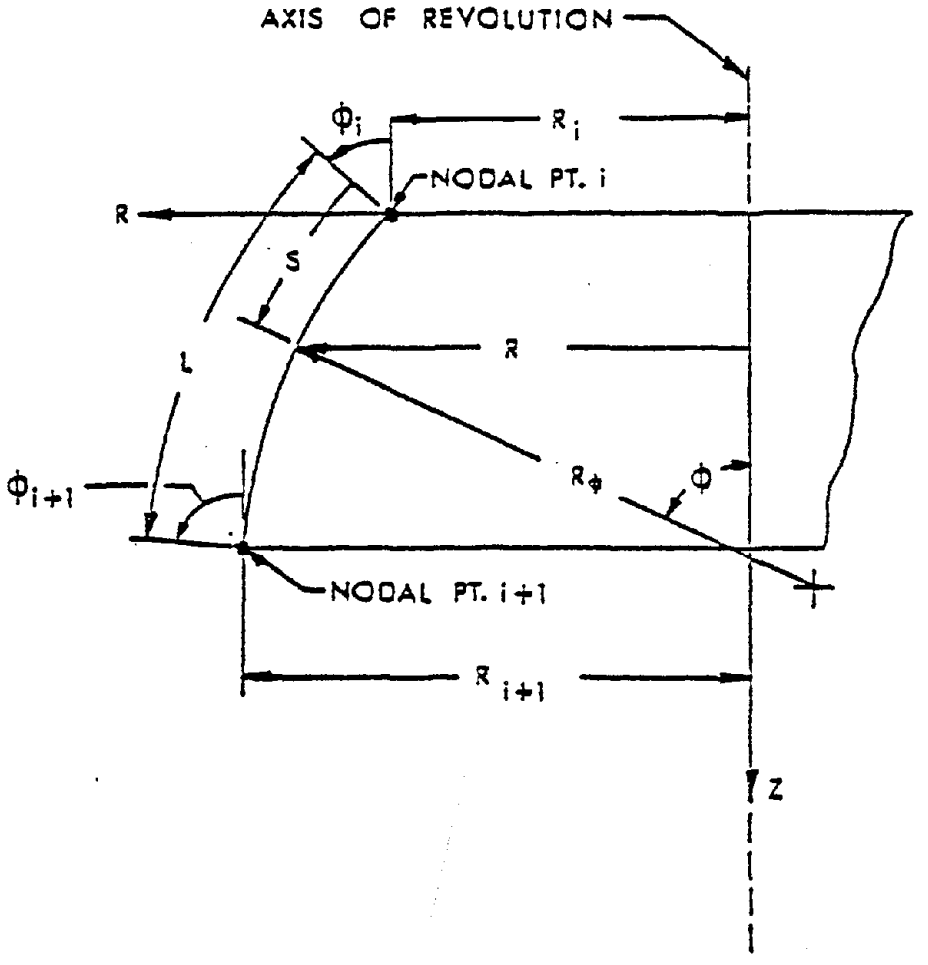

Figure 20. Shell F.E.

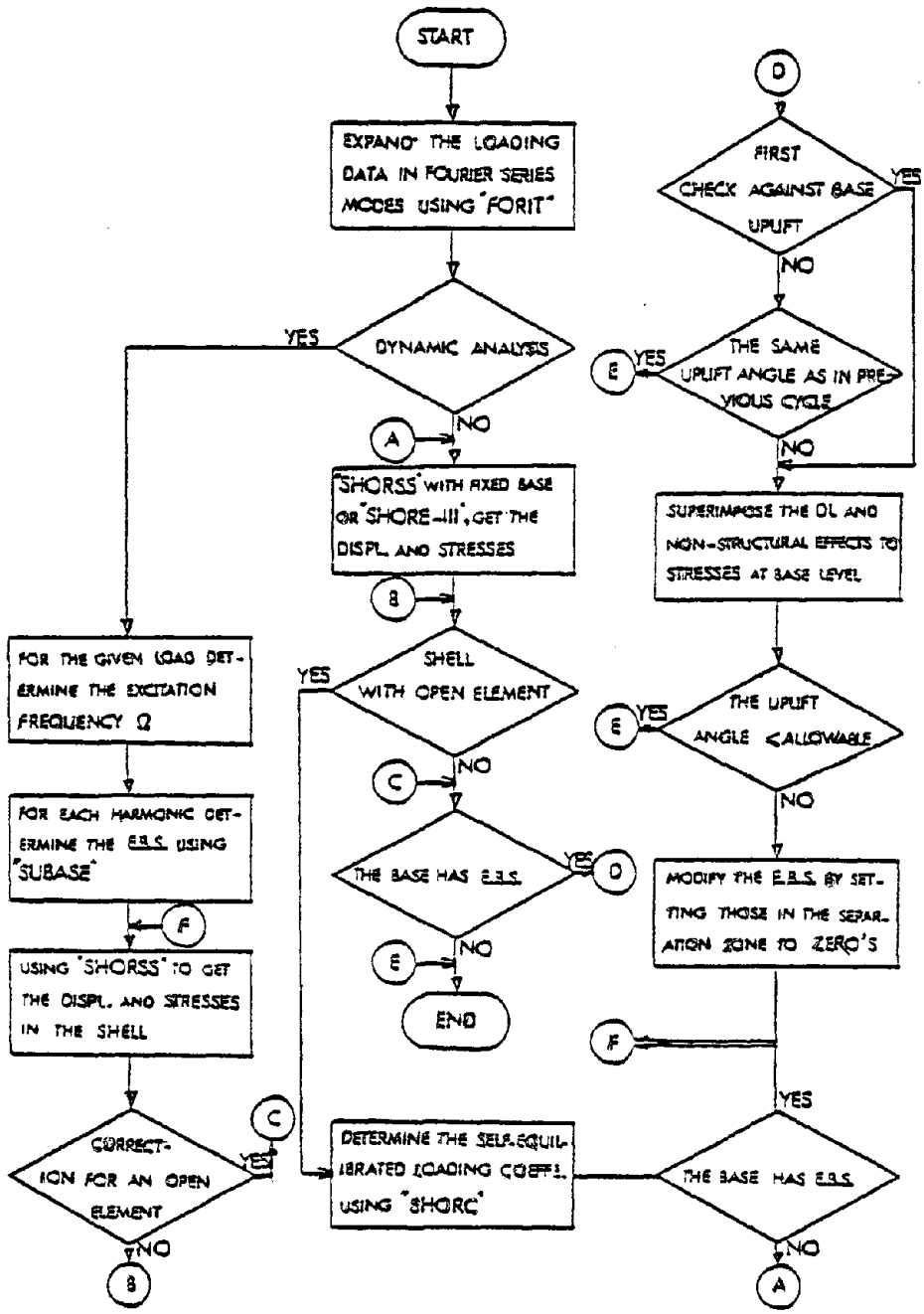

Figure 21. Computational Scheme

is required to carry out the analysis harmonicwise. The Shell of Revolution Soil System program (SHORE IV),with a fixed lower boundary (infinite stiffness and zero damping for the EBS), follows the same computational algorithm as contained in the SHORE-III program (37-38) in this case.

In case of dynamic analysis, the soil effect is introduced to provide a more realistic model. The EBS may be evaluated and referred to the foundation level using the program SUBASE; then the dynamic analysis is carried out harmonicwise using the SHORE IV program which is described in the companion volumes to this report (39-40).

To account for the possibility of uplift, the stresses at the foundation level should be checked, with any net tensile stresses corresponding to uplift; however, the dead load stresses as well as the effect of any non-structural elements tied to the shell foundation should be included in calculating the net tensile stress at the soil-foundation interface. If the separation zone is significant, the analysis should be carried out again with a modified EBS with zero stiffness and damping in the separation zone. The modification may be accomplished by expanding the modified EBS in Fourier series and introducing the resulting modal values into the ring footing. The analysis is completed if the resulting separation angle, Figure 22, is the same as in the previous cycle.

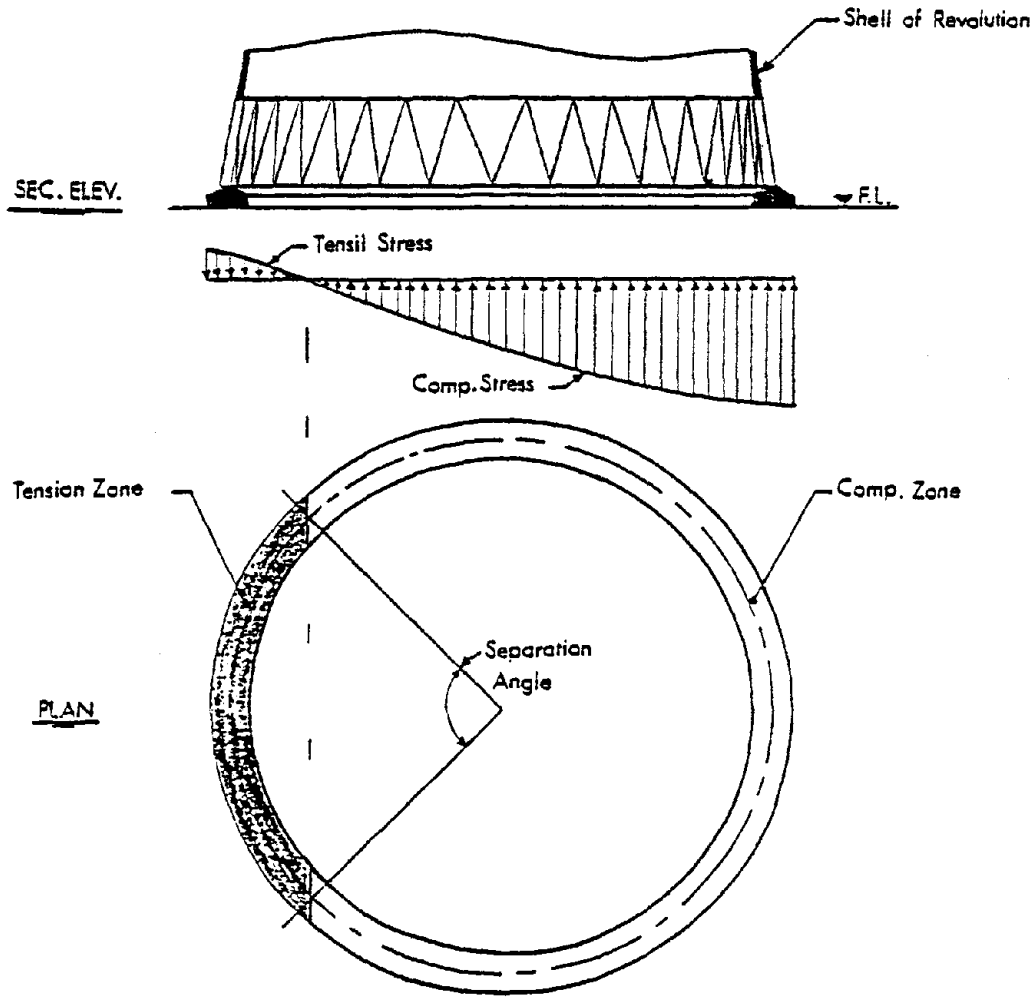

Figure 22. Base Uplift

For shells with column supports, the local stresses near the base should be corrected. This is facilitated by the application of a static superposition technique whereby the solution is taken as a combination of the continuous boundary case and a self-equilibrated line load case, both of which are represented in Fourier series, Figure 23. A computer program to evaluate the Fourier coefficients, the SHORC program, was developed by the authors of this report and is described and listed elsewhere (41). The correction should be carried out in the ring footing as well. It should be noted here that the FORIT program (see Figure 6) is capable of evaluating the Fourier coefficient for any loading distribution including the particular case of a self-equilibrated line load.

4-4 FREE VIBRATION ANALYSIS OF A COOLING TOWER ON RING FOOTING

To investigate the soil effect on the dynamic properties of rotational shells, a free vibration analysis of the reinforced concrete cooling tower shell shown in Figure 24 is carried out. The tower is assumed to have a shallow ring footing foundation and the shell meridian consists of three curves with slope continuity at the junction points (nodal points #4 and #7). Equations for the shell meridian are given in Table 3. Three soil cases are considered: (I) a soft to intermediate soil; (II) an intermediate to stiff soil; and (III) a soil with fundamental frequency close to

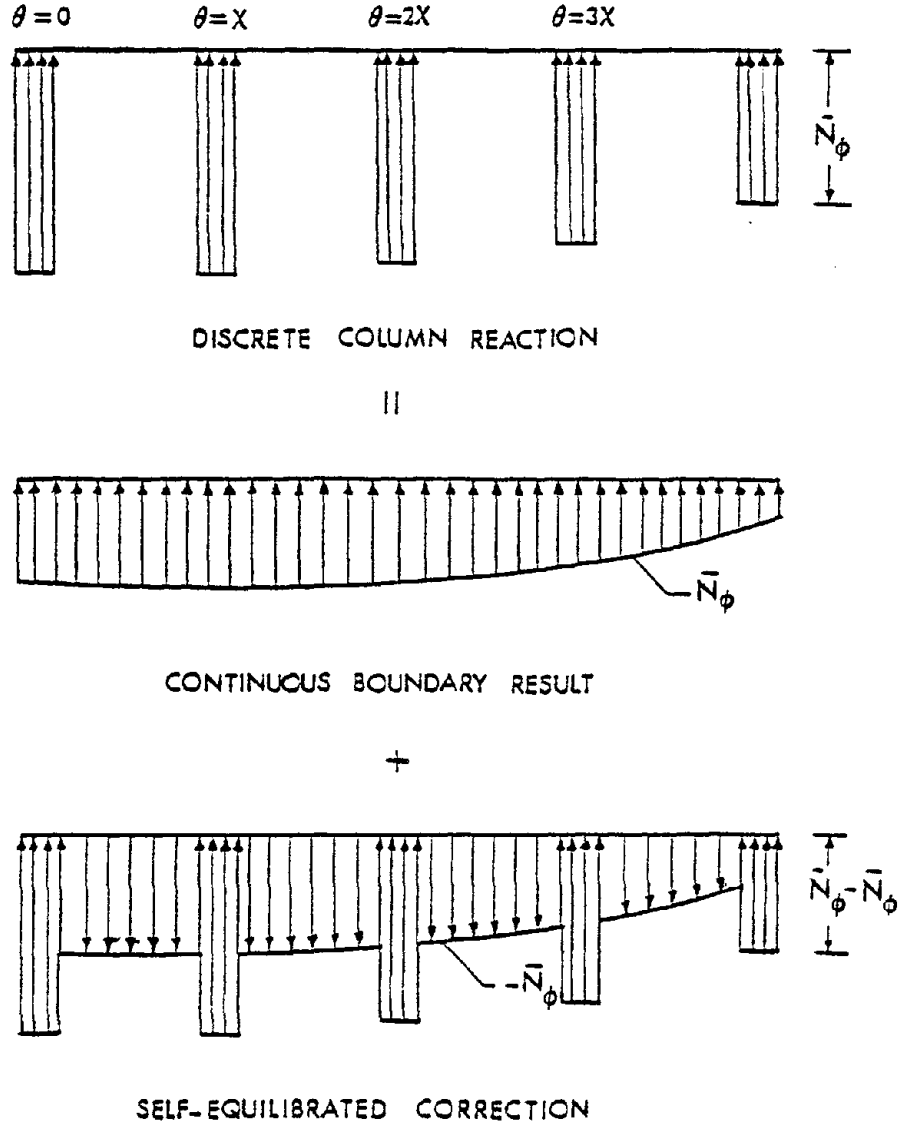

Figure 23. Discrete Column Analysis

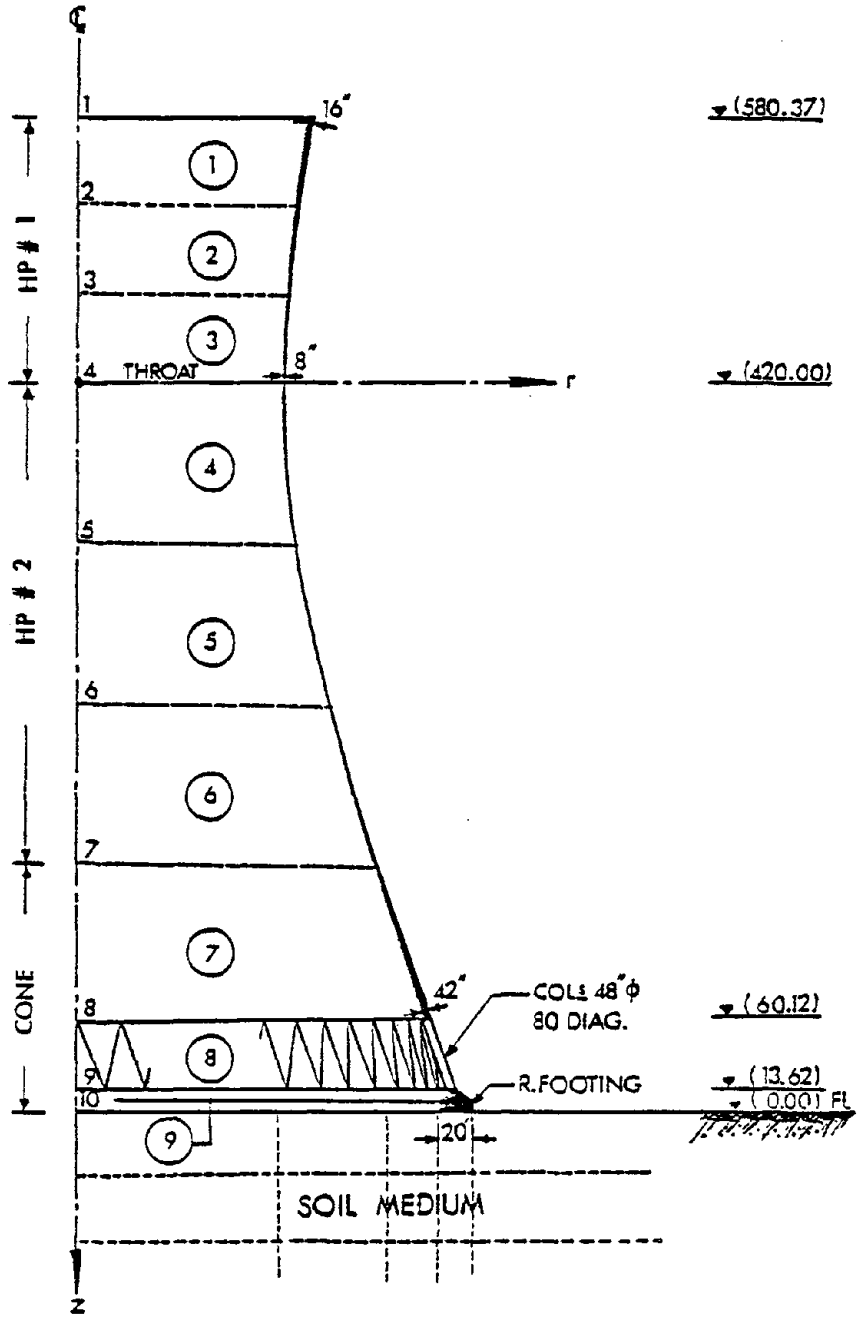

Figure 24. Cooling Tower on a Hypothetical Foundation

Table 3. Shell Meridian of the Structure Under Study

Shell Type	Nodes		Equation
	From	To	
HP #1	1	4	$z^2-123.68377\ r^2 + 27587.5165\ r - 1536846.5 = 0$
HP #2	4	7	$z^2-9.40153\ r^2 + 1302.5923\ r - 25462.9 = 0$
CONE	7	10	$0.3z - r + 87.2112 = 0$

that of the structure so that strong amplification due to resonance effects, if present, would show up. An additional case (IV), structure founded directly on competent rock, is considered as a basis of comparison. The details of the soil properties are given in References 16 and 31.

The analysis is carried out with a driving frequency of Ω = 12.34 rad/sec (the fundamental frequency of the shell on a fixed foundation) for the antisymmetrical mode (j = 1). The EBS are computed using a soil model with 24 elements and a depth ratio H/r_o in the range of 3, except for Case II where the bed rock is at 250 ft. below the foundation level.

The natural frequencies for the first three modes are given in Table 4. The change in the fundamental frequency is found to be only in the range of 5% of the fixed base frequency so that any further approximation in the EBS using the resulting interactive frequencies is unnecessary. On the other hand, the decrease in the frequency of the second mode reaches 25% of the fixed base case (Case IV). The change decreases as the soil gets stiffer, as may be observed by comparing the frequencies of the four cases in Table 4.

In Figure 25, the first three normalized eigenvectors for cases I and IV, which represent the extreme soil conditions, are shown. For the soft to intermediate soil case (Case I), the interactive eigenvectors of the second mode are drastically different than the fixed case (Case IV),

Table 4. First Three Natural Frequencies of the Studied Cases

	ω_1 Rad./sec.	ω_2 Rad./sec.	ω_3 Rad./sec.
Case I	11.84	14.86	27.19
Case II	12.02	17.46	32.41
Case III	11.85	14.98	27.33
Case IV	12.34	19.26	36.37

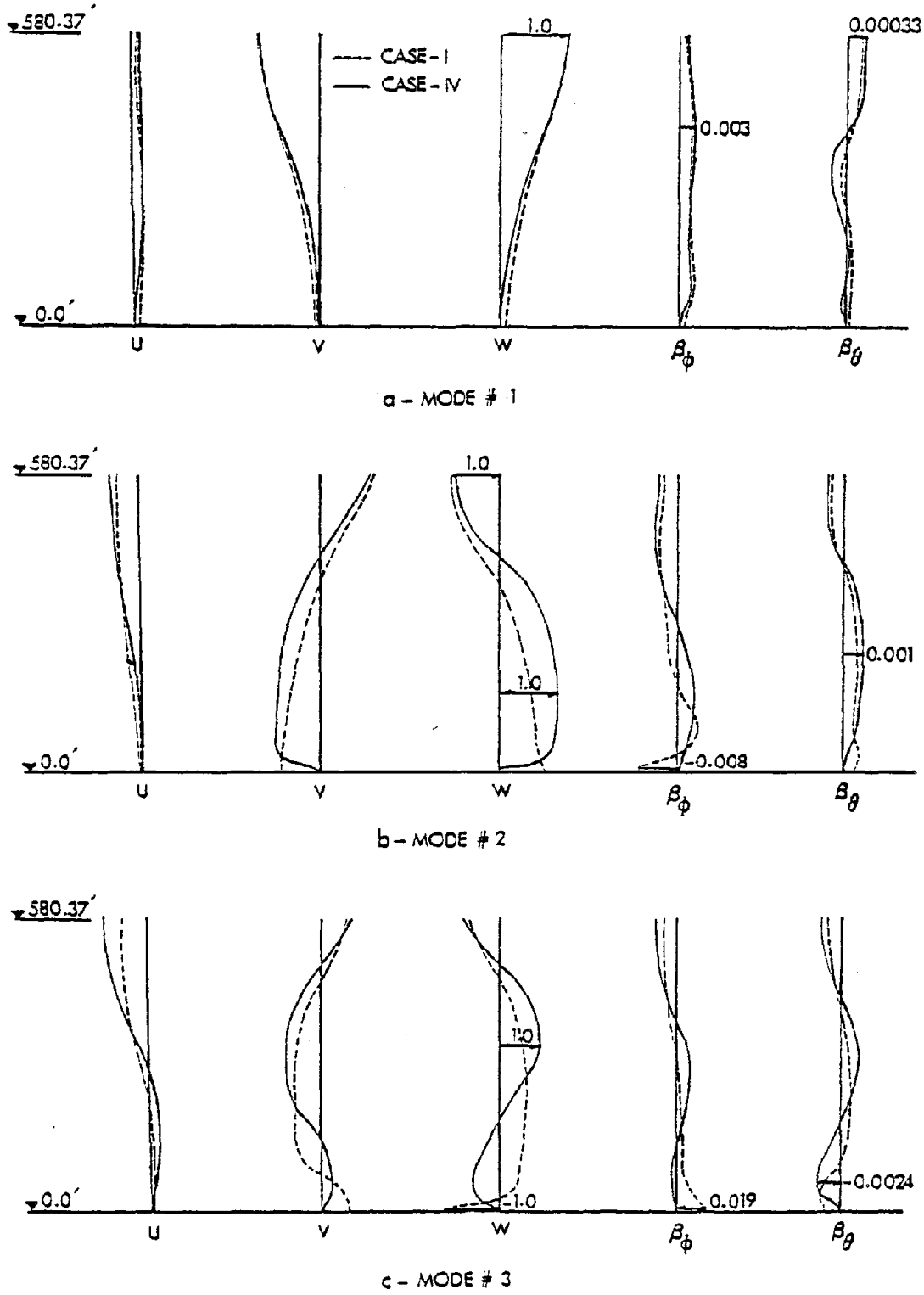

Figure 25. Soil Effect on the Antisymmetrical Eigenvectors of a Cooling Tower

whereas there is not much difference between the eigenvectors of the first mode for the two soil cases. A similar but less predominant influence of the soil on the interactive eigenvectors is observed for Case II (the stiff-shallow soil case). The eigenvectors of Case III are found to be very similar to those of Case I. This may be attributed to the combined effect of the soil depth and the shear modulus producing very similar compliances for the first and the third soil cases.

4-5 RESPONSE SPECTRUM ANALYSIS

To assess the importance of soil-structure interaction on the stress resultants and stress couples in the shell, a response spectrum analysis is carried out using the same four soil cases employed in the free vibration analysis as a supporting medium for the tower of Figure 24. The shell-soil systems for the four cases are subjected to a horizontal response spectrum with 20%g ground acceleration, Figure 26, and a damping ratio of 5% is considered for the first three modes of vibration in all cases. The high intensity of the ground motion is chosen for the purpose of approaching the case of foundation uplift, if present.

The stress resultants and stress couples at $\theta = 0^{o}$ for the shell are given in Figures 27 through 30. It can be seen that the fixed base case produces resultant forces which envelop all soil cases, except for N_{ϕ}, when a fixed base

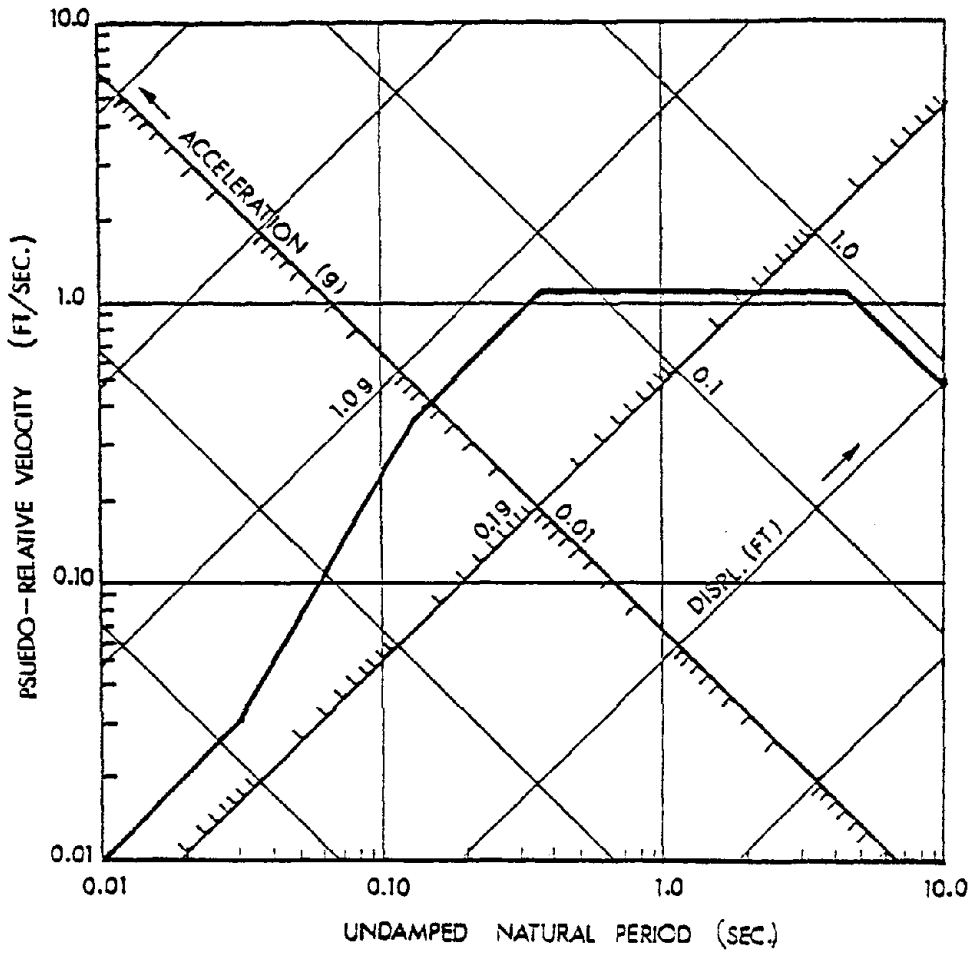

Figure 26. Horizontal Response Spectrum

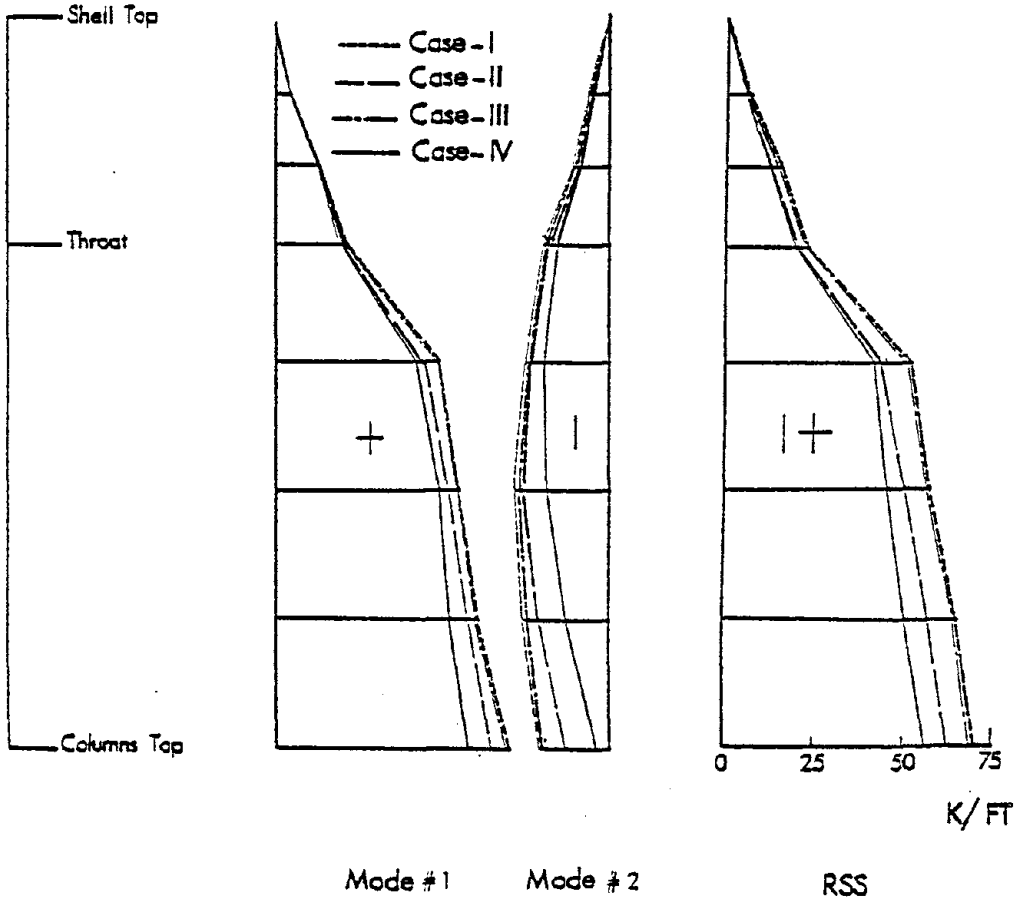

$(J = 1\ ,\ \theta = 0^{\circ})$

Figure 27. N_ϕ-Component, Earthquake Load

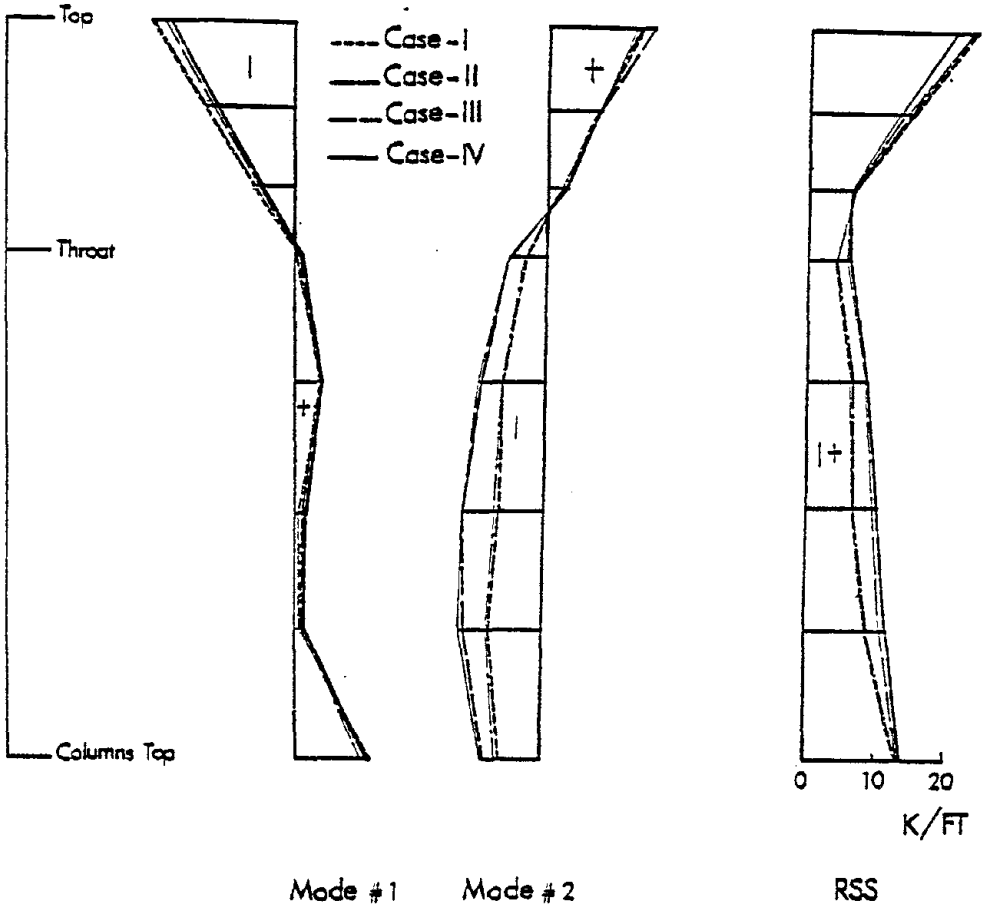

(J=1 , $\theta = 0^\circ$)

Figure 28. N_θ-Component,
Earthquake Load

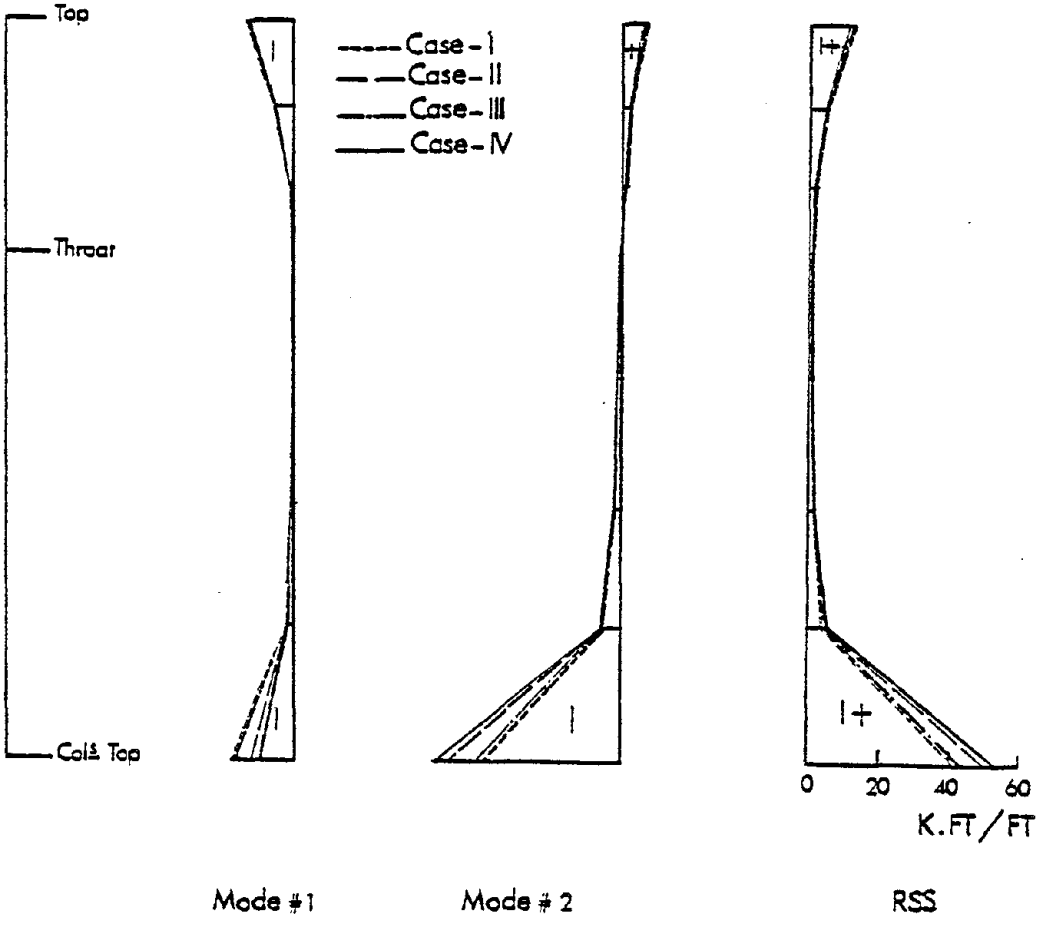

$(J=1\ ,\ \theta=0^{\circ})$

Figure 29. M_{ϕ}-Component, Earthquake Load

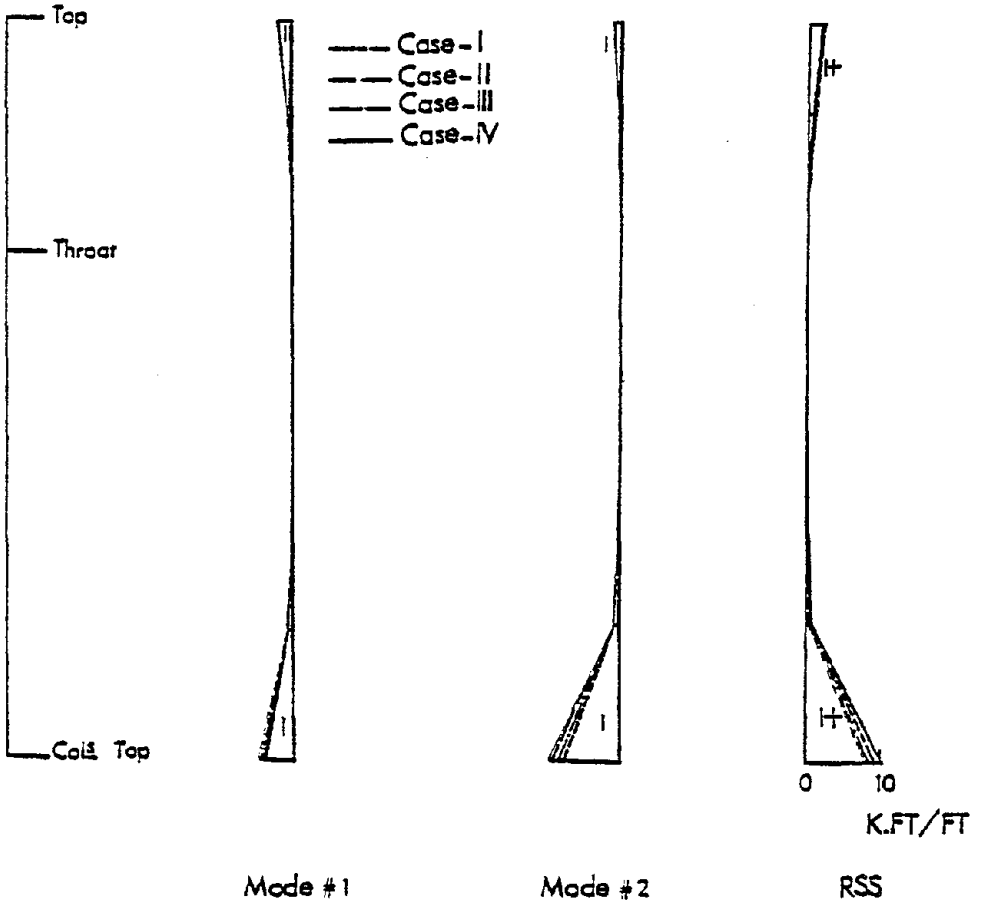

(J = 1 , $\theta = 0^{\circ}$)

Figure 30. M_{θ}-Component, Earthquake Load

condition (Case IV) is used, but this may be an extremely conservative approach.

No significant amplification due to suspected resonance effects is seen in the stress resultants and stress couples for Case III. This is due to the fact that the rocking and swaying motions tend to suppress the response of the structure at the fundamental frequency of the fixed base structure. This observation is in accord with the results reported in Ref. 16.

The axial forces, bending moments and twisting moments in the columns are calculated at $\theta = 0^{o}$ and the results are shown in Table 5. It may be observed that there is a sharp decrease in the axial forces and bending moments as the soil stiffness decreases. The decrease in the bending moment may be attributed to the smoothing of the second mode shape (Figure 25) in the lower region, whereas the 15 percent reduction of the axial forces may be due to the reduction in the total base shear as a result of a smaller input inertial forces due to the interaction effect.

The twisting moment in the columns increases as the soil stiffness decreases. However, the values of the twisting moments are not large enough to be a controlling factor in the column design as can be seen from Table 8. The response of the concentric ring footing is given in Table 9. The results presented in this table are the complete solution

Table 5. Maximum Column Forces at $\theta = 0^{\circ}$ (Horizontal Ground Motion)

Mode	Axial Force (K)				Bending Moment (K.ft)				Twisting Moment (K.ft)			
	Case I	Case II	Case III	Fixed	Case I	Case II	Case III	Fixed	Case I	Case II	Case III	Fixed
1	539.7	592.9	543.3	826.8	160.2	88.8	153.6	160.5	-14.4	-1.7	-13.1	-6.1
2	-450.1	-364.4	-451.2	-141.3	166.5	143.4	157.9	615.1	-30.3	7.8	-28.6	-17.2
3	0.2	-42.2	1.1	-19.6	1.0	398.8	9.4	17.5	-0.1	16.4	-0.3	-0.1
RSS	±702.2	±697.2	±706.2	±838.9	±240.3	±432.9	±220.5	±636.0	±33.7	±18.2	±31.5	±18.2

Table 6. Ring Footing Forces due to Horizontal Ground Motion (RSS)

Soil Case	θ	Axial Force (K)		V. Moment (K.Ft)		H. Moment (K.Ft)		Torsion (K.Ft)	
		Col.	Field	Col.	Field	Col.	Field	Col.	Field
Case I	0°	±1867.4	±1805.7	±10953.2	∓11837.4	∓809.2	±911.6	±3767.7	±4340.5
	90°	±152.4	±157.9	±715.7	∓731.6	∓32.7	±64.4	±7762.0	±7699.3
Case II	0°	±1385.0	±1361.6	±6705.0	∓7007.8	∓620.7	±701.0	±5013.1	±4897.6
	90°	±141.6	±150.7	±682.3	∓695.9	∓24.1	±54.9	±9267.4	±9226.3
Case III	0°	±1751.1	±1691.8	±9817.4	∓10911.1	∓752.5	±839.6	±4266.1	±4703.8
	90°	±146.7	±152.2	±700.5	∓715.9	∓30.8	±62.8	±8117.7	±8100.4
Case IV	0°	±392.4	±388.8	±745.7	∓699.0	∓110.0	±118.1	±6946.2	±5988.1
	90°	±23.0	±27.7	±47.7	∓50.6	∓6.7	±7.2	±11207.0	±11200.6

which consists of the continuous boundary solution and the self-equilibrated correction (See Figure 23). In the self-equilibrated correction, the SHORC program is used to calculate the Fourier coefficients for the loads and the resulting self-equilibrated loads are applied as line loads at the top of the beam which is modeled as two rotational shell elements. The highest harmonic number used in expanding the self-equilibrated loads was 440. The lower boundary of the footing consisted of static springs with zero masses and damping, i.e., the correction is carried out as static self-equilibrated forces.

Table 9 shows that the three cases of soil structure interaction give responses for the axial forces and bending moments sharply higher than the fixed base response, while the torsional moment decreases as the soil becomes softer. Convergence to the fixed base results as the soil gets stiffer is evident from Table 6. Incidentally, the values presented for the vertical moment are computed from N_ϕ results along the footing depth, since the vertical bending moment corresponds to the rotational degree of freedom about the normal axis which is neglected in linear shell theories (42).

To check against foundation uplift, the N_ϕ component of the stress resultants is computed at the foundation level for D. L., factored by 0.9 and then added to the unfactored earthquake response. The results are tabulated in Table 7.

Table 7. N_ϕ - Component at F.L. (j = 1)

D.L.	0.9(D.L.)	Case I		Case II		Case III		Case IV	
		EQ	Net	EQ	Net	EQ	Net	EQ	Net
-77.8	-70.0	64.8	-5.2	59.2	-10.8	61.9	-8.1	58.3	-11.7

Units: K/ft.

It may be seen from Table 10 that the net stress as the foundation level for all cases is compressive and no uplift occurs for the severe 20%g spectrum used in the analysis. However, it is clear that the softer the soil the more likely the uplift to occur. To investigate this possibility more closely,the vertical component of the earthquake may be included. A vertical response spectrum with 13%g ground acceleration and 5% damping is considered and the analysis is carried out at driving frequency of Ω = 32.75 rad/sec, which is the fundamental frequency of the structure on fixed base for j = 0. The RSS of N_ϕ at the foundation level for the vertical and horizontal ground motions for Case I is computed and the net value for N_ϕ is found by combining the resulting RSS value of N_ϕ with the factored D.L. value. The net value of N_ϕ is computed from the equation:

$$N_\phi(\text{net}) = (N^2_{\phi_h} + N^2_{\phi_v})^{1/2} - 0.9\, N_{\phi_d} \qquad (4\text{-}1)$$

where

N_{ϕ_h} = N_ϕ at the foundation level due to horizontal ground motion

N_{ϕ_v} = N_ϕ at the foundation level due to vertical ground motion

and

N_{ϕ_d} = N_ϕ at the foundation level due to the dead load

For Case I N_ϕ(net) is computed from Equation (4-1), with N_{ϕ_V} = 29.8 K/ft, and the resulting value of N_ϕ(net) is found to be a tensile stress of 1.3 K/ft which can cause uplift. However, N_ϕ(net) is probably too small to cause a real uplift as this net stress could be counteracted by the soil friction on the sides of the footing.

4-6 TIME HISTORY ANALYSIS

The tower of Fig. 24 was first analyzed under the El-Centro earthquake (5/18/40) EW Comp. with input in the form of Fig. 31. The soil medium is considered as an elastic half space as in the response spectrum analysis (Case 2) and then the analysis repeated with fixed lower boundary at node #10 (Case b). The time duration of the analysis is taken as five seconds and the time step for Newmark β method integration is taken 0.02 second in case a, and 0.005 second in case b. The damping coefficients (α=0.715779 and β=0.003356) are obtained based on 5% damping ratio for the first two modes of vibration (the modes of vibrations are obtained during the response spectrum analysis).

The results for both cases are plotted at selected nodes on Figs. 32-38. The use of computer plotting,which is encompassed in the SHORE-IV program,enhances the output of a time history analysis by presenting the voluminous results in a readily assimilated form. Although a wide range of parametric studies were not conducted for this time history analysis, the results are adequate to demonstrate the

Pages 116 and 117 have been removed.

Due to legibility problems, the following figure has been omitted:

Figure 31 - Input Data Echo for Time History Analysis of Hyperboloidal Shell with Soil Effect

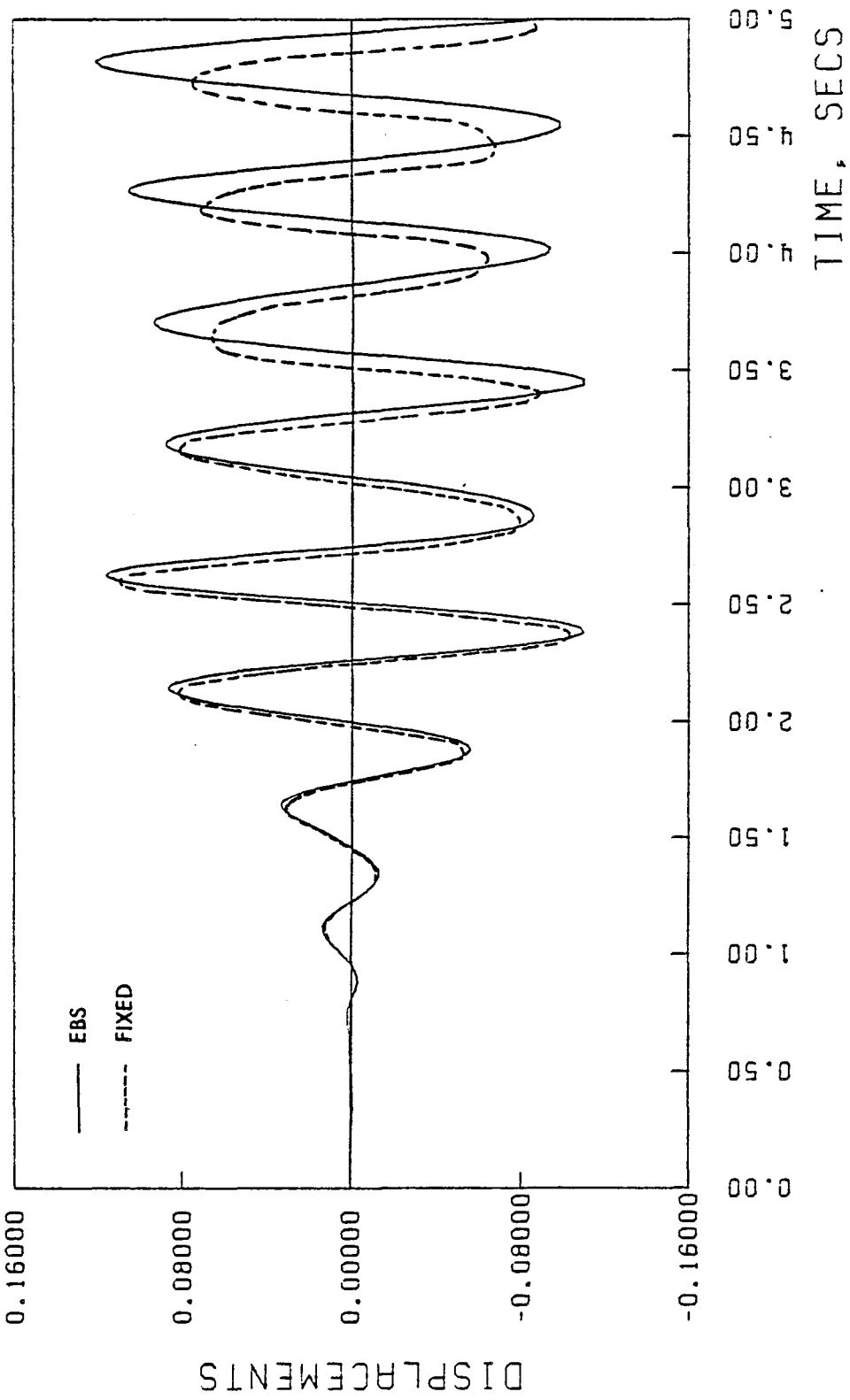
TIME HISTORY PLOT FOR HARMONIC NUMBER = 1
COMPONENT NO. 3 AT NODE NO. 1
EBS
FIXED
DISPLACEMENTS
0.16000
0.08000
0.00000
-0.08000
-0.16000
0.00
0.50
1.00
1.50
2.00
2.50
3.00
3.50
4.00
4.50
5.00
TIME, SECS

Figure 32.

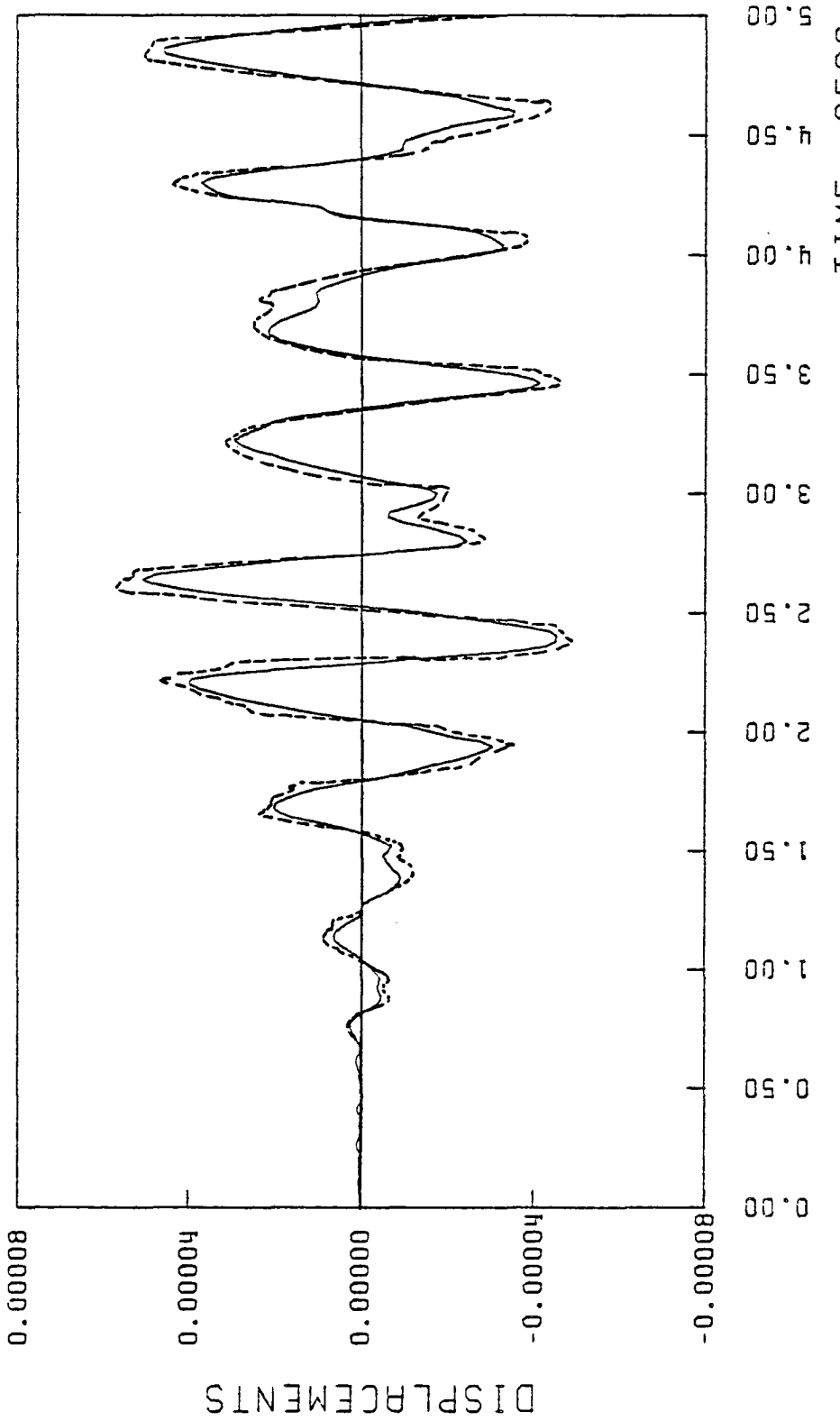

Figure 33. TIME HISTORY PLOT FOR HARMONIC NUMBER = 1
COMPONENT NO. 5 AT NODE NO. 1

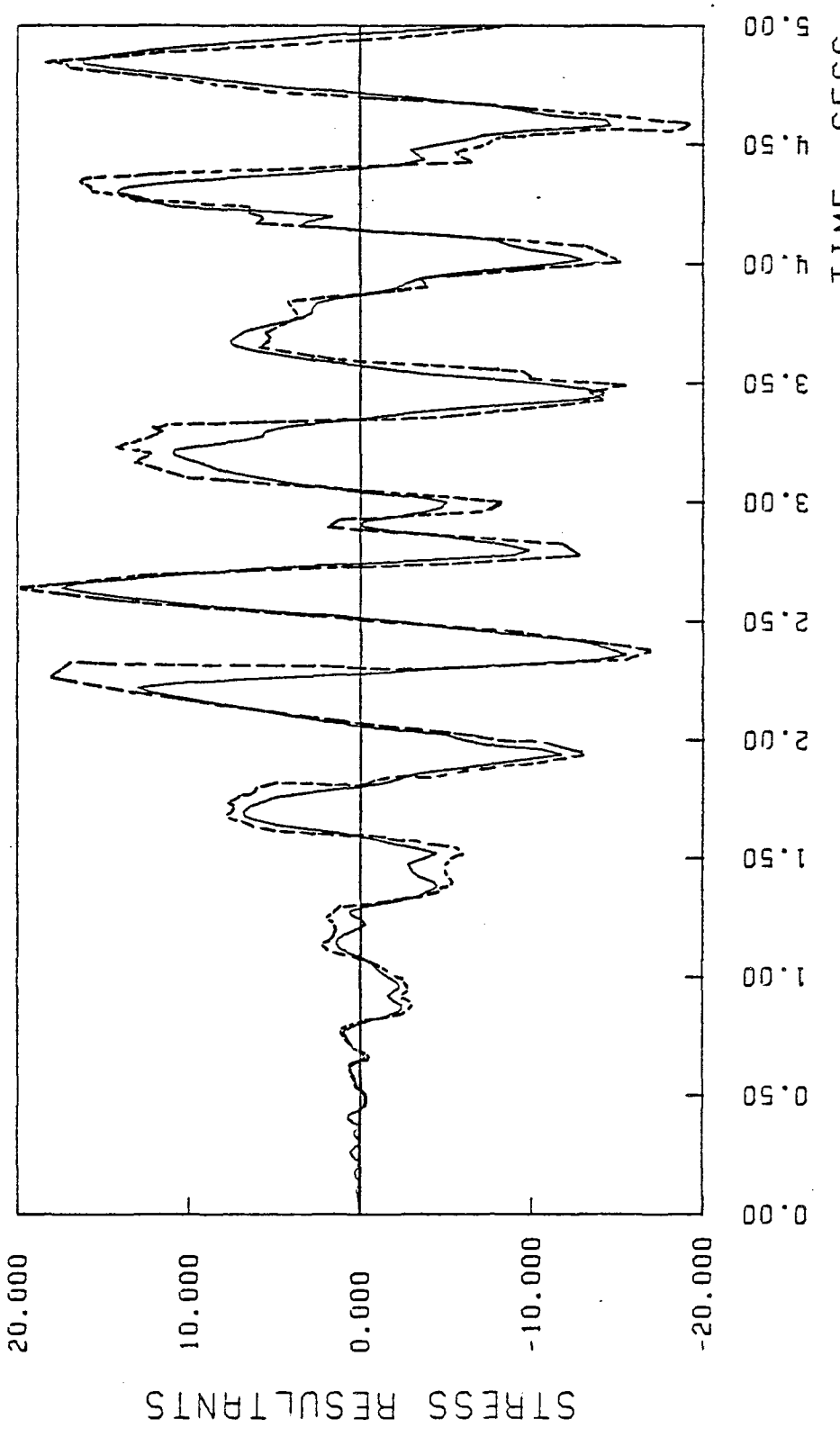
TIME HISTORY PLOT FOR HARMONIC NUMBER = 1
COMPONENT NO. 2 AT NODE NO. 1
STRESS RESULTANTS
20.000
10.000
0.000
-10.000
-20.000
0.00
0.50
1.00
1.50
2.00
2.50
3.00
3.50
4.00
4.50
5.00
TIME, SECS

Figure 34.

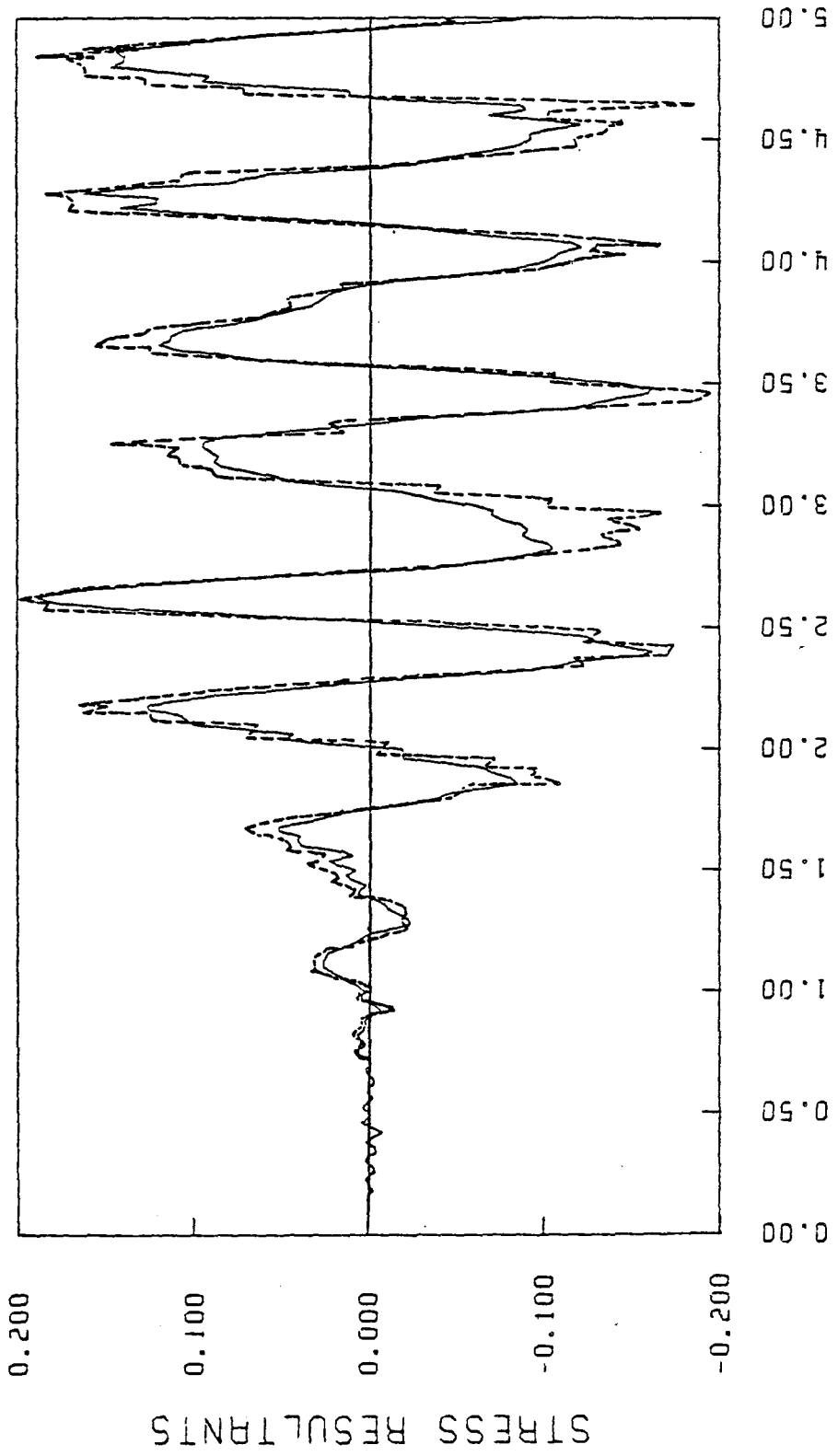

Figure 35. TIME HISTORY PLOT FOR HARMONIC NUMBER = 1
COMPONENT NO. 4 AT NODE NO. 1

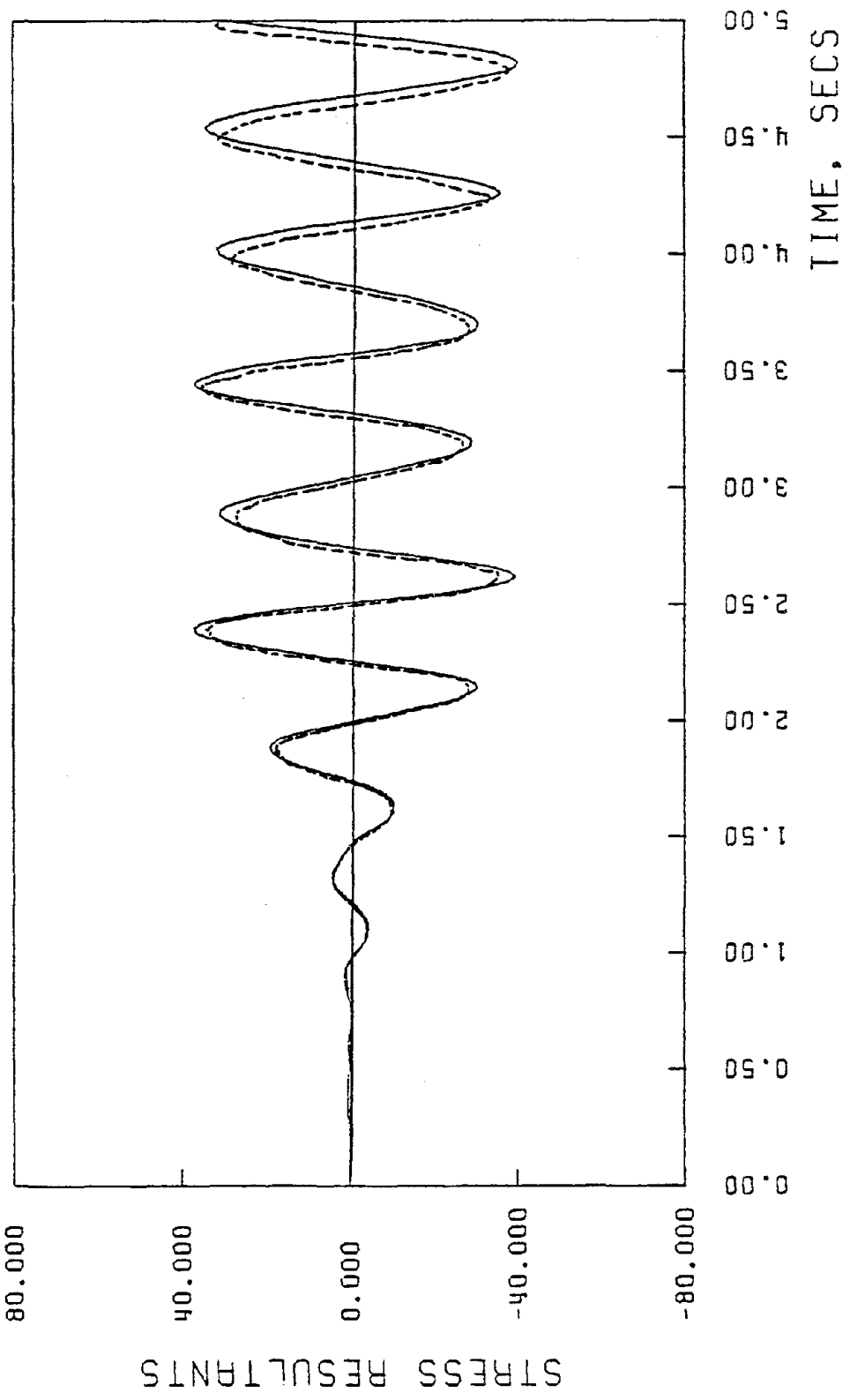

Figure 36. TIME HISTORY PLOT FOR HARMONIC NUMBER = 1
COMPONENT NO. 1 AT NODE NO. 7

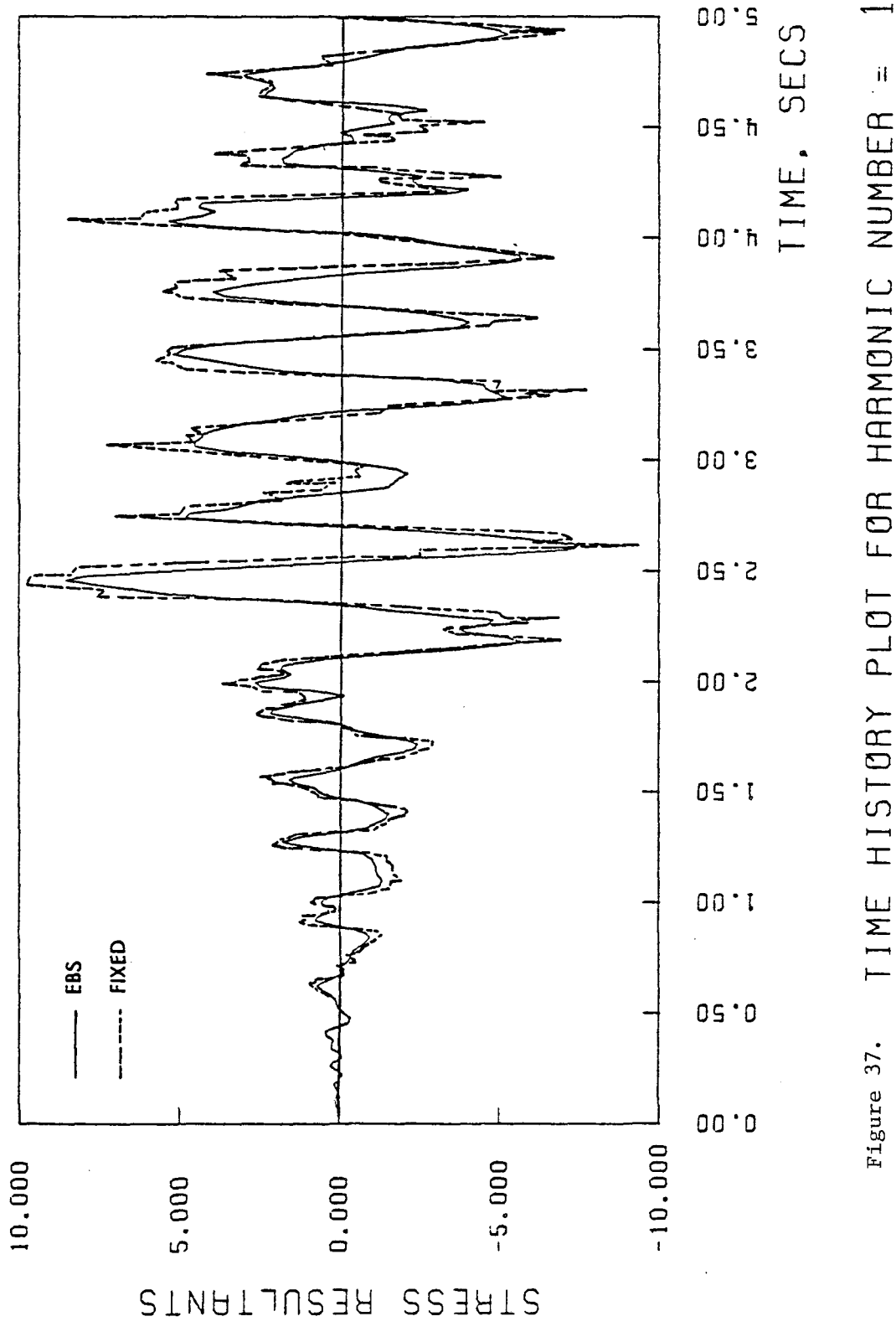

Figure 37. TIME HISTORY PLOT FOR HARMONIC NUMBER = 1
COMPONENT NO. 2 AT NODE NO. 7

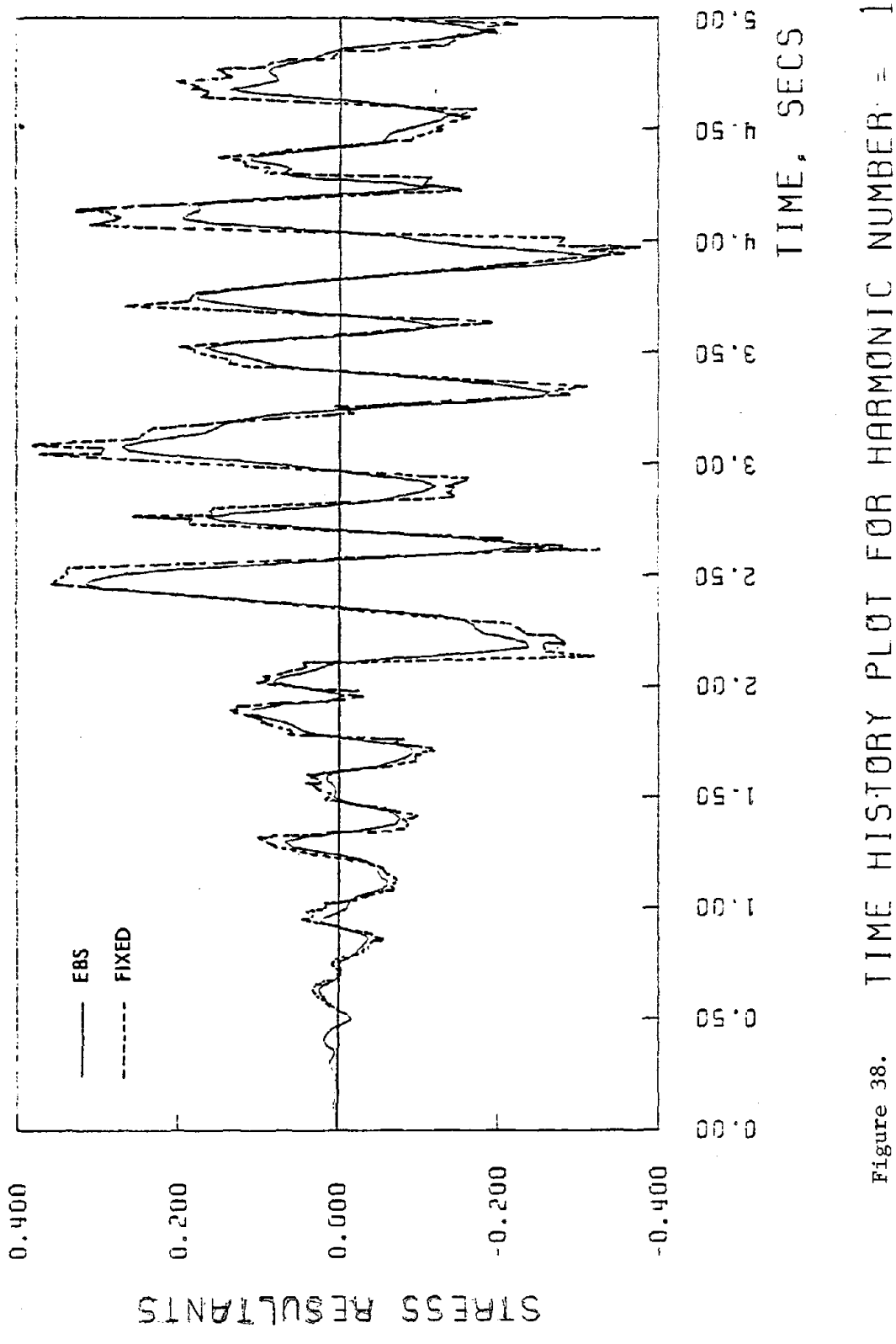
TIME HISTORY PLOT FOR HARMONIC NUMBER = 1
COMPONENT NO. 3 AT NODE NO. 7
STRESS RESULTANTS
0.400
0.200
0.000
-0.200
-0.400
0.00
0.50
1.00
1.50
2.00
2.50
3.00
3.50
4.00
4.50
5.00
TIME, SECS
EBS
FIXED

Figure 38.

possible influence of the flexible foundation on the maximum stresses and displacements.

For a specified earthquake time history and realistic field data to represent the soil, the SHORE-IV computer program can be used directly to carry out an analysis such as that presented in Figs. 32-38 for the El-Centro Earthquake and the elastic half space soil medium.

As a further example, the tower of Figure 24 is analyzed under the El-Centro earthquake (5/18/40) EW Comp. using the same four soil cases employing in the free vibration analysis as a supporting medium. The time of the analysis is taken as five seconds and the time step for Newmark β method integration is taken 0.02 seconds for the three soil cases and 0.005 seconds in the fixed base case. The damping coefficients (α=0.715779 and β=0.003356) are obtained based on 5% damping ratio for the first modes of vibration which are obtained during the response spectrum analysis. Due to the difficulty in grouping the results together for the four cases, they are shown individually in Figs. 39 through 54. Figures 39 to 42 and 43 to 46 show the plots of N_θ and M_θ respectively at node #1 ($\theta=0^\circ$). Also, Figs. 47 to 50 and 51 to 54 show the plots of N_ϕ and N_θ respectively at node #7 ($\theta=0^\circ$). The results are in the sequence of four soil cases for each stress resultant or stress couple. In order to

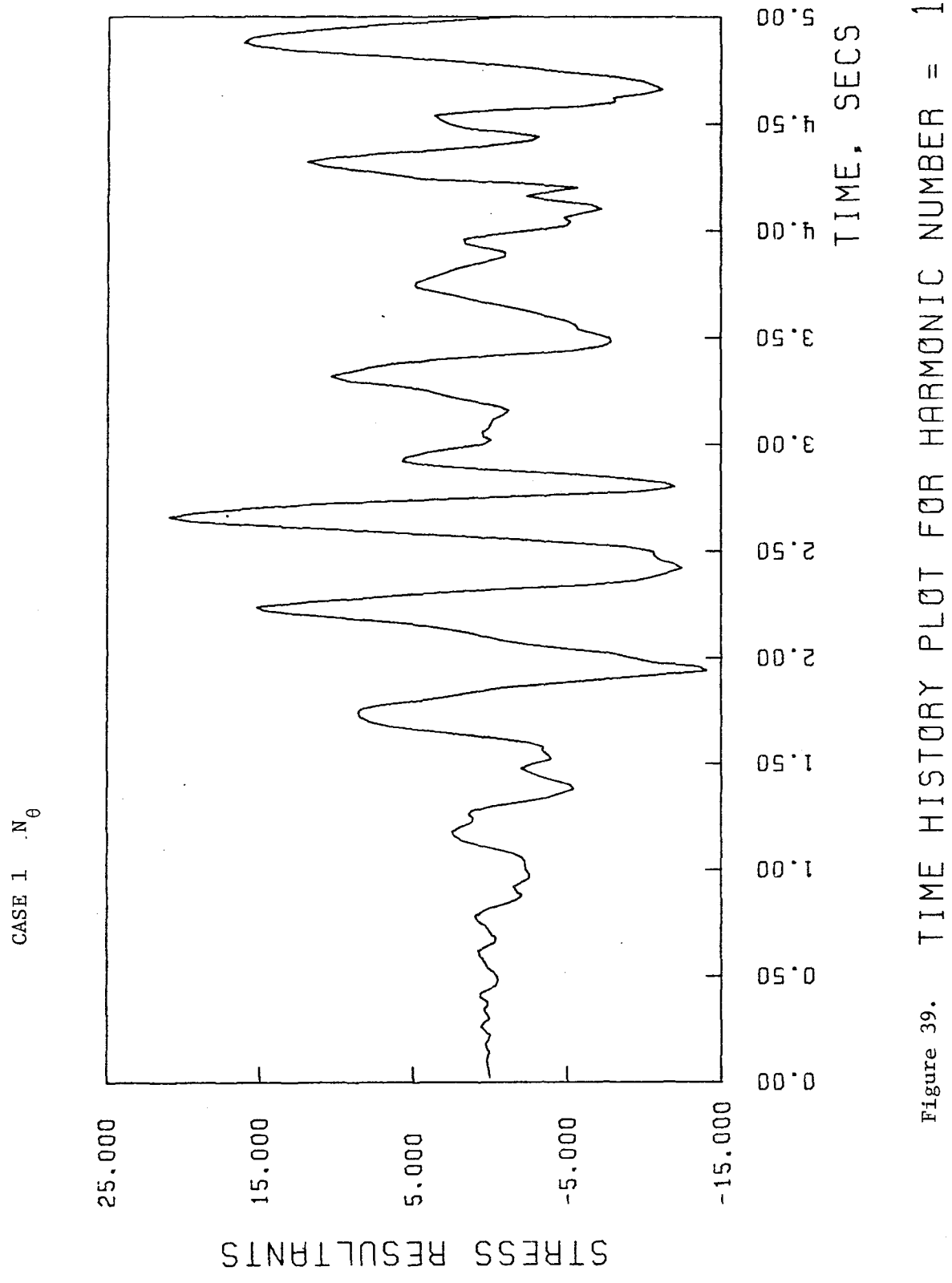

Figure 39. TIME HISTORY PLOT FOR HARMONIC NUMBER = 1
COMPONENT NO. 2 AT NODE NO. 1

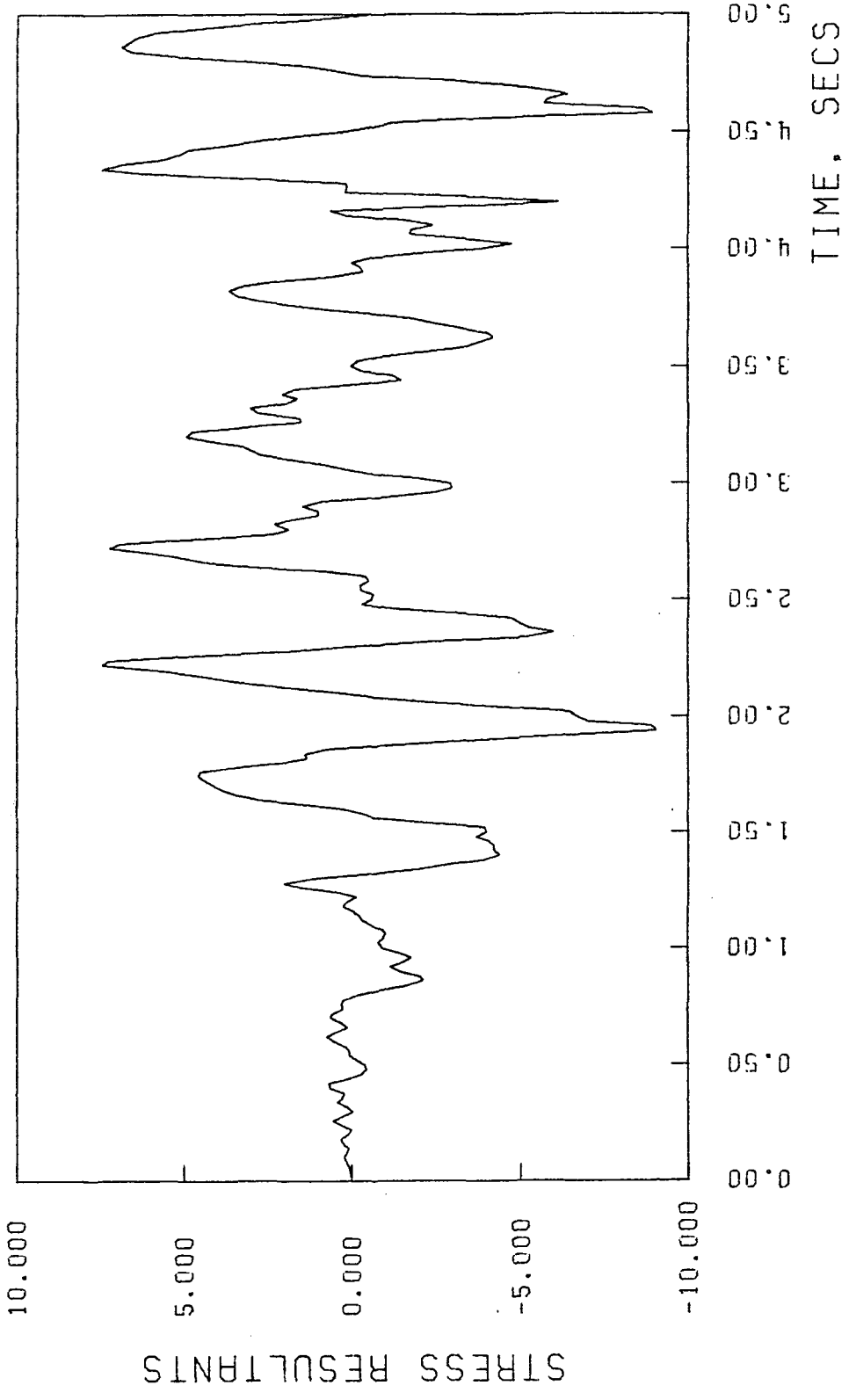

Figure 40. TIME HISTORY PLØT FØR HARMØNIC NUMBER = 1
COMPØNENT NØ. 2 AT NØDE NØ. 1

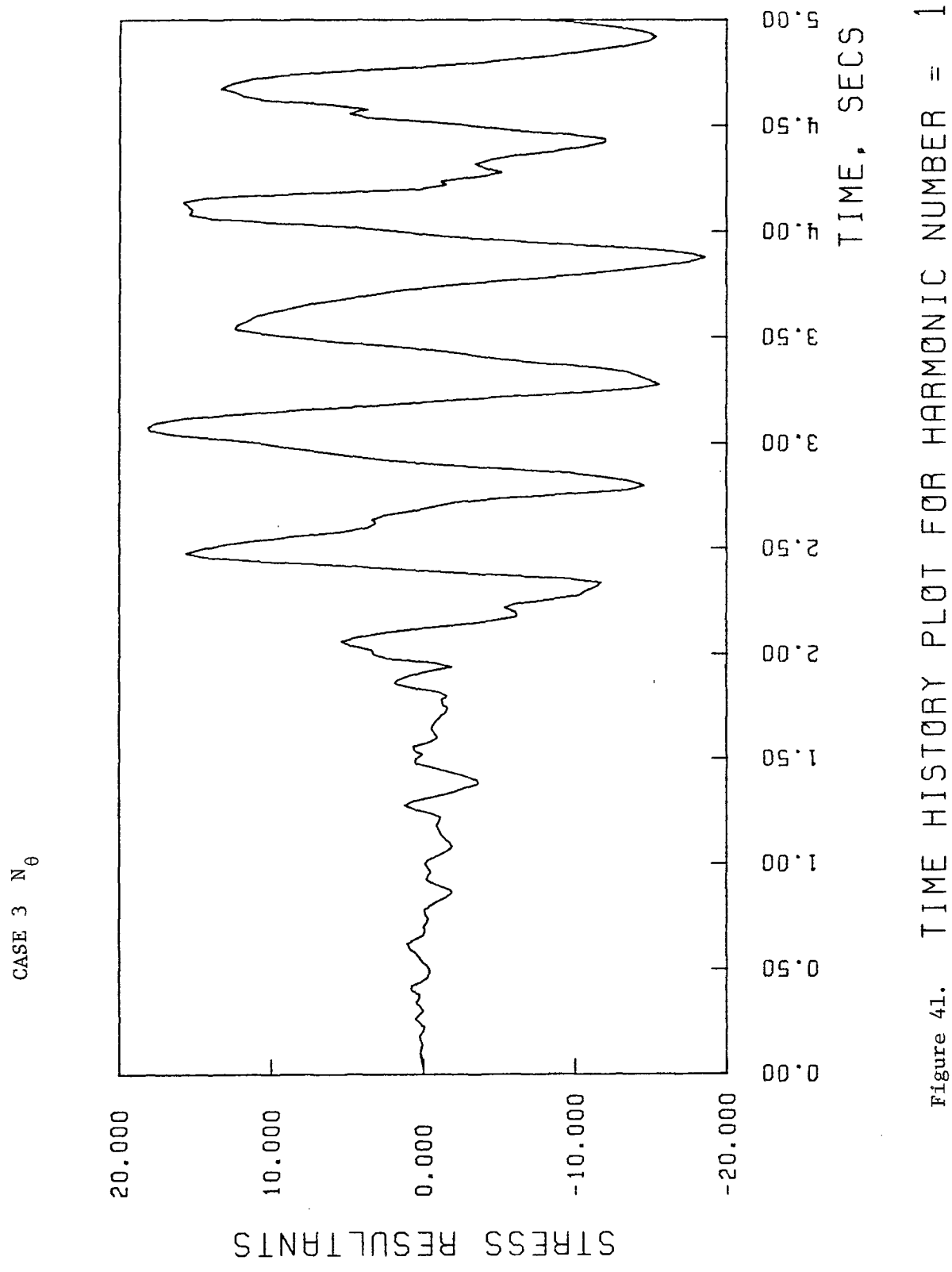

Figure 41. TIME HISTORY PLOT FOR HARMONIC NUMBER = 1
COMPONENT NO. 2 AT NODE NO. 1

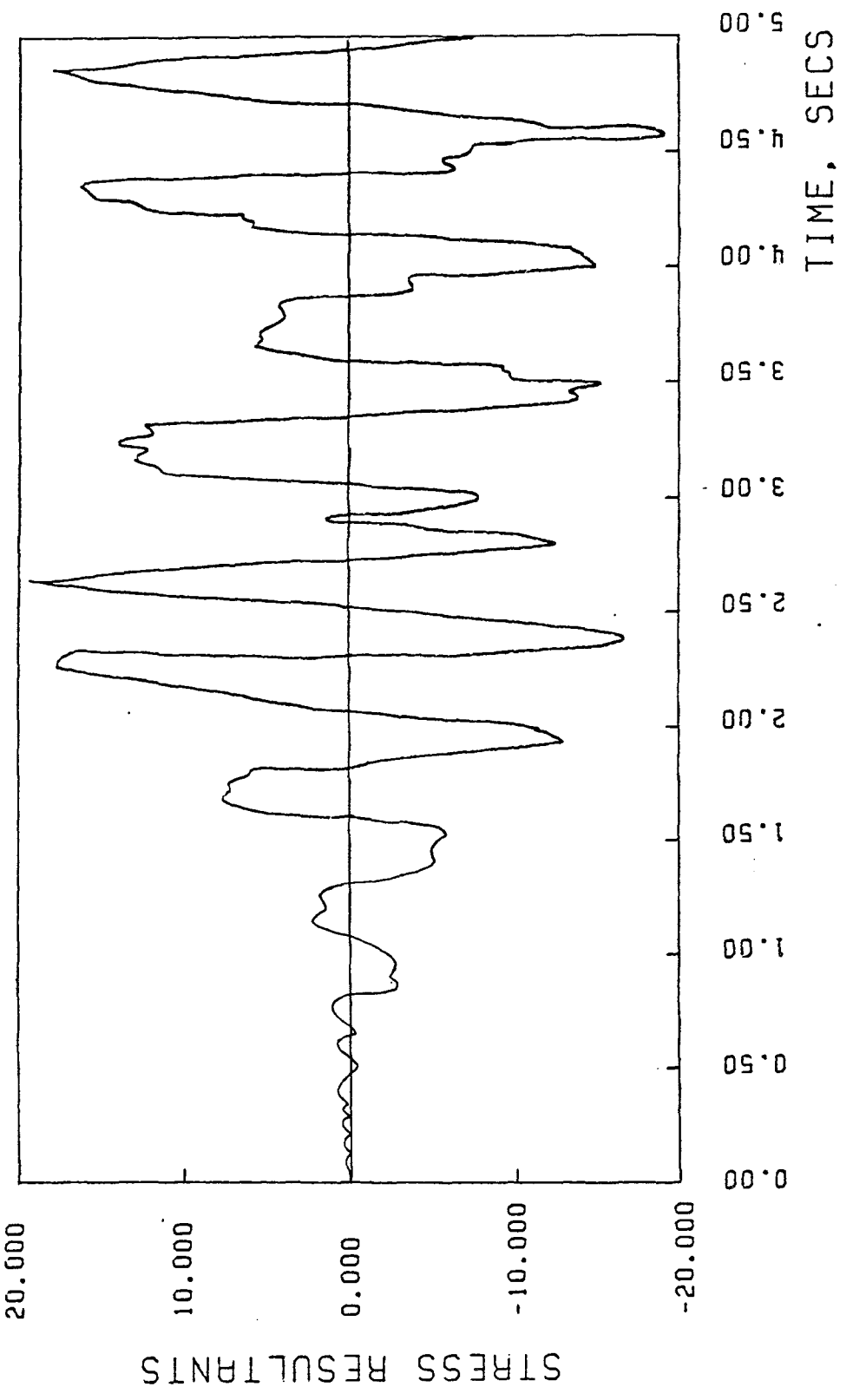

Figure 42. TIME HISTORY PLOT FOR HARMONIC NUMBER = 1
COMPONENT NO. 2 AT NODE NO. 1

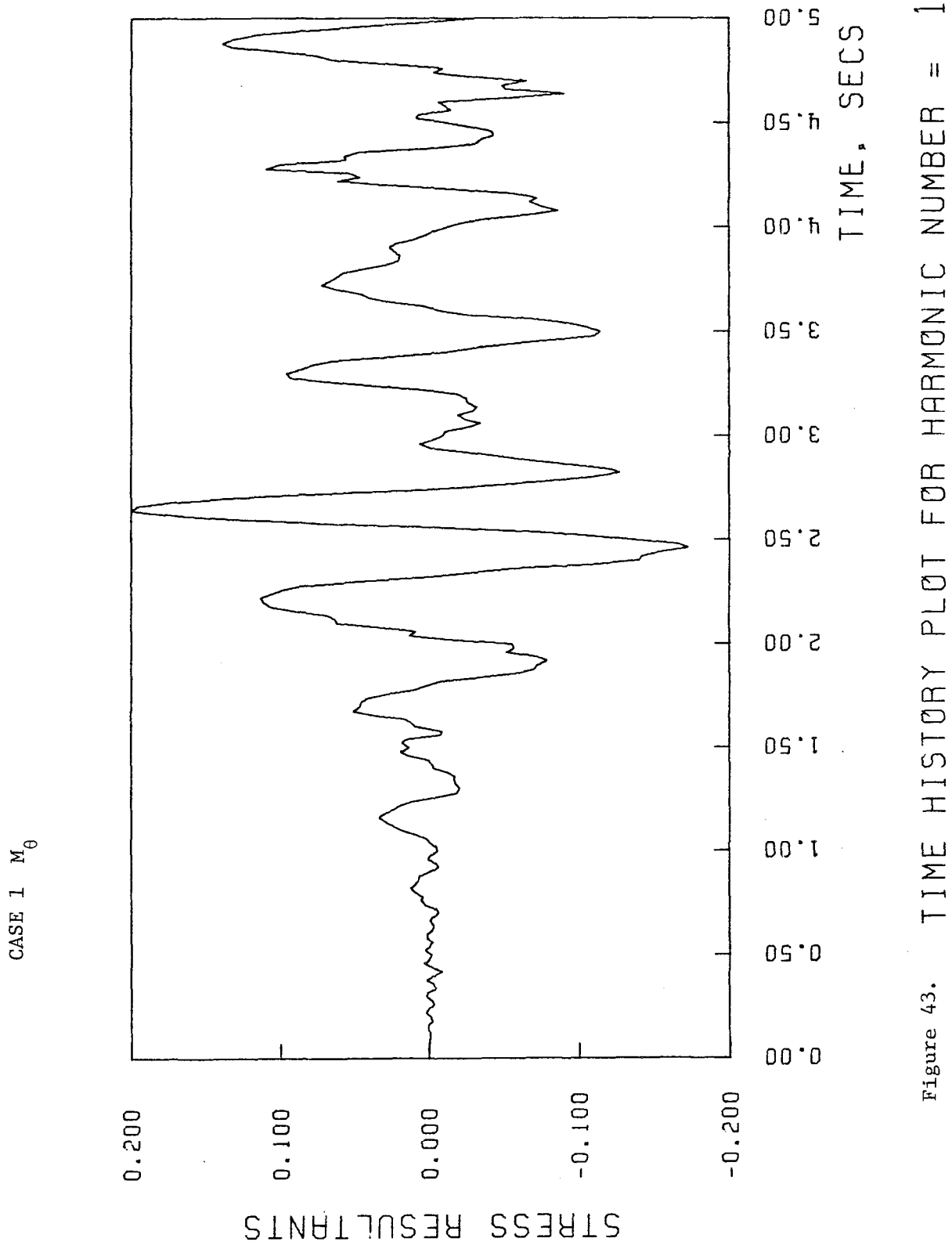

Figure 43. TIME HISTORY PLOT FOR HARMONIC NUMBER = 1
COMPONENT NO. 4 AT NODE NO. 1

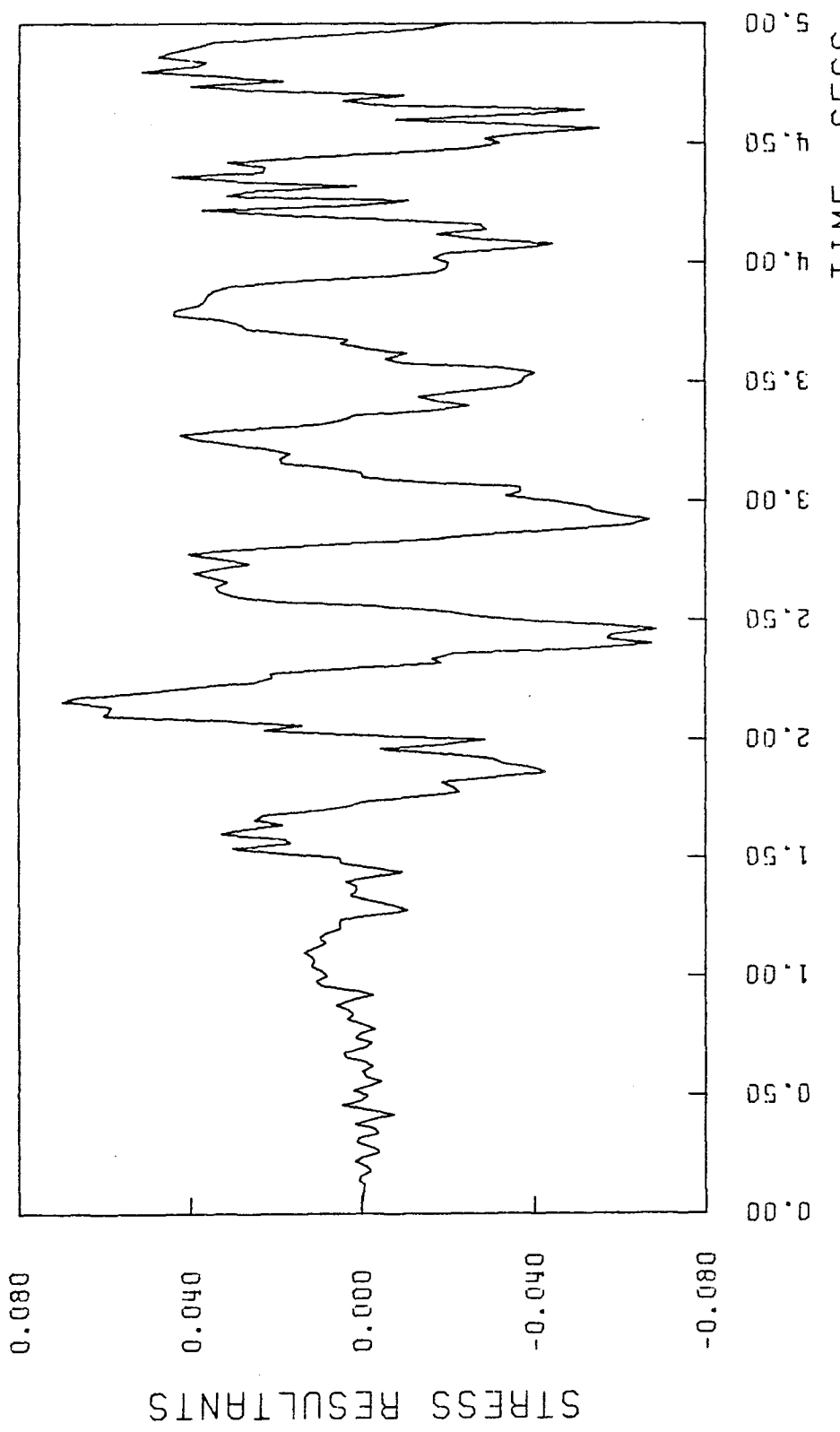

Figure 44. TIME HISTORY PLOT FOR HARMONIC NUMBER = 1
COMPONENT NO. 4 AT NODE NO. 1

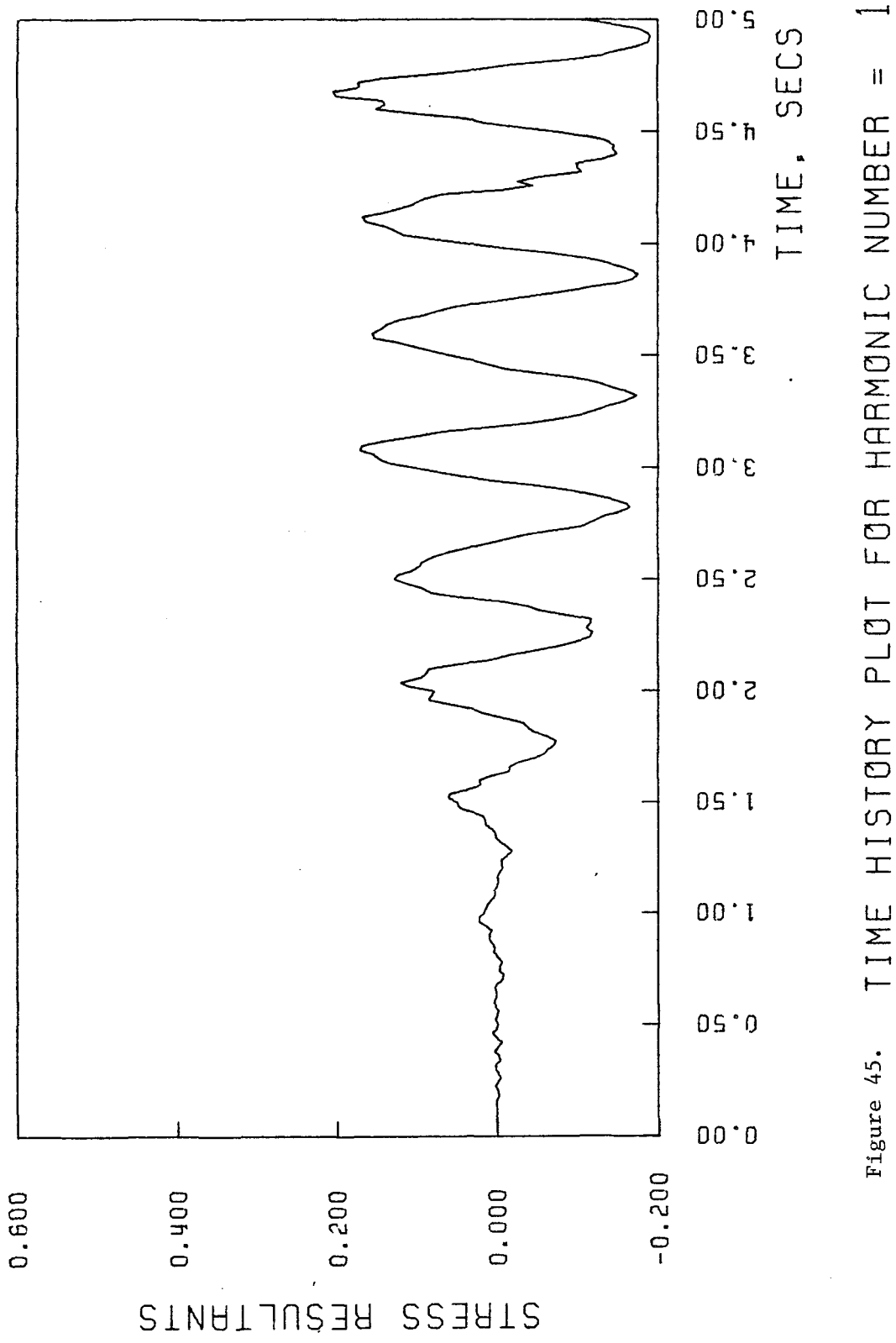

Figure 45. TIME HISTORY PLOT FOR HARMONIC NUMBER = 1
COMPONENT NO. 4 AT NODE NO. 1

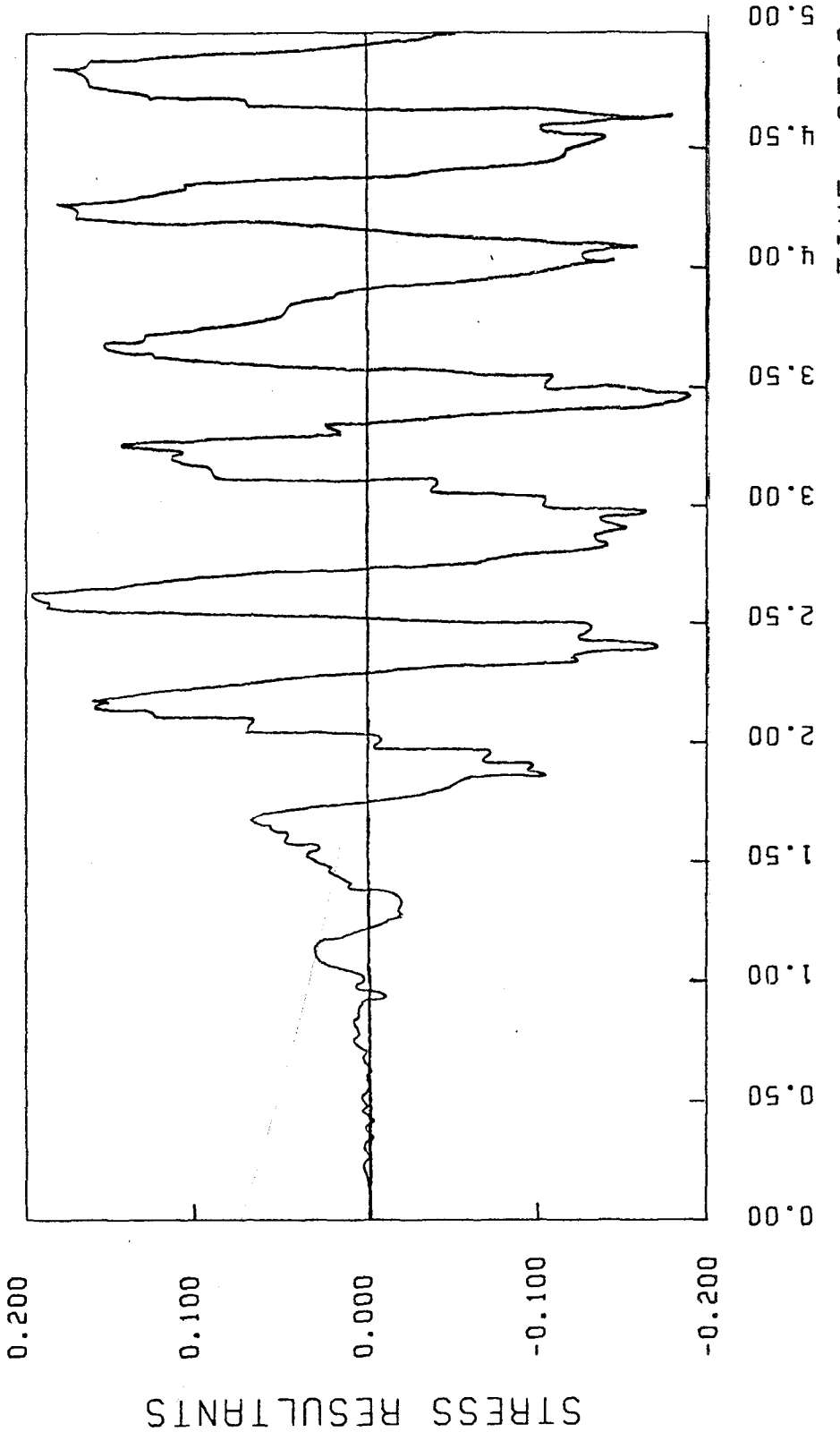

Figure 46. TIME HISTORY PLOT FOR HARMONIC NUMBER = 1
COMPONENT NO. 4 AT NODE NO. 1

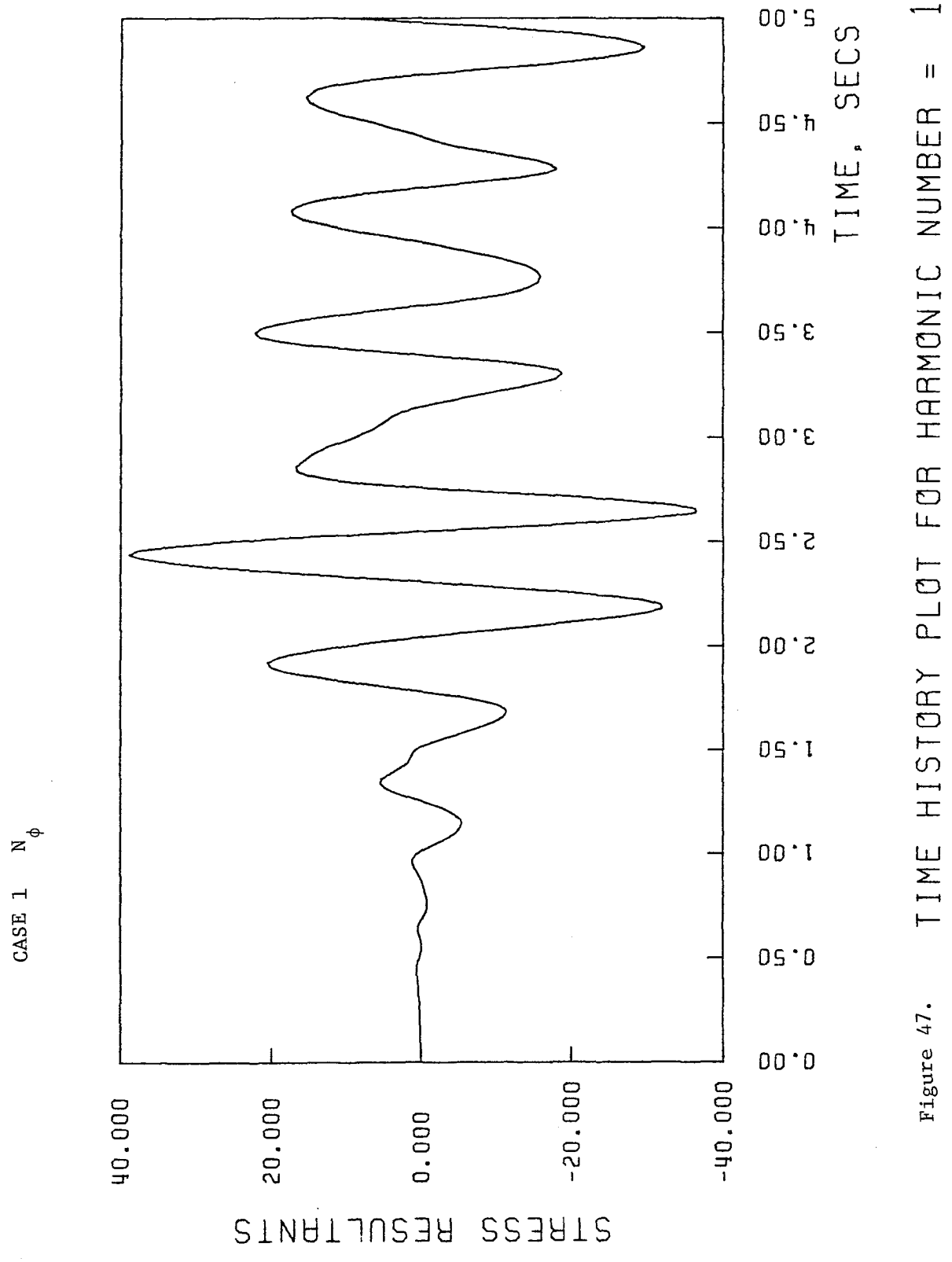

Figure 47. TIME HISTORY PLOT FOR HARMONIC NUMBER = 1
COMPONENT NO. 1 AT NODE NO. 7

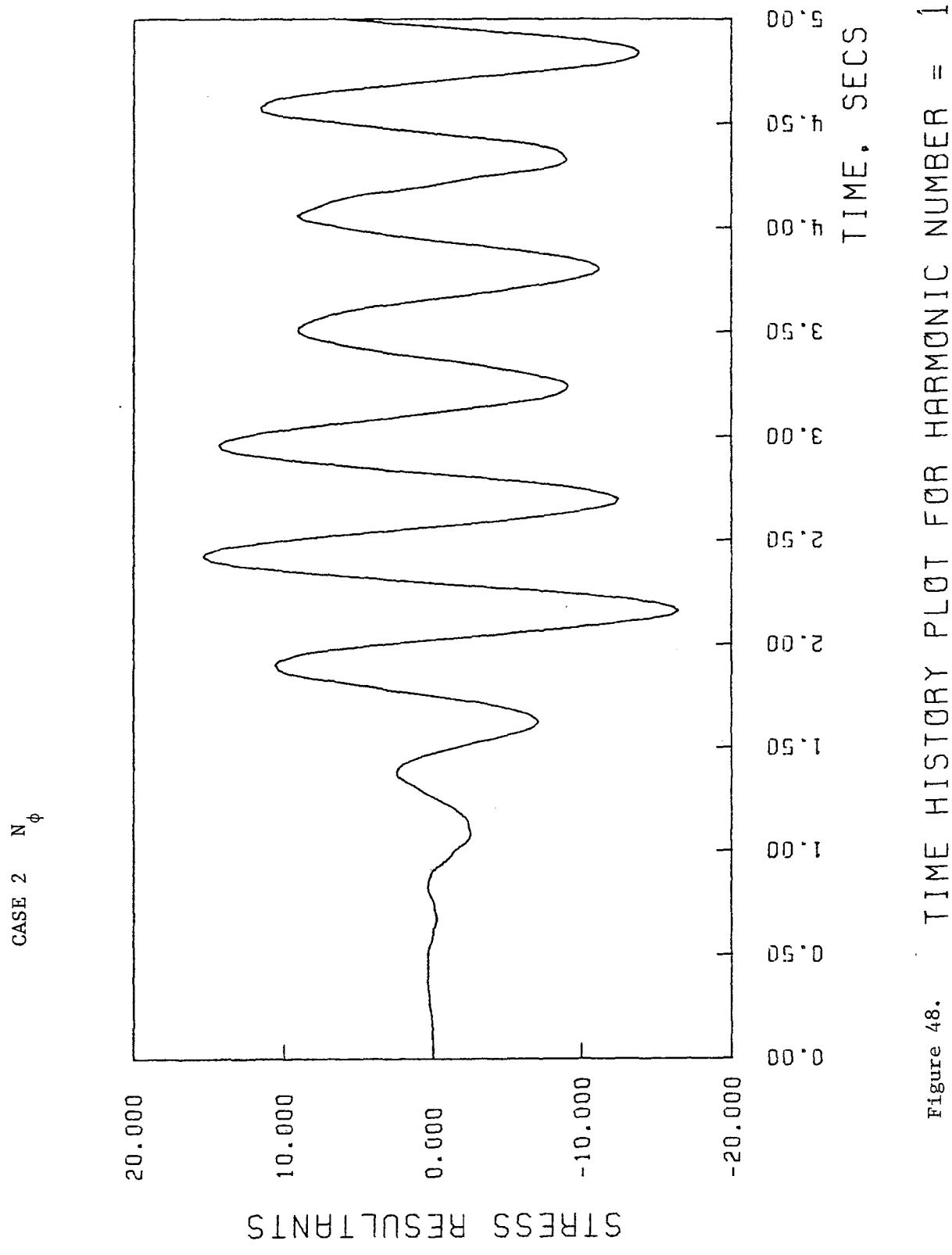

Figure 48. TIME HISTORY PLOT FOR HARMONIC NUMBER = 1
COMPONENT NO. 1 AT NODE NO. 7

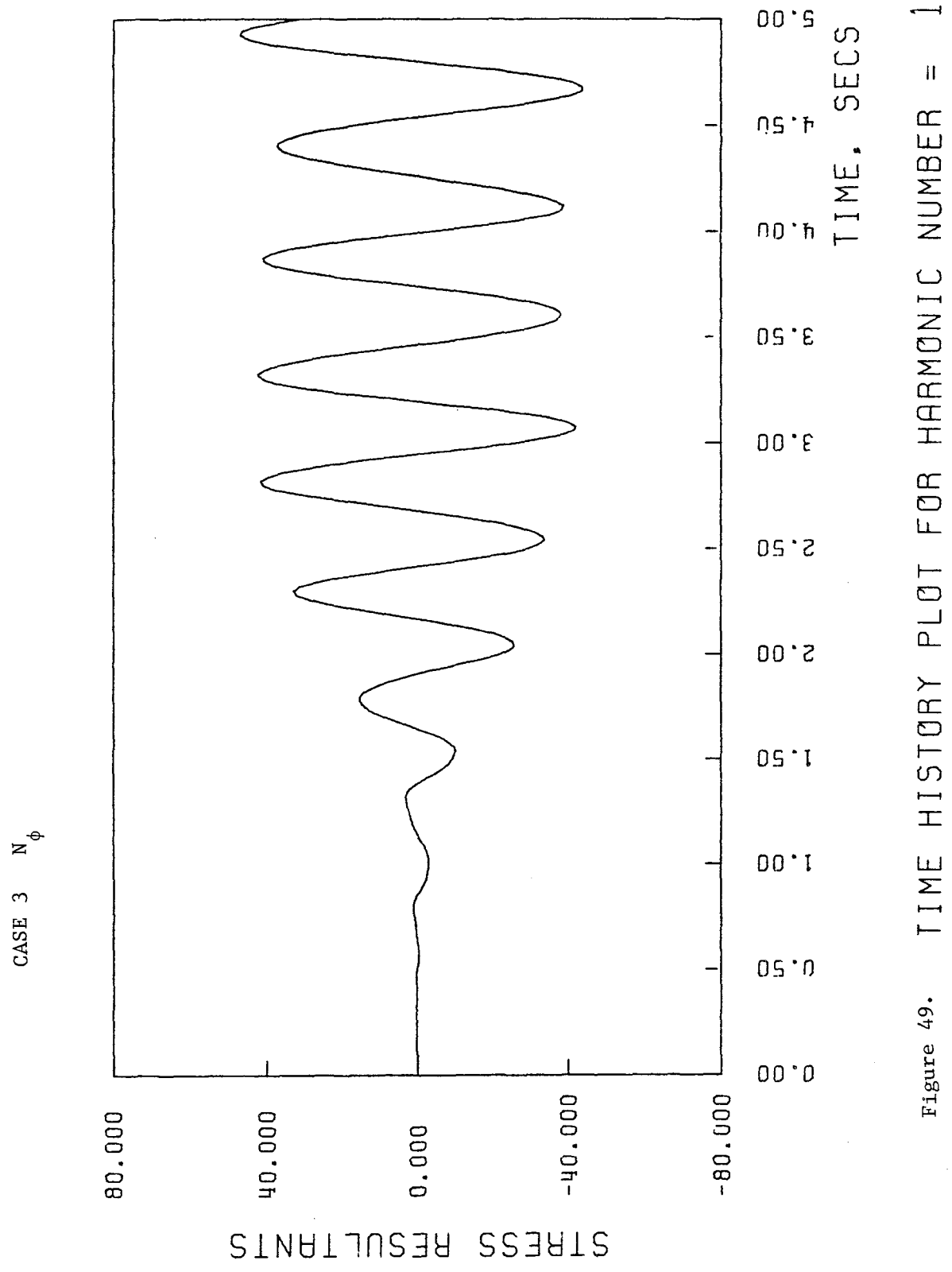

Figure 49. TIME HISTORY PLOT FOR HARMONIC NUMBER = 1
COMPONENT NO. 1 AT NODE NO. 7

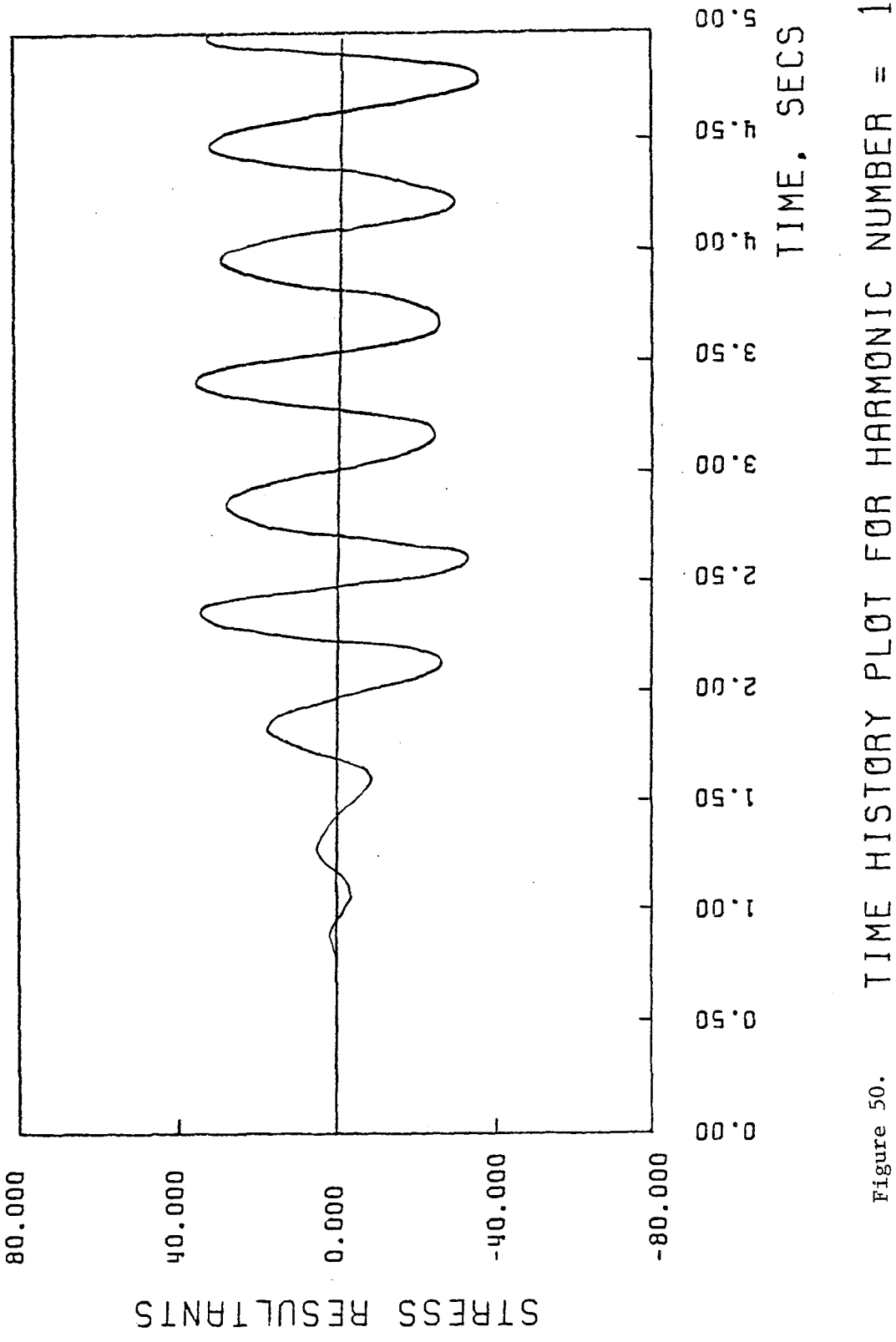
TIME HISTORY PLOT FOR HARMONIC NUMBER = 1
COMPONENT NO. 1 AT NODE NO. 7
CASE 4 N_ϕ
STRESS RESULTANTS
80.000
40.000
0.000
-40.000
-80.000
0.00
0.50
1.00
1.50
2.00
2.50
3.00
3.50
4.00
4.50
5.00
TIME, SECS

Figure 50.

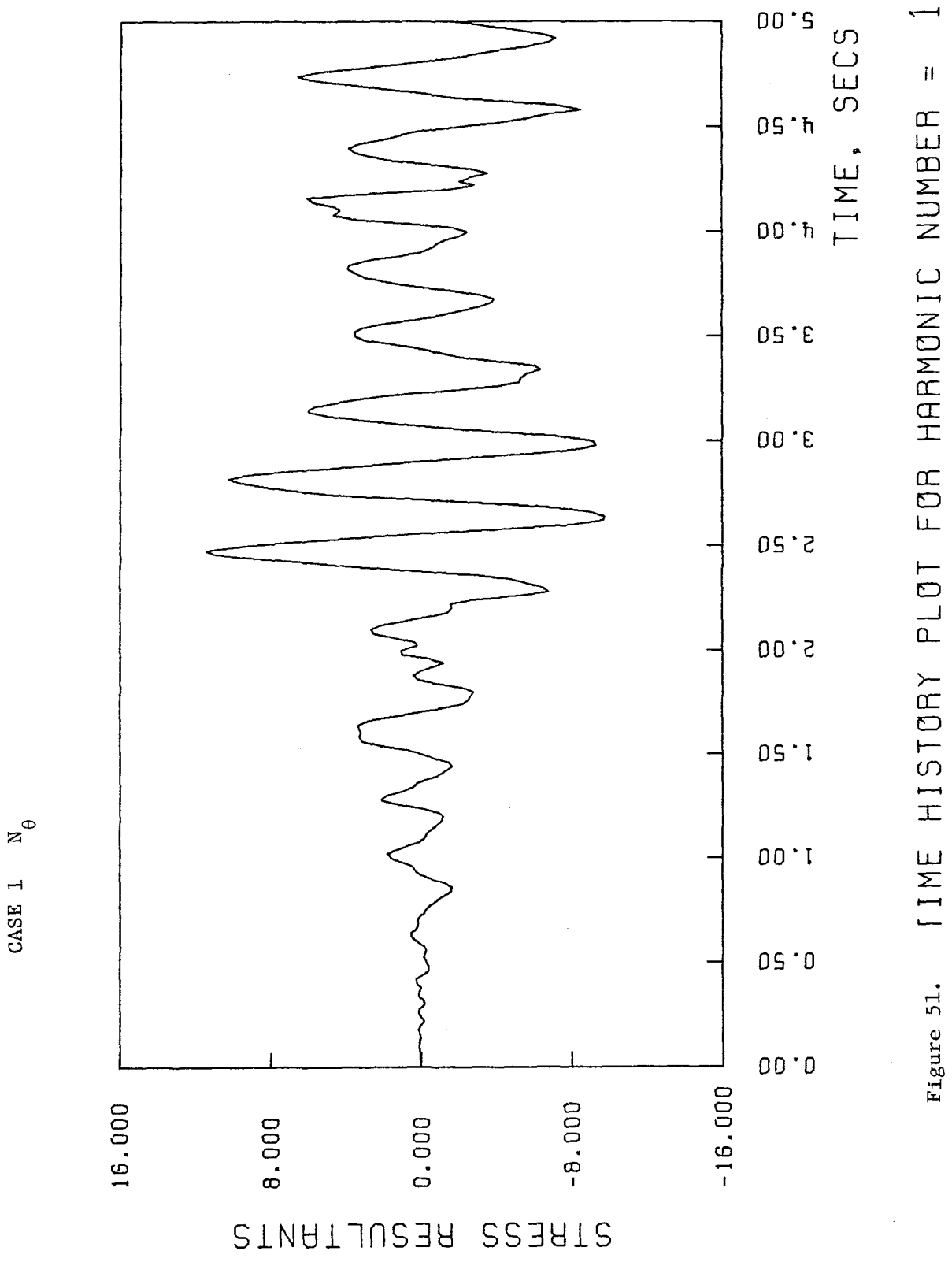

Figure 51. TIME HISTORY PLOT FOR HARMONIC NUMBER = 1
COMPONENT NO. 2 AT NODE NO. 7

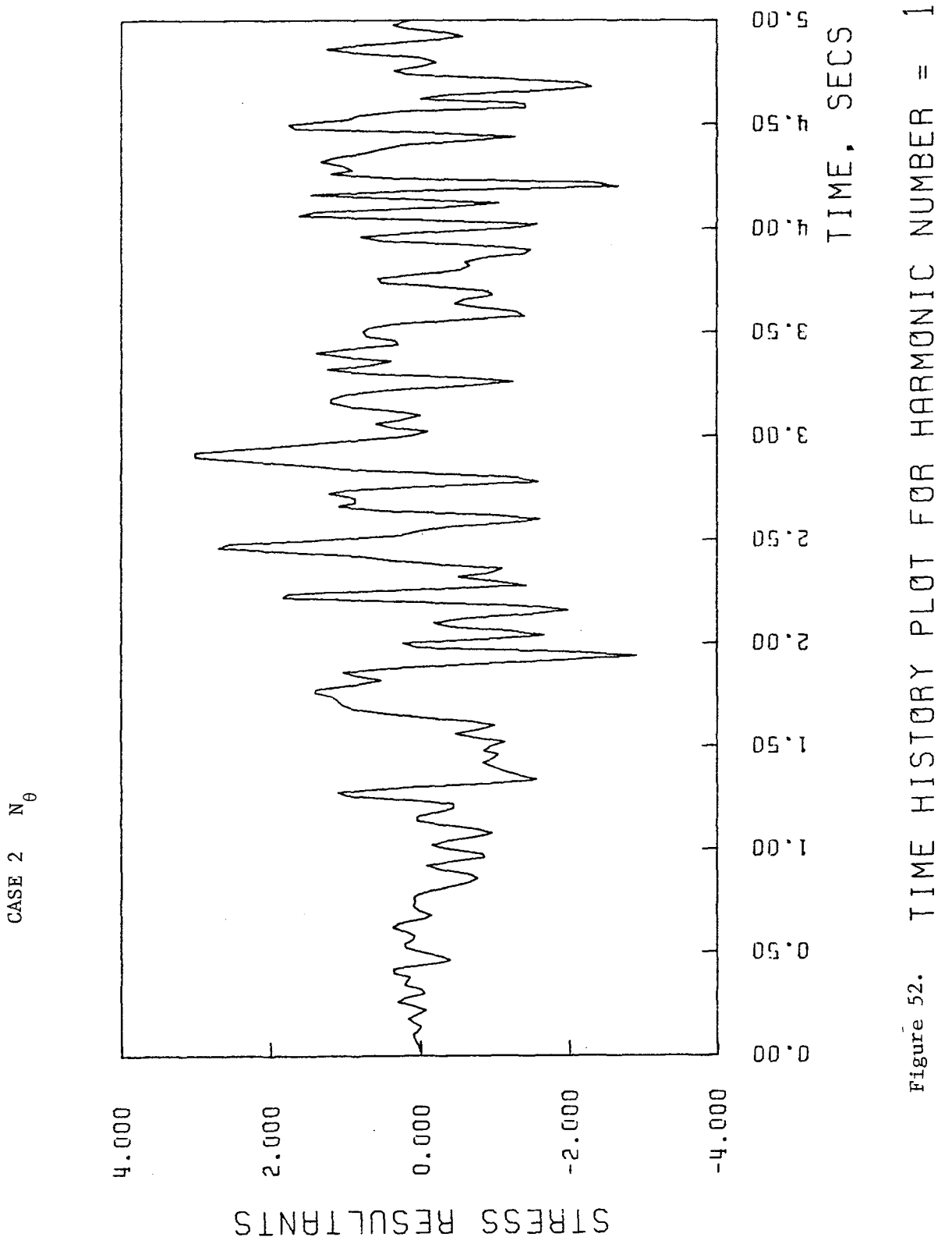

Figure 52. TIME HISTORY PLOT FOR HARMONIC NUMBER = 1
COMPONENT NO. 2 AT NODE NO. 7

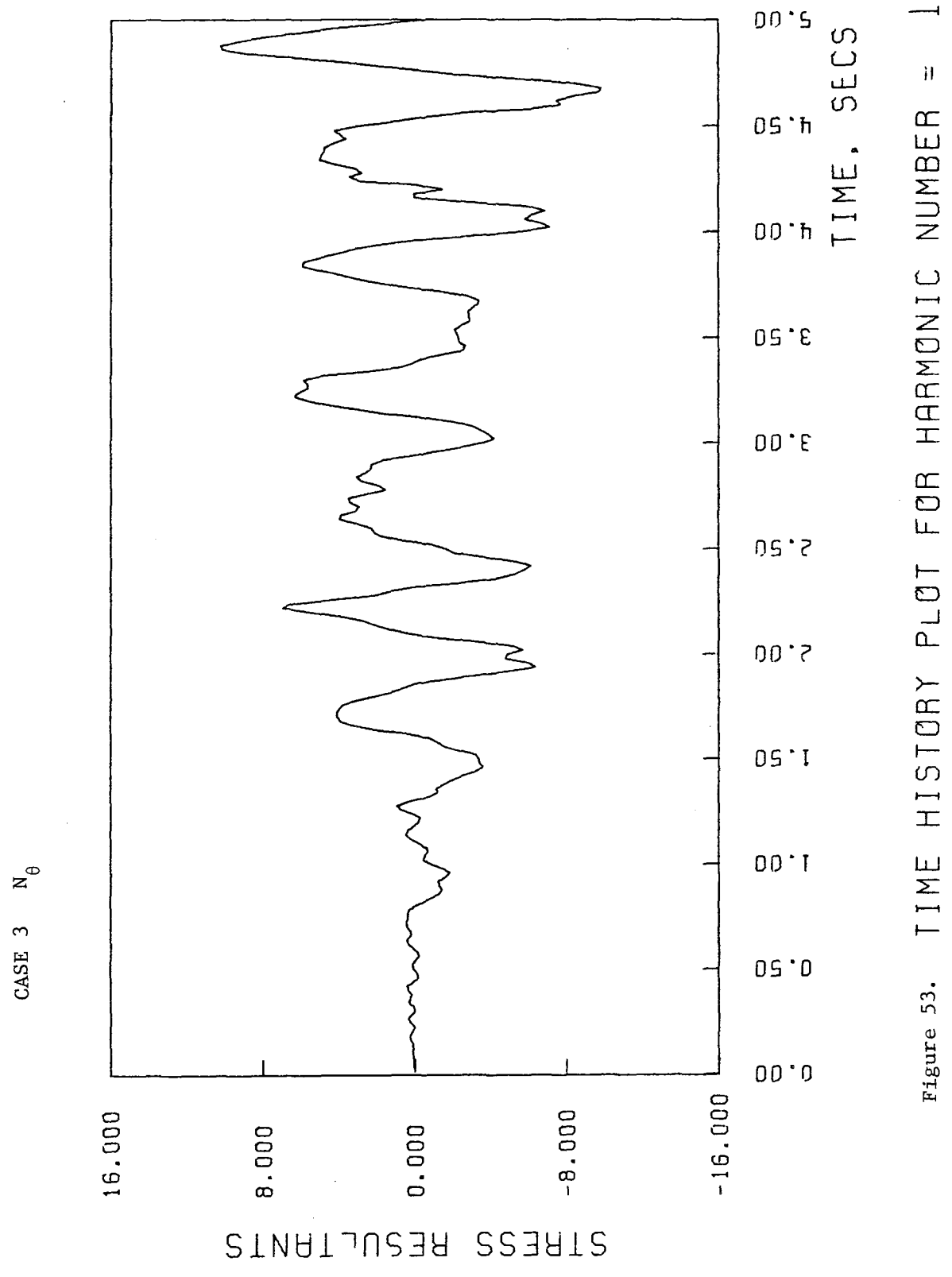

Figure 53. TIME HISTORY PLOT FOR HARMONIC NUMBER = 1
COMPONENT NO. 2 AT NODE NO. 7

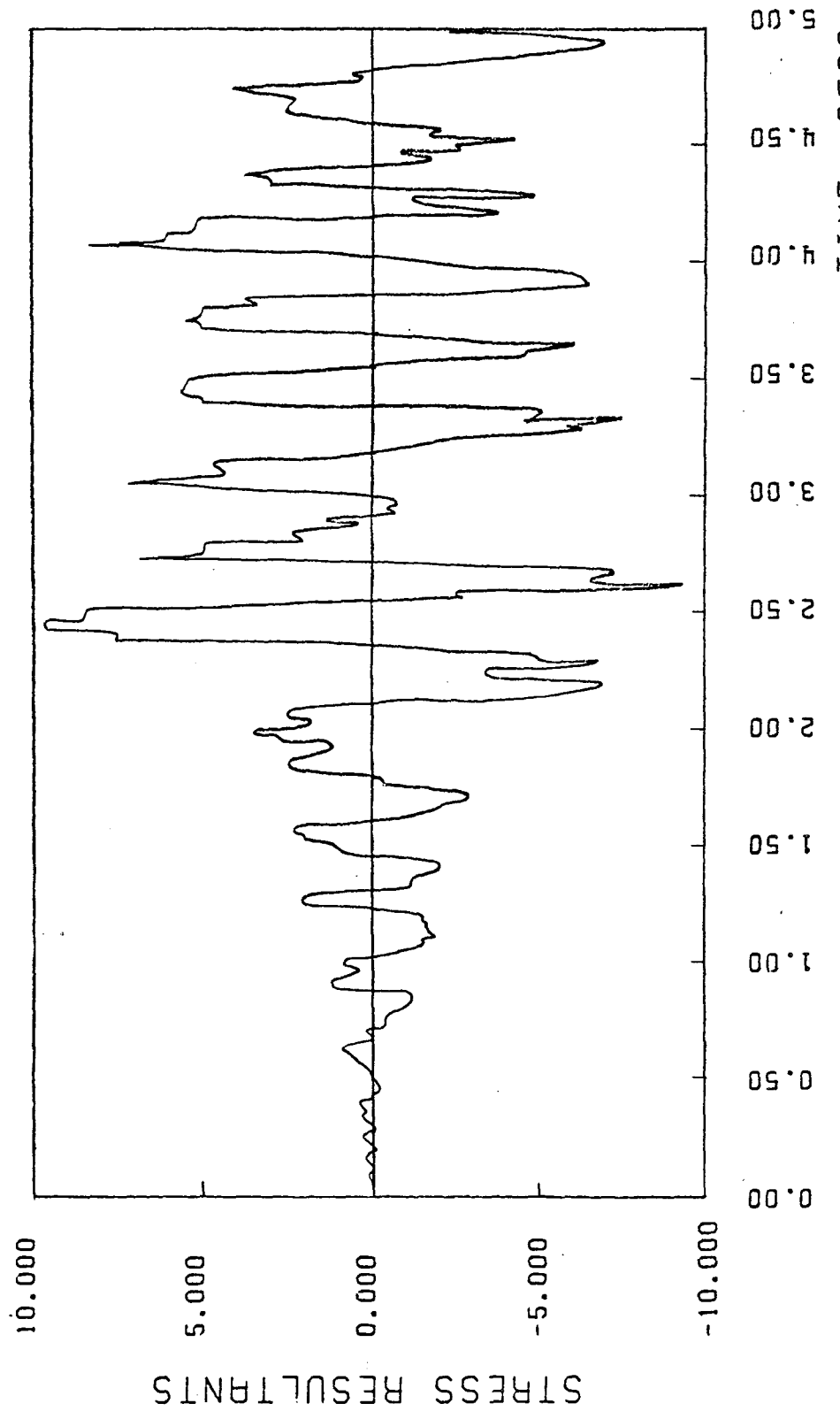

Figure 54. TIME HISTORY PLOT FOR HARMONIC NUMBER = 1
COMPONENT NO. 2 AT NODE NO. 7

identify the differences between three soil cases and the fixed base case (Case IV), the maximum responses are listed in Table 8. The comparison of the maximum response values show that the soil indeed influences the response of the shell when a strong motion earthquake loading is applied. Within the constraints of the present research, based on linear theories for the shell and the soil, similar information is obtained from the response spectrum approach. However, the capability for performing and displaying the results of a time history analysis demonstrated in this exercise are important in extended applications incorporating more realistic soil models.

Table 8. Maximum Response in Time History Analysis

Soil Case	NODE #1				NODE #7			
	Max. N_θ (K/Ft)		Max. M_θ (FtK/Ft)		Max. N_ϕ (K/Ft)		Max. N_θ (K/Ft)	
	Value	Time	Value	Time	Value	Time	Value	Time
Case I	+20.95 -14.08	2.66 1.94	+0.20 -0.15	2.64 2.45	+38.87 -36.46	2.44 2.64	+11.42 -9.80	2.48 2.64
Case II	+7.46 -9.07	4.34 1.94	+0.07 -0.07	2.16 2.46	+15.42 -16.50	2.42 2.16	+3.01 -2.92	2.90 1.94
Case III	+18.17 -18.65	3.08 3.88	+0.21 -0.19	4.68 -4.92	+46.73 -42.11	4.88 3.08	+10.24 -9.86	4.88 4.68
Case IV	+20.00 -19.28	2.63 4.60	+0.20 -0.19	2.64 3.47	+35.20 -37.50	3.40 4.75	+9.81 -9.80	2.45 2.67

5-CONCLUSIONS AND RECOMMENDATIONS

5-1 Conclusions

A finite element model for axisymmetric shell or shell-like structures founded on shallow ring footings was developed. The model consists of high-precision rotational shell elements to represent the axisymmetric shell structures and isoparametric solid elements with an energy transmitting boundary at the ring footing extremities to represent the soil medium. The substructure approach was chosen in the soil-structure interaction analysis, which simplifies the connection problem between the soil medium and the structure. Also, by using the substructure approach, the free field of the ground motion may be input directly at the foundation level.

The connection problem between the three dimensional soil medium and the two dimensional shell elements is solved by introducing a frequency dependent dynamic boundary system at the common degrees of freedom between the shell foundation and the underlaying soil. The soil model components were computed at the fundamental frequency of the shell structure without the soil system for the free vibration and response spectrum analysis, whereas the dominant driving frequency of the time history excitations was used with the time history analysis. For dynamic wind analysis the fundamental frequency of the system would likely be suitable; however, dynamic wind analysis using the present model has not been carried out.

It was shown that the require size of the finite element mesh is controlled throughout the dynamic pressure bulb by the shortest shear wave length and that this bulb exists through a depth of about one and half times the footing radius. The influence of the lower boundary on the soil model components is significant only for depths less than three times the footing radius due to the reflections of the waves on the assumed rock-soil interface, which tends to increase the stiffness elements and decrease the damping elements (convergence to the fixed base case). Based on the dynamic pressure bulb study, an economical finite element mesh for the soil medium was suggested for use with shells having a small B/r_o ratio.

A sensitivity study of the equivalent boundary system to the driving frequency showed that the stiffness components are more sensitive than the damping components, and also that the rotational components are the most sensitive to the driving frequency. A similar conclusion may be drawn for the sensitivity of the EBS to Fourier harmonic number j. It is also concluded that the EBS components are fairly independent of the harmonic number j for $j > 1$, which suggests an efficient procedure to determine the EBS components for $j > 1$ based on a single harmonic number ($j \geq 2$) analysis.

The free vibration analysis of a cooling tower on a shallow foundation showed that the overall flexibility of the shell increases with a decrease in the soil stiffness. Consequently, there is a reduction of the inertial forces on the shell. The study also revealed a dramatic change in the second mode of vibration as the soil gets more flexible. This relieves the lower region of the shell (column supports in cooling towers) from the high stresses which often occur when the soil interaction is neglected. It is concluded from this study that the soil flexibility or compliance is a very important parameter in the soil-structure interaction phenomenon and that a given flexibility can be realized by a non-unique combination of the basic parameters. This finding is in agreement with Pandya and Setlur's conclusions (16).

The importance of soil-structure interaction on the stress resultants and stress couples in the shell was shown by a response spectrum analysis of the cooling tower used in the free vibration analysis. It was shown that the fixed base or very stiff coil case produces resultant forces which envelope all soil cases, except for the N_{ϕ} component. The reduction, which is in the range of 20% of the fixed base solution, may permit reduction of the shell cross section and the circumferential steel in the shell, resulting in a considerable cost savings. Perhaps, the segment in the shell structure most affected by soil-structure interaction are the

column supports as may be seen from Table 5. The reduction in the stresses may reach 50% for certain soil flexibilities.

The analysis of the concentric ring footing, which has not been studied previously so far as the authors can determine, revealed very large twisting moments on the footing which increases with increasing the soil stiffness. On the other hand, the axial force and bending moments increase with decreasing the soil stiffness. With the present model, the footing can be analyzed as a ring resting on a continuous elastic foundation, bringing forth the axial forces and the torsion which were not possible to obtain with the continuous beam-over-point support model used before. Confidence in the ring footing response was established by comparing the present model results to the result of a space frame model.

The possibility of foundation uplift increases with increasing the soil flexibility. In the design earthquake considered here, uplift could occur only if the two components (vertical and horizontal) of the ground motions were considered simultaneously. However, the net tensile stress after adding the dead load effect is too small to cause a real uplift, as shown in the analysis.

5-2 Recommendations for Further Study

The subject of axisymmetric shells-soil interaction is a new topic in soil-structure interaction and the research

presented in this report may be extended to include or account for several other factors which may prove very important for certain types of problems. Among these are the effect of non-uniform earthquake excitation which may yield further reduction in the structure response due to the inherent self-diminishing feature to this type of earthquake excitation, as suggested by Scanlan (19). For such an excitation, time history analysis is most suitable and the analysis must include more than the first two Fourier harmonics ($j > 1$).

Another factor which may prove very important is the fact that the soil material may not be elastic but more likely viscoelastic or nonlinear. For a realistic analysis of viscoelastic soil material, experimental data for the Lame' constant seems to be necessary. Unfortunately, there is not much available data for various types of soil, especially when the soil layers are saturated so that the water pressure could add to the complexity of the soil material. In this kind of soil problem, the damping may be very sensitive and more study is needed for the choice of the damping ratio to adequately represent the material and radiation damping. The relationship between the damping ratio and the viscous damping where complex Lame' constants of the soil material are used needs further study.

For axisymmetric shells founded on pile foundations, an inertial interaction mode may not be sufficient and complete interaction may be more realistic. However, in this type of analysis the use of the transmitting boundary is still valid and probably can save in the computation cost. More investigation is required to account for pile-pile interaction in the pile group and also for the possibility of modelling the pile group as an equivalent axisymmetric element. In case of friction piles the problem may be more complicated due to the settlement and creep action with time.

Separate shallow footings may be an option in the list of alternatives for shell structures with column supports. This type of foundation could be the most economical type. However, very little is known about the individual behavior of those footings under dynamic loading when the soil-interaction is included, which suggests further investigation in this area as well.

6-REFERENCES

1. Brombolich, L. and Gould, P. L., "High-Precision Finite Element Analysis of Shells of Revolution", Research Report No. 16, Structural Division, Washington University, St. Louis, MO, Feb. 1971.

2. Sen, S., Gould, P. and Suryoutomo, H., "High-Precision Static and Dynamic Finite Element Analysis of Shells of Revolution with Application to Hyperboloidal Shells on Discrete Supports", Research Report No. 23, Structural Division, Washington University, St. Louis, MO., Nov. 1973.

3. Gould, P. L., Szabo, B. A. and Suryoutomo, H. B., "Curved Rotational Shell Elements by the Constraint Method", Proceedings of the International Conference on Variational Methods in Engineering, Vol. II, Southampton University, England, Sept. 1972, pp. 8/33-8/42.

4. "Analysis for Soil-Structure Interaction Effects for Nuclear Power Plants", Report by the Ad Hoc Group in Soil-Structure International, Nuclear Structures and Material Committee of the Structure Division, ASCE (draft) Dec. 5, 1975.

5. Vaish, A. K. and Chopra, A. K., "Earthquake Finite Element Analysis of Structure-Foundation Systems", Journal of Engineering Mechanics Division, ASCE, Vol. 108, No. EM6, Dec. 1974, pp. 1101-1116.

6. Chopra, A. K. and Gutierrez, J. A., "Earthquake Response Analysis of Multistory Buildings Including Foundation Interaction", International Journal of Earthquake Engineering and Structural Dynamics, Vol. 3, 1974, pp. 65-77.

7. Veletsos, A. S., "Dynamics of Structure-Foundation Systems", Presented at the Symposium on Structural and Geotechnical Mechanics Honoring Nathan M. Newmark, Univ. of Illinois, Urbana, Champaign, Oct. 2 & 3, 1975.

8. Kausel, E., Roesset, J. M. and Waas, G., "Dynamic Analysis of Footing on Layered Media", Journal of Engineering Mechanics Division, ASCE, Vol. 101, No. EM5, Oct. 1975, pp. 679-693.

9. Luco, J. E. and Westmann, R.A., "Dynamic Response of Circular Footing" Journal of Engineering Mechanics Division, ASCE, No. EM5, Oct. 1971, pp. 1381-1395.

10. Novak, M., "Effect of Soil on Structural Response to Wind and Earthquake", International Journal of Earthquake Engineering and Structural Dynamics, Vol. 3, 1974, pp. 79-96.

11. Bielak, J., "Modal Analysis for Building-Soil Interaction", Journal of Engineering Mechanics Division, ASCE, Vol. 102, No. EM5, Oct. 1976, pp. 771-786.

12. Rainer, J. H., "Damping in Dynamic Structure-Foundation Interaction", Canadian Geotechnical Journal, Vol. 12, 1975, pp. 13-22.

13. Roesset, J. M., Whitman, R. V. and Dobry, R., "Modal Analysis for Structure with Foundation Interaction", Journal Structure Division, ASCE, Vol. 99, No. ST3, Proceedings Paper 9603, March 1973, pp. 399-416.

14. Tsai, N. C., "Modal Damping for Soil-Structure Interaction", Journal of the Engineering Mechanics Division, ASCE, Vol. 100, No. EM2, Proceedings Paper 10490, April 1974, pp. 323-341.

15. Clough, R. and Mojtahedi, S., "Earthquake Response Analysis Considering Non-Proportional Damping", International Journal of Earthquake Engineering and Structural Dynamics, Vol. 4, 1976, pp. 489-496.

16. Pandya, V. and Setlar, A. Y., "Seismic Soil-Structure Interaction by Finite Elements: Case Studies", Proceedings of the 2nd ASCE Specialty Conference on Structural Design of Nuclear Plant Facilities, Vol. 1-A, Dec. 1975, pp. 826-848.

17. Penzien, J., "Soil-Pile Foundation Interaction", Earthquake Engineering, Wiegel, Prentice-Hall, 1970.

18. Veletsos, A. S. and Nair, V., "Seismic Interaction of Structures on Hystretic Foundations", Journal of the Structural Division, ASCE, ST1, Jan. 1975, pp. 109-129.

19. Scanlan, R. C., "Seismic Wave Effects on Soil-Structure Interaction", International Journal of Earthquake Engineering and Structural Dynamics, Vol. 4, 1976, pp. 379-388.

20. Akiyoshi, T., "Compatible Viscous Boundary for Discrete Models", Journal of the Engineering Mechanics Division, ASCE, No. EM5, Oct. 1978, pp. 1253-1266.

21. Kausel, E., "Forced Vibration of Circular Foundation on Layered Media", MIT Research Report R74-11, Soils Publication No. 336, Structures Publication No. 38, Massachusetts Institute of Technology, Cambridge, Mass., Jan., 1974.

22. Luco, J. E., Wong, H. L. and Trifunac, M. D., "A Note on the Dynamic Response of Rigid Embedded Foundations", International Journal of Earthquake Engineering and Structural Dynamics, Vol. 4, 1975, pp. 119-127.

23. Arnold, R. N., Bycroft, G. N., Warburton, G. B., "Forced Vibrations of a Body on an Infinite Elastic Solid", Journal of Applied Mechanics, No. 77, pp. 391-401, 1955.

24. Veletsos, A. S. and Verbic, B., "Dynamics of Elastic and Yielding Structure-Foundation Systems", Proceedings Fifth World Conference on Earthquake Engineering, Rome, Italy, pp. 2610-2613.

25. Veletsos, A. and Wei, Y., "Lateral and Rocking Vibration of Footings", Journal of the Soil Mechanics and Foundation Division, ASCE, Vol. 97, Sept. 1971.

26. Veletsos, A. and Meek, J., "Dynamic Behaviour of Building-Foundation Systems", International Journal of Earthquake Engineering and Structural Dynamics, Vol. 3, 1974, pp. 121-138.

27. White, J. E., "Seismic Waves: Radiation, Transmission and Attenuation", McGraw-Hill, 1965.

28. Bullen, K. E., "An Introduction to the Theory of Seismology", Cambridge Press, 1963.

29. Ewing, W. M., Jardetsky, W. S. and Press, F., "Elastic Waves in Layered Media", McGraw-Hill, New York, 1957.

30. Langhaar, H. L., "Energy Methods in Applied Mechanics", J. Wiley and Sons, 1962.

31. El-Shafee, O. M., "Dynamic Analysis of Shells of Revolution-Soil Systems", Dissertation presented to Sever Institute of Technology, Washington University, St. Louis, MO, May 1979.

32. Lysmer, J., and Richart, F.E., Jr., "Dynamic Reponse of Footings to Vertical Loading", Journal of Soil Mechanics and Foundation Division, ASCE, Vol. 92, No. SM1, Proceedings Paper 4592, Jan., 1966, pp. 65-91.

33. Lysmer, J. and Kuhlemeyer, R.L., "Finite Dynamic Model for Infinite Media", Journal of Engineering Mechanics Division, ASCE, No. EM4, Aug., 1969, pp. 859-877.

34. Vaish, A. K. and Chopra, A. K., "Earthquake Finite Element Analysis of Structure-Foundation Systems", J. of Engineering Mech. Division, ASCE, Vol. 108, No. EM6, Dec. 1974, pp. 1101-1116.

35. Wong, H. L. and Luco, J. E., "Dynamic Response of Rigid Foundations of Arbitrary Shape", International Journal of Earthquake Engineering and Structural Dynamics, Vol. 4, 1976, pp. 579-587.

36. Bazant, Z. P., "Spurious Reflection of Elastic Waves in Nonuniform Finite Element Grids", Journal of Computer Methods in Applied Mech and Engineering, 16, 1978, pp. 91-100.

37. Basu, P. K. and Gould, P. L., "SHORE-III, Shell of Revolution Finite Element Program-User's Manual", Research Report No. 49, Structural Division, Washington University, St. Louis, MO, Sept. 1977.

38. Basu, P. K. and Gould, P. L., "SHORE-III,Shell of Revolution Finite Element Program-Theoretical Manual", Research Report No. 48, Structural Division, Washington University, St. Louis, MO, Sept. 1977.

39. El-Shafee, O. M., Basu, P. K., Lee, B. J. and Gould, P.L., "SHORE-IV, Finite Element Program for Dynamic and Static Analysis of Shells of Revolution-User's Manual", Structural Engineering Research Report No. 56, Department of Civil Engineering, Washington University, St. Louis, Mo., October 1981.

40. El-Shafee, O. M., Basu, P. K., Lee, B. J. and Gould, P.L., "SHORE-IV, Finite Element Program for Dynamic and Static Analysis of Shells of Revolution-Theoretical Manual", Structural Engineering Research Report No. 57, Department of Civil Engineering, Washington University, St. Louis, Mo., October 1981.

41. Gould, P. L., and El-Shafee, O. M., "Local Stress Analysis of Discretely Supported Rotational Shells: Method and Computer Program," Engineering Structures, Vol. 1, No. 3, April, 1979, pp. 153-161.

42. Gould, P. L., "Static Analysis of Shells," Lexington Books, D. C. Heath and Company, 1977.

APPENDIX I

Details Of Stiffness Matrix For An Isoparametric Solid Element

This appendix presents the details of the 24×24 stiffness matrix components of a quadratic isoparametric solid element for a general Fourier harmonic j. The shape function ϕ_i and first derivatives are given in Table 1 , which are chosen to represent the element geometry as well as the displacements within the element. From Equations (3-6) to (3-9), using the partitioned form of B, D and Φ matrices one can get

$$K_k = \iint \left[\begin{array}{c|c} (b_{11}^T D_1 b_{11} + b_{21}^T D_2 B_{21}) & (b_{11}^T D_1 b_{12} + b_{21}^T D_2 b_{22}) \\ 16\times16 & 16\times8 \\ \hline (b_{11}^T D_1 b_{12} + b_{21}^T D_2 b_{22})^T & (b_{22}^T D_2 b_{22} + b_{12}^T D_1 b_{12}) \\ 8\times16 & 8\times8 \end{array}\right]_{24\times24} \quad \text{(I-1)}$$

= the stiffness matrix of the kth element.

and with Equation (2-11) we can write

$$b_{1n} = \frac{\partial g_n}{\partial r} \quad , \qquad b_{1m} = 0$$

$$b_{2n} = b_{2s} = 0 \quad , \quad b_{2\ell} = \frac{\partial g(\ell-8)}{\partial z}$$

$$b_{3n} = \frac{g_n}{r} \quad , \quad b_{3\ell} = 0 \quad , \quad b_{3s} = \frac{-jg(s-16)}{r}$$

$$b_{4n} = \frac{\partial g_n}{\partial z} \quad , \quad b_{4\ell} = \frac{\partial g(\ell-8)}{\partial r} \quad , \quad b_{4s} = 0$$

$$b_{5n} = \frac{jg_n}{r} \quad , \quad b_{5\ell} = 0 \quad , \quad b_{5s} = r\,\frac{\partial}{\partial r}\left(\frac{g(s-16)}{r}\right)$$

$$b_{6n} = 0 \quad , \quad b_{6\ell} = \frac{j}{r}\, g(\ell-8) \quad , \quad b_{6s} = \frac{\partial g(s-16)}{\partial z} \qquad \text{(I-2)}$$

where

$(n = 1,\ldots,8)$

$(m = 9,\ldots,24)$

$(\ell = 9,\ldots,16)$

$(s = 17,\ldots,24)$

Using the above values of the B matrix in Equation I-1 yields,

$$* \quad b_{11}^T\, D_1\, b_{11} + b_{21}^T\, D_2\, b_{21} = \left[\begin{array}{c|c} \bar{K}_{11} & \bar{K}_{12} \\ \hline \bar{K}_{12}^T & \bar{K}_{22} \end{array}\right]_{16\times 16} \qquad \text{(I-3)}$$

where each of $\bar{K}_{11}$, $\bar{K}_{12}$ and $\bar{K}_{22}$ are submatrices of order 8×8.

$$* \quad b_{21}^T\, D_2\, b_{22} + b_{11}^T\, D_1\, b_{12} = \left[\begin{array}{c} \bar{K}_{13} \\ \hline \bar{K}_{23} \end{array}\right]_{16\times 8} \qquad \text{(I-4)}$$

$$* \quad (b_{21}^T D_2 b_{22} + b_{11}^T D_1 b_{12})^T = \underset{8\times16}{\left[\bar{K}_{13}^T \vdots \bar{K}_{23}^T\right]} \qquad (I\text{-}5)$$

$$* \quad b_{22}^T D_2 b_{22} + b_{12}^T D_1 b_{12} = \underset{8\times8}{\left[\bar{K}_{33}\right]} \qquad (I\text{-}6)$$

In Equations (I-3) to (I-6) the elements of the sub-matrices are defined as:

$$\bar{K}_{11mn} = (\lambda+2\mu)[g_{m,r}\, g_{n,r} + g_m\, g_n/r^2] + \frac{\lambda}{r}(g_m\, g_{n,r} + g_n\, g_{m,r}) + \mu g_{m,z}\, g_{n,z} + \mu\left(\frac{j}{r}\right)^2 g_m\, g_n$$

$$\bar{K}_{12mn} = \lambda[g_{n,z}(g_{m,r} + g_m/r)] + \mu g_{m,z}\, g_{n,r}$$

$$\bar{K}_{13mn} = j\mu g_m(g_n/r)_{,r} - \frac{j}{r}\, g_n[\lambda g_{m,r} + (\lambda+2\mu) g_m/r]$$

$$\bar{K}_{22mn} = (\lambda+2\mu)[g_{m,z}\, g_{n,z}] + \mu[g_{m,r}\, g_{n,r}] + \mu\left(\frac{j}{r}\right)^2 g_m\, g_n$$

$$\bar{K}_{23mn} = \mu\, \frac{j}{r}\, g_m\, g_{n,z} - \frac{j}{r}\, \lambda g_n\, g_{m,z}$$

$$\bar{K}_{33mn} = (\lambda+2\mu)\left(\frac{j}{r}\right)^2 g_m\, g_n + \mu\left[r\left(\frac{g_m}{r}\right), r\left(\frac{g_n}{r}\right), r + g_{m,z}\, g_{n,z}\right] \qquad (I\text{-}7)$$

where (m = 1,...,8), and (n = 1,...,8)

Now, the element stiffness element K_k can be written as:

$$K_k = \iint \left[\begin{array}{c|c|c} \bar{K}_{11} & \bar{K}_{12} & \bar{K}_{13} \\ \hline \bar{K}_{12}^T & \bar{K}_{22} & \bar{K}_{23} \\ \hline \bar{K}_{13}^T & \bar{K}_{23}^T & \bar{K}_{33} \end{array}\right] \text{ rdrdz} \qquad \text{(I-8)}$$

and with the transformation of Equation (3-12) together with (3-17), the submatrices of Equation (I-7) can be expressed in terms of the natural coordinates ξ and η, as follows:

$$\begin{aligned} \bar{K}_{11mn} = {} & (\lambda+2\mu)(IJ_{11}\, g_{m,\xi} + IJ_{12}\, g_{m,\eta})(IJ_{11}\, g_{n,\xi} + IJ_{12}\, g_{n,\eta}) \\ & + \frac{\lambda}{RG}[g_m(IJ_{11}\, g_{n,\xi} + IJ_{12}\, g_{n,\eta}) + g_n(IJ_{11}\, g_{m,\xi} + IJ_{12}\, g_{m,\eta})] \\ & + \mu(IJ_{21}\, g_{m,\xi} + IJ_{22}\, g_{m,\eta})(IJ_{21}\, g_{n,\xi} + IJ_{22}\, g_{n,\eta}) \\ & + \left(\frac{j}{RG}\right)^2 \mu\, g_m\, g_n + (\lambda+\mu)[g_m g_{n/(RG^2)}] \end{aligned} \qquad \text{(I-9)}$$

$$\begin{aligned} \bar{K}_{12mn} = {} & \lambda(IJ_{21}\, g_{n,\xi} + IJ_{22}\, g_{n,\eta})(IJ_{11}\, g_{m,\xi} + IJ_{12}\, g_{m,\eta} + g_{m/RG}) \\ & + \mu(IJ_{21}\, g_{m,\xi} + IJ_{22}\, g_{m,\eta})(IJ_{11}\, g_{n,\xi} + IJ_{12}\, g_{n,\eta}) \end{aligned} \qquad \text{(I-10)}$$

$$\bar{K}_{13mn} = \frac{\mu j}{RG} g_m (IJ_{11} g_{n,\xi} + IJ_{12} g_{n,\eta} - g_{n/RG}) - \frac{\lambda j}{RG} g_n \cdot$$

$$(IJ_{11} g_{m,\xi} + IJ_{12} g_{m,\eta}) - \frac{j(\lambda+2\mu)}{(RG)^2} g_m g_n \qquad (I-11)$$

$$\bar{K}_{22mn} = (\lambda+2\mu)(IJ_{21} g_{m,\xi} + IJ_{22} g_{m,\eta})(IJ_{21} g_{n,\xi} + IJ_{22} g_{n,\eta})$$

$$+ \mu(IJ_{11} g_{m,\xi} + IJ_{12} g_{m,\eta})(IJ_{11} g_{n,\xi} + IJ_{12} g_{n,\eta})$$

$$+ \left(\frac{j}{RG}\right)^2 \mu g_m g_n \qquad (I-12)$$

$$\bar{K}_{23mn} = \frac{\mu j}{RG} g_m (IJ_{21} g_{n,\xi} + IJ_{22} g_{n,\eta}) - \frac{\lambda j}{RG} \cdot$$

$$g_n (IJ_{21} g_{m,\xi} + IJ_{22} g_{m,\eta}) \qquad (I-13)$$

$$\bar{K}_{33mn} = \left(\frac{j}{RG}\right)^2 (\lambda+2\mu) g_m g_n + \mu[(IJ_{21} g_{m,\xi} + IJ_{22} g_{m,\eta}) \cdot$$

$$(IJ_{21} g_{n,\xi} + IJ_{22} g_{n,\eta}) + (IJ_{11} g_{m,\xi} + IJ_{12} g_{m,\eta}$$

$$- g_{m/RG})(IJ_{11} g_{n,\xi} + IJ_{12} g_{n,\eta} - g_n/RG)] \qquad (I-14)$$

In the above equations IJ_{11}, IJ_{12}, IJ_{21} and IJ_{22} are defined by Equation (3-11), and;

$(m = 1,\ldots,8)$

$(n = 1,\ldots,8)$

The final stiffness matrix K_k is obtained by substituting Equations (I-9) to (I-14) in Equation (I-8), and with Equation (3-18), one can write

$$K_k = \int_{-1}^{1}\int_{-1}^{1} \left[\begin{array}{c|c|c} \bar{K}_{11_{mn}} & \bar{K}_{12_{mn}} & \bar{K}_{13_{mn}} \\ \hline \bar{K}^T_{12_{mn}} & \bar{K}_{23_{mn}} & \bar{K}_{23_{mn}} \\ \hline \bar{K}^T_{13_{mn}} & \bar{K}^T_{23_{mn}} & \bar{K}_{33_{mn}} \end{array}\right]_{24X24} \text{RGdet.Jacd}\xi d\eta \qquad \text{(I-15)}$$

$(m = 1,\ldots,8)$ and $(n = 1,\ldots,8)$

The integration in the above equation is carried out by means of four points Gaussian integration with the natural cooredinates ξ, η.